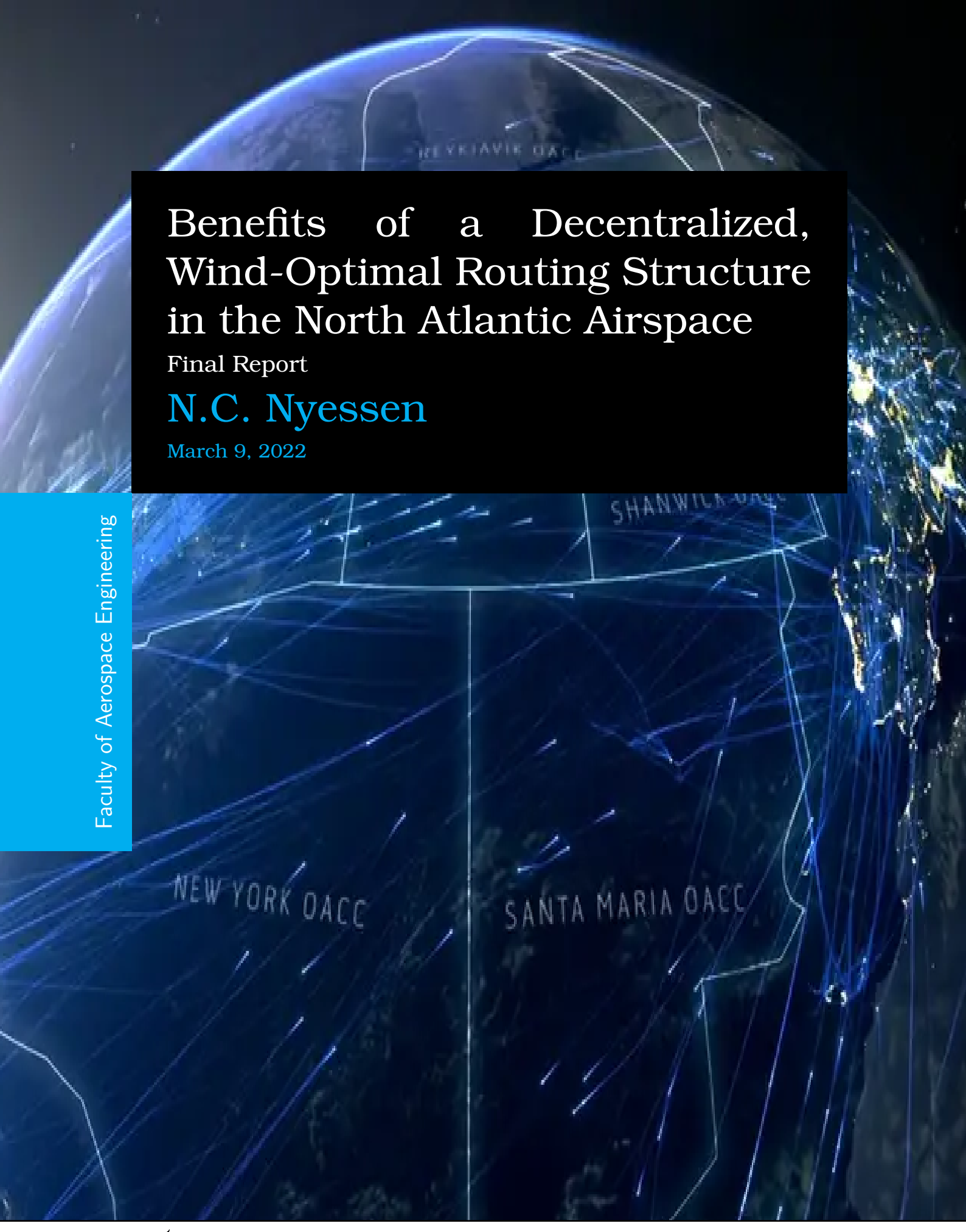

Benefits of a Decentralized, Wind-Optimal Routing Structure in the North Atlantic Airspace

Final Report

N.C. Nyessen

March 9, 2022

Faculty of Aerospace Engineering

TU Delft Delft University of Technology

Challenge the Future

Benefits of a Decentralized, Wind-Optimal Routing Structure in the North Atlantic Airspace

Final Report

by

N.C. Nyessen

Student number: 4377079
Supervisors: prof.dr.ir. J.M. Hoekstra
dr.ir. J. Ellerbroek

March 9, 2022

Cover: NATS - Flight Global (Air Traffic Visualization)
https://d1a2ot8agkqe8w.cloudfront.net/web/2019/10/main-image-air-space-atlantic-c-nats_79264.jpg

Faculty of Aerospace Engineering · Delft University of Technology

Delft University of Technology
Department of

The undersigned hereby certify that they have read and recommend to the Faculty of Aerospace Engineering for acceptance a thesis entitled

Benefits of a Decentralized, Wind-Optimal Routing Structure in the North Atlantic Airspace

by

N.C. Nyessen

in partial fulfillment of the requirements for the degree of

Master of Science.

Dated: March 9, 2022

Supervisor: _____
dr.ir. J. Ellerbroek

Readers: _____
prof.dr.ir. J.M. Hoekstra

Preface

Dear reader,

Thank you for showing an interest in this MSc Thesis. The research has been a challenging and enjoyable time in which trajectory optimization and decentralization air traffic control took a major part. As a result, a paper is included in this thesis titled; Benefits of a Decentralized, Wind-Optimal Routing Structure in the North Atlantic Airspace.

First, I would like to thank my daily thesis supervisor dr.ir. Joost Ellerbroek for his guidance and enthusiasm for the field of air traffic management. Also, I would like to thank my supervisor prof.dr.ir Jacco Hoekstra for his expertise and ability to put problems in a clear context. I would like to thank them both for the considerable amount of work they put into the BlueSky air traffic management simulator. It has been a pleasure working on and with it and I am confident that it will be of great use in our faculty's mission to challenge current aviation standards.

This thesis marks the end of my student time at the TU Delft. I would like to thank all faculty members, my friends, and my parents in particular. They all made it a most enjoyable time.

Nino Nyessen
Delft, February 2022

Contents

List of Acronyms

ACC	Area Control
ADS-B	Automatic Dependent Surveillance-Broadcast
API	Application Programming Interface
APP	Approach Control
ATC	Air Traffic Control
ATCo	Air Traffic Controller
ATS	Air Traffic Services
ATM	Air Traffic Management
ASAS	Airborne Separation Assurance System
BADA	Base of Aircraft Data
CAR	Caribbean Region
CAT	Clear Air Turbulence
CTA	Control Areas
CTR	Control Zones
CWAM	Convective Weather Avoidance Model
DCPC	Direct Controller Pilot Communications
DEP	Domino Effect Parameter
ECMWF	European Centre for Medium-Range Weather Forecast
EMS	Environmental Management System
EUR	European Region
FIR	Flight Information Region
FL	Flight Level
FR24	FlightRadar24

GCR	Great Circle Route
GNSS	Global Navigation Satellite System
GPWS	Ground Proximity Warning System
GWP	Global Warming Potential
IAS	Indicated Airspeed
IATA	International Air Transport Association
ICAO	International Civil Aviation Organization
ISA	International Standard Atmosphere
LoS	Loss of Separation
MID	Middle East Region
MSL	Mean Sea Level
MTOW	Maximum Take-Off Weight
MVP	Modified Voltage Potential
NAM	North American Region
NASA	National Aeronautics and Space Administration
NAT	North Atlantic Region
NAT-OTS	North Atlantic Organized Track System
NextGen	Next Generation Air Transportation System
NLP	Non-Linear Programming
NMAC	Near Mid-Air Collision
NOAA	National Oceanic and Atmospheric Administration
NOTAM	Notice to Airman
PDE	Partial Differential Equation
OEW	Operational Empty Weight
OTS	Organized Track System
PRM	Preferred Route Message
SESAR	Single European Sky ATM Research
SID	Standard Instrument Departures
SSD	Solution Space Diagram
STAR	Standard Arrival Routes
SUA	Special Use Airspace
TAS	True Airspeed
TCAS	Traffic Alert and Collision Avoidance System
TMA	Terminal Control Area
TMI	Track Message Identification

TWR	Tower Control
UAC	Upper Airspace Control
UTA	Upper Control Area
VO	Velocity Obstacles
WOR	Wind-Optimal Route
WTC	Wake Turbulence Category

List of Symbols

χ	Track angle
ϵ	Thrust angle
η	Thrust specific fuel consumption
γ	Flight path angle
μ	Bank angle
ϕ	Latitude
ψ	Heading angle
ρ	Air density
$\rho_{0,ISA}$	Sea level air density
$\rho_{trop,ISA}$	Tropopause level air density
ρ_{AC}	Traffic density
θ	Longitude
ξ	Penalty function constant
$\xi(x)$	Smoothing function
A	Airspace area
b	Scaling variable
$C_{D0,\Delta LDG}$	Parasitic drag coefficient (landing gear)
$C_{D0,AP}$	Parasitic drag coefficient (approach)
$C_{D0,CR}$	Parasitic drag coefficient (cruise)
$C_{D0,LDG}$	Parasitic drag coefficient (landing)
C_{D0}	Zero lift drag coefficient
$C_{D2,AP}$	Induced drag coefficient (approach)
$C_{D2,CR}$	Induced drag coefficient (cruise)

$C_{D2,LDG}$	Induced drag coefficient (landing)
C_{D2}	Induced drag coefficient
C_D	Drag coefficient
C_{f1}	First thrust specific fuel consumption coefficient
C_{f2}	Second thrust specific fuel consumption
C_{f3}	First descent fuel flow coefficient
C_{f4}	Second descent fuel flow coefficient
C_{fcr}	Cruise fuel flow correction coefficient
C_f	Fuel component
C_L	Lift coefficient
$C_{T_{des,app}}$	Approach thrust coefficient
$C_{T_{des,high}}$	High altitude descent thrust coefficient
$C_{T_{des,ldg}}$	Landing thrust coefficient
$C_{T_{des,low}}$	Low altitude descent thrust coefficient
$C_{Tc,1}$	First max. climb thrust coefficient
$C_{Tc,2}$	Second max. climb thrust coefficient
$C_{Tc,3}$	Third max. climb thrust coefficient
$C_{Tc,4}$	Fourth max. climb thrust coefficient
$C_{Tc,5}$	Fifth max. climb thrust coefficient
C_{Tcr}	Maximum cruise thrust coefficient
C_t	Time component
$C_t(\cdot)$	Conflict count
CO	Carbon monoxide
CO_2	Carbon dioxide
D	Drag
f	Fuel flow
$f(X, a)$	Speed of the mobile
$F(X, n)$	Speed of the wavefront
$f_{app/ldg}$	Fuel flow approach/landing
f_{cr}	Fuel flow cruise flight
f_{min}	Minimum fuel flow
f_{nom}	Nominal fuel flow
FC_{tot}	Total fuel consumption
g	Gravitational acceleration
h	Altitude
H_{gnd}	Ground altitude
H_{hi}	High altitude
H_{lo}	Low altitude
h_{opt}	Optimal altitude

h_{opt}^{Legal}	Flyable altitudes
H_p	Geopotential pressure altitude
HC	Hydro carbon
I_H	Horizontal intrusion
I_V	Vertical intrusion
$Int_{severity}$	Intrusion severity
J	Cost function
K_T	Temperature gradient
L	Lift
L_{path}	Average nominal path distance
m	Mass
m_{ref}	Reference mass
n	Outward unit vector normal to the front
N_{AC}	Number of aircraft
NO_x	Nitrogen oxides
R	Radius
$R1$	Stabilizing effect
$R2$	Common conflicts
$R3$	Destabilizing effect
R_E	Earth radius
R_{gas}	Gas constant for air
RoC_+	Positive rate of climb
RoC_-	Negative rate of climb
RoC_0	Zero rate of climb
S	Wing surface
$S1$	Conflict alerts without resolution
$S2$	Conflict alerts with resolution
T	Thrust
t	Time
$T_{0,ISA}$	Sea level temperature
$t_{0_{int}}$	Start time intrusion
t_0	Initial time
$t_{1_{int}}$	End time intrusion
$T_{cr_{max}}$	Maximum cruise thrust
T_{cruise}	Cruise thrust
$T_{des,app}$	Approach thrust
$T_{des,high}$	High altitude descent thrust
$T_{des,ldg}$	Landing thrust
$T_{des,low}$	Low altitude descent thrust

T_{eff}	Effective thrust
t_f	Final time
$T_{maxclimb}$	Maximum climb thrust
$T_{maxclimb}$	Maximum climb thrust
$T_{trop,ISA}$	Tropopause level air temperature
$Temp$	Temperature
u	Eastward component wind velocity
$u(X)$	Value function at point X
V	Velocity
v	Northward component wind velocity
V_{avg}	Average aircraft speed
V_a	Aircraft velocity
V_{CAS}	Calibrated airspeed
V_{ground}	Ground speed
V_{hi}	High velocity
v_{lon}	Longitudinal velocity
V_{lo}	Low velocity
V_{mid}	Medium velocity
V_{ref}	Reference speed
V_{TAS}	True airspeed
v_{w_θ}	Wind velocity in the longitude direction
v_{w_φ}	Wind velocity in the latitude direction
v_{w_z}	Wind velocity in the vertical direction
V_{wind}	Wind speed
W	Weight
$W_y(x, y)$	Northward wind component
W_{fuel}	Fuel weight
W_{MTO}	Maximum takeoff weight
W_{OE}	Operational empty weight
$W_{payload}$	Payload weight
$W_x(x, y)$	Eastward wind component
X	Point on grid
Y	Maximal deviation value
z	Altitude
z'	New solution
z_c	Current solution

List of Figures

List of Tables

Reading Guide

Part I

Scientific Paper

Benefits of a Decentralized, Wind-Optimal Routing Structure in the North Atlantic Airspace

N.C. Nyessen
Supervisors: dr. ir. J. Ellerbroek, Prof. dr. ir. J.M. Hoekstra
Section Control & Simulation, Department Control and Operations, Faculty of Aerospace Engineering
Delft University of Technology, the Netherlands

***Abstract*—In an effort to increase the operational efficiency in the North Atlantic region, the benefits of a decentralized, wind-optimal routing structure are researched. Such a routing structure allows for direct routing by optimizing trajectories on the individual level. Implementing a tactical conflict detection and resolution method eliminates the capacity limits imposed by air traffic control by shifting control to the flight deck. The benefits in terms of safety, capacity, and efficiency are assessed by comparing this routing structure to the current routing structure by simulating a year of real flight data. Furthermore, it is researched if such a routing structure remains viable for forecasted traffic levels by creating a future direct routing scenario with the use of dummy flights. Trajectory optimization is performed for the part of the trajectory above 10,000 ft in a decoupled manner with the ordered upwind algorithm for the horizontal domain and the base of aircraft data performance model for the vertical domain. Conflicts are solved on the tactical level with the modified voltage potential method in the horizontal domain. On average, a 5.1% fuel reduction, or 1.9% time reduction, is established for the new routing structure. A total of 18 loss of separations with an intrusion severity above 1% occur, of which the most severe intrusion still assures 734 ft vertical and/or 3.67 NM horizontal separation. The routing structure appears to be robust for future traffic levels as the airspace density scales linearly with the amount of aircraft and the conflict to loss of separation ratio remains constant with only three loss of separations slightly exceeding the 1% limit.**

Keywords: Airspace Structure, Air Traffic Control, Decentralized Airspace, Direct Routing, Free Flight, Modified Voltage Potential, North Atlantic Airspace, Wind-Optimal Routing

I. Introduction

Ever-growing customer demand and an increasing incentive to reduce aviation climate impact challenge the sectors' current standards. One way aviation impacts the environment is by in-flight emissions. Being the busiest oceanic airspace with around 730,000 crossings in 2017 [1], the North Atlantic corridor contributes to 6.5% of all aviation emissions of which 97% is emitted above an altitude of 7 km [2]. The airspace in this area is structured by the Organized Track System (OTS), also known as "highways in the sky", which guarantees safe separation as Direct Controller Pilot Communications (DCPC) and Air Traffic Services (ATS) surveillance are limited in remote areas [3]. The OTS aims to safely facilitate as many flights as possible. However, the capacity of the airspace is currently constrained by large separation standards and a limited economically viable height band. Further limitations are imposed by two time-constrained westbound and eastbound flows. The current OTS structure facilitates inefficient routing [4], keeping aviation emissions unnecessarily high and posing limitations on the airspace capacity. What makes the problem even more imminent is the prediction of the International Civil Aviation Organization (ICAO) that North Atlantic traffic will almost double in the coming twenty years [5], despite the COVID-19 setback from which aviation is expected to bounce back [6]. Two ways to reduce emissions and cope with the predicted growth are either by technological advancements or operational improvements. The latter yields the highest short-term benefits and is promising for the North Atlantic region (NAT).

General research on airspace restructuring often focuses on introducing the free flight concept [7] as this provides a safe and efficient airspace structure. As surveillance, communication, and navigation methods have improved over the past years, the free-flight concept has become viable. This as these technological advancements allow for on-board Conflict Detection and Resolution (CD&R). Also, with aviation expected to grow and sector densities to increase, the workload of the Air Traffic Controller (ATCo) will increase. Free flight takes a decentralized approach by shifting control from Air Traffic Control (ATC) to the flight deck, reducing this workload and Air Traffic Management (ATM) costs. This shift allows for maximizing behavior instead of satisficing behavior [8], improving the overall efficiency.

Previous research addressing inefficiencies in the North Atlantic region in particular mainly focused on either OTS modification or airspace restructuring. Adjustments to the tracks are made by taking oceanic winds into account, decreasing separation standards, and/or allowing for along-track rerouting [1], [9]. Airspace restructuring mainly focuses on investigating the benefits of wind-optimal routing on an individual level combined with a centralized strategic deconflicting method to reduce congestion clusters and obtain less congested trajectory sets [4], [10]. This reduces the workload during the tactical conflict resolution stage. Uncertainties in wind have been modeled for strategic methods to improve the model robustness [11]. A study investigating the benefits of direct routing in the North Atlantic region by optimizing routes on the individual level while taking winds into account and solving conflicts by a decentralized, tactical approach has not yet been conducted. Technological advancements assure

that all commercial aircraft in the USA and Europe, hence above in the North Atlantic region, have to be equipped with Automatic Dependent Surveillance-Broadcast (ADS-B) as of 2020. Aircraft equipped with such a device constantly transmit their state information which is received by a global network. This data is used to construct both the actual flown and wind-optimal trajectories. These trajectories are used to compare the difference in safety, capacity, and efficiency between the routing structures.

An overview of the current airspace structure and the NAT, in particular, is presented in section II. Besides this, the concept of free flight and its corresponding conflict detection and resolution requirements are discussed. Wind-optimal routing is discussed in section III. With this information, the experiment is designed in section IV and it states the assumptions that are made. section V presents the results of the research which are discussed in section VI together with some recommendations. At last, a conclusion is drawn in section VII.

II. Airspace Characteristics

Aviation is a heavily regulated transportation sector with a major focus on safety. Therefore, it is of importance to have a thorough understanding of the current systems and routing structures before these can be challenged with new concepts. First, the current routing structure and its emergence are discussed. Then, attention is paid to the characteristics of the NAT in particular. Further, the free flight concept is elaborated upon. At last, conflict detection and resolution methods to allow for airspace decentralization is touched upon.

A. Current Routing Structure

In the early days of aviation, navigation was performed similarly to naval navigation with maps, compasses, and pilots' senses. When traffic levels increased, a more structured way of coordinating and planning became necessary to handle complex situations and safely separate aircraft [12]. This resulted in a centralized control approach through ATC that was made possible with the emergence of more advanced navigation systems, such as radar detection and navigation beacons. The increased intervention of ATC reduced the freedom of pilots to fly their preferred routes as they had to fly predefined routes consisting of a series of waypoints.

Nowadays, aircraft routing is still based on these waypoints. The airspace is structured into layers and sectors for ATCo to be able to cope with the complexity of the system and assure safe separation and a smooth flow of traffic. These layers and sectors can be roughly divided into the airspace below and above Flight Level (FL) 100. The airspace below this level consists of Standard Instrument Departures (SID) and Standard Arrival Routes (STAR) to reduce Air Traffic Controller (ATCo) workload and comply with noise regulations around airports. These routes depend on weather and runway conditions. The task of the ATCo in this airspace is to safely separate aircraft and perform the guidance around airports in an efficient manner. The airspace above this level (FL100) is less complex and the main task of ATCo is to safely separate aircraft and perform en-route guidance from sector entry to sector exit. As the airspace above FL100 is less restricted, it allows for more optimization. Furthermore, areas that restrict or prohibit commercial flights are denoted as Special Use Airspace (SUA). The division of airspace into sectors and layers can be used as an advantage for the partial implementation of new routing structures.

ATC plays a crucial role in the current routing system and aircraft always have to obey ATC orders unless there is an imminent danger appointed by the prevention systems (Traffic alert and Collision Avoidance System (TCAS)). This centralized airspace structure comes at the cost of overall efficiency. First of all, aircraft can not fly their most optimal route due to waypoint restrictions. Secondly, airlines tend to maximize profits. All ATC services have to be paid for and each entity charges a fee to all passing aircraft based on their flown distance and weight. Some airlines base their strategic advantage on reducing these costs as they fly through more economical airspace, accepting additional fuel consumption. At last, capacity and routing efficiency are limited by the ATCo workload. Reducing the ATCo numbers also reduces the cost of ATC.

B. NAT Characteristics

The airspace of special interest is the NAT, which consists of the OTS in which aircraft have to follow predefined routes. These tracks assure safe separation throughout the NAT with a reduced vertical separation (1000 ft), longitudinal separation defined by clock minutes, and a standard lateral separation distance of 60 NM (one degree latitude). Most aircraft fly within the economically viable FL290-410 region, therefore, the flight levels associated with the OTS are FL310 to FL400 [9], [13]. Minimum time tracks are established daily, based on all individually filed routes that take weather systems into account up to a certain extent (to the airlines' standards). Together, all flight plans are used to produce a basic minimum time track. Multiple tracks may be established during periods of high demand. This changing system is called the OTS. The OTS tracks are mainly located in the Gander and Shanwick (G/S) oceanic Flight Information Regions (FIR). Deviation from the OTS is possible if a flight remains clear of the established tracks and ATC has the responsibility that these flights do not interfere, which can lead to substantial route deviations. About half of all flights crossing the North Atlantic follow the NAT-OTS, [3] (8.1.7).

Altogether, some general characteristics relevant in the North Atlantic region can be stated. Aircraft operate at or near both cruise altitude and speed. The structure of the tracks causes aircraft to mainly fly in (near)parallel in the NAT. They are expected to do so in absence of the tracks due to the location of the major airports and dominant flight directions in the network. Therefore, conflicts are likely to be in the shallow angle or head-on (large angle) region. Jet streams play a significant role in the North Atlantic region. Their location is subjected to seasonal patterns being stronger and more south during winter and vice versa during summer [14].

C. Free Flight

As mentioned above, a centralized routing structure with ATC imposes limitations on the overall efficiency. Emerging technologies allow implementing the free flight principle by shifting back control from ATC to the flight deck, drastically reducing ATCo numbers [15]. When aircraft fly their most optimal route in free-flight airspace, it is called direct routing. Current initiatives that look into improving current airspace structures and implementing direct routing with the use of modern technologies such as ADS-B are SESAR (Europe) and its US counterpart, NextGen.

Introducing such free-flight airspace has the practical disadvantage that countries have to share their airspace. However, this is a minor implication compared to the potential benefits in terms of capacity, efficiency, and safety that can be experienced. The airspace capacity can be increased as a result of a reduced average flight time and a more evenly spread of aircraft throughout the airspace as they are not bounded by fixed structures anymore [16], [17]. However, some research shows that free flight could decrease the airspace capacity for high levels of traffic density due to the conflict chain reaction property [18]. Solving conflicts in an unstructured manner could cause the system to destabilize [19]. Another advantage is the possibility for aircraft to fly their desired optimal route by optimizing their vertical and horizontal flight trajectory [16]. Yielding a higher fuel efficiency and a reduction of overall flight time. Generally, there appears to be a negative correlation between the level of structuring and the overall efficiency [20]. However, when traffic density levels become too high, the efficiency benefits may no longer be realized [18]. At last, it can be said that free-flight airspace increases safety compared to structured routing airspace as fewer conflicts are counted due to increased spreading of traffic [20], [21]. Furthermore, the cockpit crew experiences the free-flight scenario as safer compared to the ATC situation on a subjective scale, [7]. This lays an important foundation as the human perception in the cockpit of the free-flight concept is of utmost importance as control shifts in that direction.

D. Conflict Detection & Resolution

Decentralizing the NAT by shifting control from ATC to the flight deck is solely possible with a well-functioning CD&R method to assure safe separation. The main goal of such a method is to solve conflicts and avoid a loss of separation (LoS). A LoS occurs when an intruder enters the Protected Zone (PZ) of the ownship (usually a disk-shaped area of 5 NM radius and 1000 ft vertical offset [3]) and a conflict occurs when a LoS is predicted within a certain look-ahead time [22]. The look-ahead time can be varied to find a balance between the time to resolve a conflict and the relevance of potential intruders as both the ownship and intruders are susceptible to trajectory uncertainties. Various levels of intent can be used to determine trajectory propagation. However, no intent is used in direct routing as aircraft are less likely to maneuver, it simplifies the implementation, and it is more transparent to the crew [7]. Furthermore, ADS-B equipment should be assumed to be fully functioning.

The absence of ATC calls for a tactical CD&R method that is capable of generating fast and efficient resolutions with some level of redundancy in case of failure aboard one aircraft. The Modified Voltage Potential (MVP) method, based on a self-organizational algorithm, is used for this research [16]. This method uses a minimum distance vector to compute an avoidance vector out of the intruder's protected zone taking the future position of both the intruder and ownship at the moment of minimum distance into account [7]. The method is fail-safe as it assumes the intruder not to move and the avoidance vector points in the opposite direction. In case of multiple conflicts, the vectors are summed. The algorithm is suited for online implementation and a look-ahead time of 5 minutes ensures sufficient time to identify and solve the conflict. No negotiation is required, mitigating the chance of a deadlock [23]. Previous research shows that airspace with a high traffic density remains manageable for a direct routing structure. With adaptations to the recovery part of the MVP [24], the algorithm is most likely suited to handle flights under NAT specific characteristics like flying in parallel and handling head-on and shallow angle conflicts.

However, no research has been performed to find the most suitable resolution domain for flights under NAT-specific conflict characteristics. On a tactical level, conflicts can be avoided by performing a maneuver in the vertical (climb/descent), lateral (turn), and longitudinal (speed) direction, [25]. In general, pilots have a preference for solving conflicts in the vertical domain due to the rapid result (shape of the PZ) and lower cognitive workload. Depending on the traffic and airspace characteristics, either of these combinations could perform best.

III. Wind-Optimal Routing

Free-flight airspace allows for aircraft to fly their desired optimal route and this section discusses a suitable optimization method. Trajectory optimization for aviation has been widely researched and is believed to result in immediate, low-cost, low-risk, and significant fuel reductions [26]. It is important to clearly define the optimization objective as, for instance, fuel-optimized routes are not necessarily climate-optimized routes. Also, additional external factors that (in)directly pose restrictions on the objective can be incorporated. These factors are mostly weather and obstacle related, such as nonlinearities around jet streams [27], convective areas [28], and SUA. As airlines and aircraft tend to seek for maximizing behavior to improve their competitive advantage [8], fuel-optimized trajectories are most promising to increase the overall routing performance. The trajectory optimization can be performed in both the horizontal and vertical domains. These domains are assumed to be weakly coupled and often considered separately to reduce the overall model complexity and increase the computational performance [29].

Vertical optimization is mainly a function of aircraft aerodynamics, engine performance, and vertical wind gradients

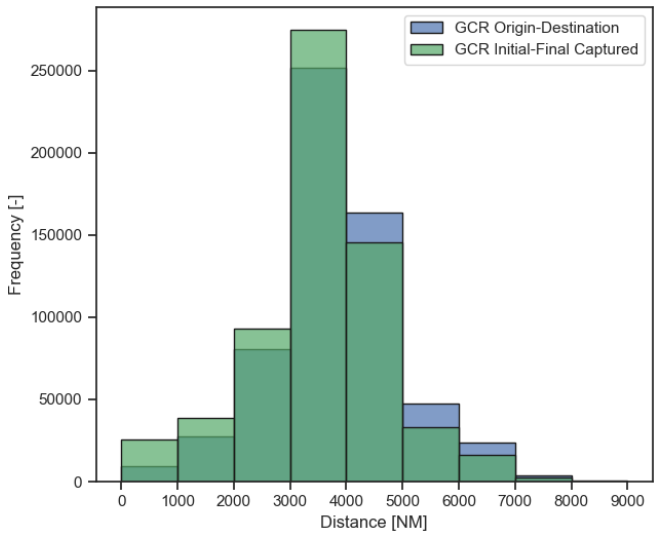

Fig. 1. Distribution of GCR distances for both the origin-destination and captured initial-final location pairs for all flights in the data set.

[29]. The vertical profile can be divided into three phases; climb, cruise, and descent. A model that contains aircraft-specific performance and operating procedure coefficients for trajectory simulations is the Base of Aircraft Data (BADA) model [30]. This can be used to construct vertical trajectories. The model complies with real-life procedures as constant Indicated Airspeed (IAS)/Mach climb and descent. The rate of climb is computed using the total-energy model and the rate of descent is computed using nominal mass values. Maximum specific range (minimum fuel consumption) is obtained by keeping airspeed constant for decreasing weight during cruise. This results in a gradual climb throughout the cruise phase where the optimal altitude is a function of mass.

Horizontal trajectory optimization is mainly limited by weather and obstacles, especially due to the strong influence of winds in the NAT. An active area of research is the computation of Wind-Optimal Routes (WOR) and this method has been proven successful in the NAT [4], [11]. Although the Great Circle Route (GCR) is shorter, taking the presence of winds into account with WOR yields a higher than 1% benefit on average fuel consumption for routes over a 2000 NM (3700 km) distance [31]. Most flights crossing the North Atlantic region cover a distance larger than this as can be seen in Figure 1. Around 95% of the flights cover a distance of more than 2000 NM from origin to destination. When only looking at the captured parts of these trajectories, still 90% of the flights have a GCR that covers more than 2000 NM. Besides the importance of taking winds into account, the horizontal optimization method should be computationally efficient as a large number of flights cross the NAT.

A suitable method is the Dijkstra-like ordered upwind method [32], [33]. The controlled parameter is the optimal heading angle ψ and this should be chosen to minimize the total travel time, also minimizing fuel consumption under the assumption of constant true airspeed and constant altitude. This standard formulation of the optimal control problem is solved by writing it in the Hamilton-Jacobi form and treating it as a front expansion problem where the speed of the wavefront depends on the speed of the mobile. The optimal path is designed by following the characteristics of the Hamilton-Jacobi Partial Differential Equation (PDE) from the arrival point to the departure point. This algorithm is highly efficient since it avoids iterations by carefully using the information on the characteristic directions of the PDE. A Lambert Conformal Conic projection [34] is applied for sphere/plane conversion. This method yields a time reduction of 2.9% for routes of 315 minutes compared to their GCR [33].

IV. Experiment Design

An experiment is designed to find the benefits in terms of efficiency, safety, and capacity of a direct routing structure compared to the current routing structure in the North Atlantic region. The aim is to research how much fuel/time can be saved by implementing this structure, while safely separating aircraft. This is researched by conducting an experiment that simulates a year of real flight data to compare the current Air Traffic Management (ATM) structure to a direct routing one and assess its benefits. Furthermore, the robustness of the direct routing structure is researched by assessing if the airspace remains safe for the forecasted increase in traffic levels in the North Atlantic region.

It is expected that the direct routing scenario performs better in terms of efficiency than the current routing scenario, meaning a fuel reduction is established. No changes in LoS are expected as it is assumed that none are present in the current scenario and all conflicts will be resolved in the direct routing scenario. The same holds for the intrusion severity. Aircraft are expected to cross the North Atlantic region faster when flying WOR, resulting in a decreased traffic density. At last, it is expected that the direct routing scenario remains safe for the forecasted traffic levels.

All simulations will be performed in the open-source, open-data ATM simulation tool developed by TU Delft [35]. Performance modeling in BlueSky based on BADA is validated [36]. All further computations and modeling is performed in Python 3.X. The used hardware is an HP ZBook 15 2014, 2.40GHz Quad-Core Intel i7-4700MQ, 16GB RAM, and a TU Delft simulation PC, Ryzen 1700x 8c16t, 32GB RAM PC.

A. Data Collection and Preprocessing

To construct these scenarios and simulate a year of flights, flight data obtained from FlightRadar24[1] (FR24) for the pre-COVID period of 1 April 2019 till 31 March 2020 is used. FR24 gathers flight and position data (as stated in Table I) with a worldwide system of 20,000 ADS-B receivers. As of 2020, all commercial aircraft in Europe and the US have to be equipped with ADS-B equipment. Therefore, it is assumed that all flights crossing the NAT are equipped as well and are

[1]https://www.flightradar24.com

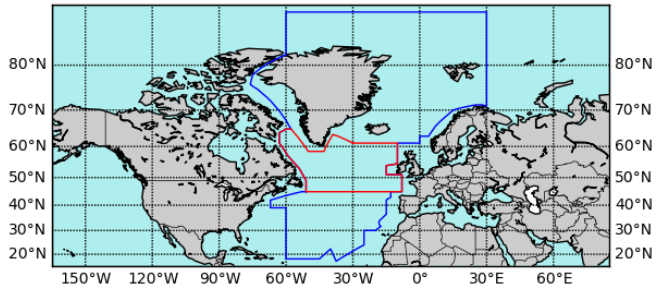

Fig. 2. The FR24 data extraction region on a cylindrical projection with the North Atlantic Flight Information Region in blue and the Gander and Shanwick Flight Information Regions in red.

captured by FR24 up to some extent (also assumed for 2019 flights). The ADS-B data is assumed to perfectly match the actual aircraft states. The extraction region covers an area from 15°N-90°N by 165°W-85°E (Figure 2) and is selected based on a trade-off between capturing as many flights crossing the NAT and limiting the total amount of data.

TABLE I
FLIGHTRADAR24 FLIGHT AND POSITION DATA.

Variable	Definition [Unit]
Flight ID	Unique decimal identifier for the flight leg
Equipment	ICAO aircraft designator
Schd from	IATA code for scheduled departure airport
Schd to	IATA code for scheduled arrival airport
Real to	IATA code for actual arrival airport
Snapshot ID	Time of position update [s]
Altitude	Height above sea level [ft]
Heading	True heading [deg]
Latitude	Floating point format [°]
Longitude	Floating point format [°]
Speed	Ground speed [kts]

Flights that cross the NAT are filtered out to be used in the simulations. First, flights with at least three coordinates within the NAT and non-equal origin-destination continent are selected. Furthermore, flights with Africa-Europe and Asia-Europe origin-destination continents (apart from entries from Iceland) are removed from the data as these are considered to be irrelevant to the problem. Before performing the continent-based filtering, it is checked based on the position data if the right arrival airport is stated in the flight data as this turns out to be incorrect for some cases. At last, flights that are considered as separate flights by flight ID, but have the same callsign, origin-destination pair, and chronological trajectory characteristics are merged into a single flight. The daily number of aircraft crossing the NAT for the extraction period is displayed in Figure 3. The start of the COVID pandemic influences North Atlantic travel from mid-March onwards. Furthermore, seasonal and weekly variations in traffic levels can be noticed.

Besides flight data, reanalysis data is required to construct the simulation scenarios and run the simulation. The reanalysis data for the trajectory construction is obtained from the European Centre for Medium-Range Weather Forecast (ECMWF)

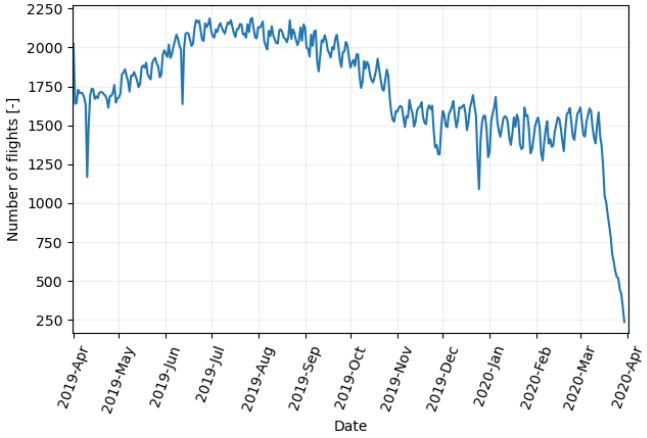

Fig. 3. Daily number of flights crossing the North Atlantic region for the extraction period.

via an easy-to-use API and consists of an eastward (u) and northward (v) wind component. An extraction region, including bounds where possible, of 165.25W, 90N, 85.25E, 14.75S is used to guarantee interpolation near the boundaries. The extracted data has a resolution of 0.25x0.25 degrees, pressure levels corresponding to 9,882-44,647 ft at ISA, and a 3-hour update interval in which wind is assumed not to vary. However, the BlueSky simulator uses readily available reanalysis data from the National Oceanic and Atmosphere Administration (NOAA) via the WindGFS plugin. This data differs slightly in grid (1x1 degrees) and pressure level resolution which makes it less data-intensive. It is expected that differences between these two data sets are minor and they are assumed to be negligible.

B. Traffic Scenarios

The preprocessed flight data is the starting point of the trajectory construction for the traffic scenarios. A total of three routing scenarios will be constructed, one based on the actual routes and two on the optimized trajectories. Before constructing these scenarios, some general assumptions are stated. First, International Standard Atmosphere (ISA) conditions apply to perform velocity conversions in absence of atmospheric pressure data. Aircraft are assumed to be in quasi-rectilinear, symmetric flight for the BADA model to hold and all flights with unspecified aircraft type are assumed to be B77W (the most frequently observed model in the NAT region). As aircraft usually cover large distances when crossing the NAT, the initial mass is set to the maximum mass rather than drawing a mass from a probability distribution to avoid aircraft from exceeding their minimum mass. This initial mass is reduced to account for the distance covered from the origin to the initial position by subtracting a ratio (the origin-initial point GCR to origin-destination GCR) of the total estimated fuel consumption (arbitrarily chosen difference of the maximum and 1.3 times the minimum mass). At last, assumptions regarding the airspace are made where fees are constant so that airlines have no incentive to prolong their

routes through more cost-efficient airspace and no SUA is present.

1) Current Routes: The current routing scenario is directly constructed from the FR24 data. Some additional filtering has to be performed before constructing the actual trajectories for this scenario. The optimization focuses on the airspace above FL100 as the airspace below this is dominated by airport procedures. Therefore, all trajectory data below FL100 and above FL550 (possible outliers) is discarded. All trajectories containing less than two points are discarded as well. The actual trajectory is constructed with all position data captured by FR24 from the first to the last data point at or above FL100, from now on called the initial and final coordinate. BlueSky requires the Calibrated Airspeed (CAS) or Mach number as velocity input. As FR24 provides the ground speed, this is converted to the CAS with the use of wind data and ISA pressure altitude for the current routes.

2) Direct Routes: The direct routing scenario consists of WOR that are constructed via a separate vertical and horizontal optimization in line with the weakly coupled optimization domain assumption. The optimization is performed not just for the part of the flight in the NAT, but for the whole trajectory within the extraction region as this gives a more accurate view of the possible fuel benefits. First, the horizontal profile is constructed for which the initial and final coordinates are used as the starting and endpoint. This horizontal trajectory is computed with the ordered upwind algorithm, assuming aircraft type-specific constant true airspeed based on reference mass optimal altitude (BADA). A random, irregular 2D grid that encloses the initial and final points with some margin is created with the Poisson disc sampling algorithm[2]. This grid is created on the Lambert Conic Conformal plane and contains a maximum of 175 points to assure sufficient computational performance. It is expected that some randomness in grid point location and quantity helps to avoid trajectory clusters around the main origin-destination pairs within the network. The accepted wavefront travels from the initial to the final point and is updated with the use of a concave hull algorithm[3]. The trajectory is constructed by following the characteristic via backward propagation with a time step of 60 seconds. When an optimal trajectory contains less than 4 points it is discarded as it covers insufficient distance. Then, the vertical trajectory is constructed based on the 2D (latitude/longitude) horizontal trajectory and the BADA model. During this optimization, the optimal altitude is determined based on decreasing mass and procedural velocities. Vertical wind components are assumed to be zero and not taken into consideration. The start of descent is determined by the difference between current and final altitude and a standard descent steepness. This optimization approach does not result in a global optimum, as such computations are too expensive.

3) Future Direct Routes: To research the sensitivity of the direct routing scenario to the predicted future growth in aviation in the North Atlantic region, a future traffic scenario is constructed. This scenario is strongly related to the current direct routing scenario as the trajectories are constructed via the same optimization method. Additionally, dummy flights are added up to the peak week traffic level forecasted by ICAO. These dummy flights are based on the current flight data as there are uncertainties as to how the network will develop in the future. First, the data is split up into eastbound and westbound traffic. Both traffic sets are scaled by a scaling factor based on the predicted growth in peak week NAT travel. It is set to $\frac{26}{14}$, as a peak week travel of approximately 26,000 flights in 2038 is forecasted compared to 14,000 flights in 2019. The scaling is done by drawing dummies from the data set with equal probability, adding them to existing data sets, and merging the eastbound and westbound sets. This way the original departure time distribution and eastbound/westbound fractions are matched. To obtain some randomness, the departure times are shuffled at random and reassigned to the flight data (initial location, final location, aircraft type, and initial mass). Wind-optimal routes are created based on this newly obtained set to construct the future direct routing scenario.

4) Simplified Routes: The actual and optimized trajectories consist of an extensive number of data points. This data is loaded into BlueSky as waypoints via scenario files and the number of waypoints directly influences the computational speed of BlueSky. To run scenarios in an acceptable time, a line reduction algorithm is used on both the actual and optimized trajectories. The Ramer-Douglas-Peucker (RDP) algorithm[4] is selected as it performs well in terms of computational speed and difference in fuel consumption w.r.t. the full trajectories. The algorithm is performed on the latitude, longitude, and altitude dimensions and a distance dimension factor of 0.0015 is selected. BlueSky operates under a soonest climb and latest descent logic based on aircraft-specific performance (BADA). The optimized trajectories follow the same logic and only the points selected by the RDP algorithm are included in the simplified trajectory. The actual trajectories do not follow this logic. To avoid loss of fidelity of the fuel burn model, the simplified actual trajectories also contain all points that are labeled as climb or descent by a fuzzy logic flight identification algorithm [37] on top of the points selected by the RDP algorithm. The simplified routes are assumed to follow the BlueSky logic by flying GCR to the next waypoint and adhere to the fastest climb/descent and speed change logic.

C. Simulation Setup

Now, the simulation setup for the different experiments is elaborated upon with the use of the different traffic scenarios stated above. It holds for all simulations that the airspace under the current routing structure is assumed to be managed by ATC, therefore, no further conflict resolution method is used. The opposite holds for the decentralized airspace under the direct routing structure, no ATC is involved to direct aircraft along a route or to resolve conflicts as this responsibility has

[2]https://scipython.com/blog/poisson-disc-sampling-in-python/, April 2017.

[3]https://gist.github.com/AndreLester/589ea1eddd3a28d00f3d7e47bd9f28fb, August 2018.

[4]https://github.com/mourner/simplify-js.git, Oct 2021

been shifted to the flight deck. The conflict detection and resolution settings for the MVP method are set to a look-ahead time of 300 seconds, horizontal separation of 5 NM, and vertical separation of 1000 ft. Conflict resolution is performed in the horizontal domain by heading and speed changes.

The MVP algorithm in BlueSky tends to underperform when aircraft spawn into each others' PZ, resulting in long-lasting loss of separations. To avoid this, a time shift is applied to any ownship of which the first trajectory waypoint interferes with an intruder's trajectory in both time and place. If a conflict is detected, shifts of 120 seconds are applied to the ownship until no more interference is present. This is only applied to the direct routing scenarios as no MVP is used for the current routing scenarios. Beware that time shifts are applied for simulation purposes only. In real life, an ATCo would safely guide flights into the free-flight zone from where the MVP algorithm handles conflict avoidance.

The simulation area is set equal to the extraction region to capture the full trajectories. Only conflicts and LoS within the NAT are considered relevant as the conflict count outside this region is not representative in absence of remaining traffic. However, the fuel consumption is computed for the whole trajectory to get a better view of the potential total fuel savings. This, as trajectories are optimized on the individual level and it is expected that the absence of remaining traffic has a negligible impact on the overall fuel consumption as tactical CD&R is performed fuel-efficient.

1) Current Routing vs. Direct Routing: The first simulation setup compares the current routing structure to the direct routing structure by simulating a full year of flight data. This allows for a comparison in overall fuel consumption, safety, and capacity while taking seasonal variation in weather and traffic levels into account. Furthermore, it validates the improved efficiency of the WOR by comparing them to the actual routes. Both simulation scenarios are split up in monthly intervals to avoid data loss. No traffic built-up is used as traffic spawns in the simulation area throughout the simulation period. The number of LoS, intrusion severity, and traffic density logging starts right away and ends at 23:59 UTC on the last day of the month. The fuel data logging starts right away and ends when the last aircraft has reached its destination to capture the entire covered distance (this will be the first day of the next month for the final flights).

2) Future Direct Routing: The future direct routing simulation is constructed based on a subset of three days with the highest number of aircraft crossing the NAT (30 June 2019, 27 July 2019, and 28 July 2019). This future scenario is compared to the direct routing scenario for the selected days. They are compared by safety and capacity only as fuel burn is considered to be unrepresentative due to uncertainties in both the future network and aircraft/engine efficiency. The wind data of the selected days will be used for the future direct routing scenario as well. One day of traffic built-up is used in advance to guarantee representative traffic levels during the eastbound OTS hours. The number of LoS, intrusion severity, and traffic density are logged over the day of interest (00:00-23:59 UTC).

D. Independent Variables

In line with the simulation scenarios, the following independent variables are defined. For the current routing vs. direct routing simulation, the airspace structure is the independent variable. Where the current routing scenario consists of the centralized, actual routing structure and the direct routing scenario consists of a decentralized, wind-optimal routing structure. The independent variable for the future direct routing simulation is the traffic level in the NAT under the decentralized, wind-optimal routing structure.

E. Dependent Variables

The airspace performance of the different scenarios is compared according to several performance criteria. These criteria are safety, capacity, and efficiency. Each of these criteria is assessed by one or more performance indicators.

1) Safety: The first and most important criterion is airspace safety, which is a measure of separation performance. This safety is measured by indicators that quantify if a direct or indirect risk on the overall safety occurs. First, the number of times aircraft intrude each others' PZ (LoS) are counted. Also, the number of conflicts is counted and compared to the number of LoS to determine if the CD&R method effectively resolves them. As one could argue that a minor LoS should not be counted equally as a near miss, the intrusion severity is measured as well, computed by Equation 1. An intrusion is considered to be severe if it exceeds a 1% intrusion limit. I_H and I_V are the horizontal and vertical intrusions that are normalized for the corresponding minimum separation requirements, while $t_{0_{int}}$ and $t_{1_{int}}$ are the start and end time of an intrusion [20].

$$Int_{severity} = \max_{t_{0_{int}} - t_{1_{int}}} \left[min \left(I_H(t), I_V(t) \right) \right] \tag{1}$$

A direct comparison of these indicators is possible for the direct routing and the future direct routing simulation scenarios as these operate under the same airspace structure. However, when comparing these indicators for the current and direct routing scenarios it has to be kept in mind that although some LoSs occur in the current scenario due to the trajectory simplification, these are actually assumed to be zero in presence of ATC.

2) Capacity: Each airspace has a maximum capacity, just like a road has one. The amount and variety in airspace structuring directly influence this capacity. To measure this capacity, the airspace density (ρ_{AC}) is computed at a fifteen-minute interval according to Equation 2. Where N_{AC} denotes the number of aircraft, A is the airspace area, Δt is the time interval over which the conflicts are counted, V_{avg} is the average aircraft speed, and L_{path} is the average nominal path distance of the aircraft in the simulation space.

$$\rho_{AC} = \frac{N_{AC}}{A \Delta t (V_{avg} / L_{path})} \tag{2}$$

The airspace density is computed for both the NAT area and the G/S area as the OTS tracks are predominantly positioned in the G/S area. Therefore, incorporating this gives a better view of the effect of the direct routing structure on traffic spreading.

3) Efficiency: All aircraft in the simulation region are taken into account when determining airspace efficiency. The airspace efficiency is measured by the amount of fuel consumed. The fuel burn is computed with the BADA performance model which is integrated into BlueSky and based on the total-energy model [30]. The fuel flow and thrust are computed for each flight phase based on aircraft-specific input (performance and operating procedure coefficient), aircraft state information (altitude, velocity, time step, and ROCD), and atmospheric conditions (ISA). The total fuel consumption is computed by integrating the fuel flow over the flight time. An overall improvement of the airspace efficiency does not guarantee that the individual aircraft efficiency improves. Therefore, it is important to investigate the whole spectrum of fuel consumption differences to see if some flights are more heavily impacted than others.

V. Results

This section elaborates upon the results for the different simulation scenarios. The results are stated in the same order as the discussed dependent variables. Outlier flights are removed from the data, including flights where the actual trajectory contains polluted data. For the paired data of sufficient sample size, it is tested if the difference between the samples is significant. The non-parametric Wilcoxon paired signed-rank test [38] is used for samples for which the null hypothesis of normally distributed samples is rejected at the 5% significance level according to the D'Agostino and Pearson's test [39], [40]. The Wilcoxon test has a null hypothesis of equal sample distribution and an alternative hypothesis of non-equal sample distribution. The null hypothesis is rejected at the 5% significance level. This test is used to assess the significance of the differences in daily conflict count, daily airspace density, and yearly fuel consumption.

The following abbreviations are used for the traffic scenarios, all scenarios consist of simplified routes:

- AR, current routing (not denoted with CR as this can be confusing with conflict resolution).
- DR, direct routing
- FR, future direct routing

A. Safety

For measuring safety, the AR and DR scenarios are compared on an annual and daily basis. Before comparing the results, all conflicts and losses that occur in the DR scenario within the look-ahead time of 300 seconds since the spawning time of one of the aircraft in conflict are excluded from the results. This, as it is assumed that these aircraft have an insufficient response time.

First, the total annual results for the number of conflicts, number of LoSs, and the maximum intrusion severity are stated in Table II. For the largest intrusion in the DR scenario, a separation of 734 ft vertically and/or 3.67 NM horizontally is obtained. While the number of conflicts increases for the DR scenario, the number of LoSs and the intrusion severity decrease. This indicates that the conflict resolution method effectively takes care of the conflicts, potentially at the cost of creating secondary conflicts. When looking at the conflict location heat map for all conflicts during the year of simulation in Figure 4 and Figure 5, it is noticed that conflicts are more evenly spread over the NAT, instead of mainly near the region borders.

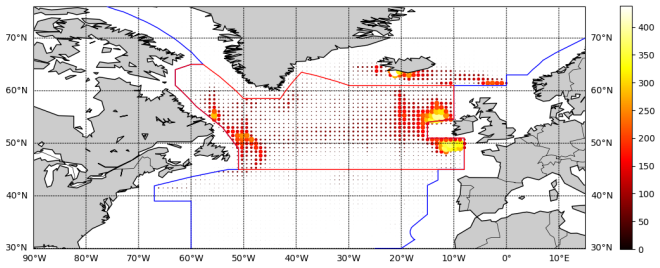

Fig. 4. Conflict locations for the AR scenario for the year of simulation.

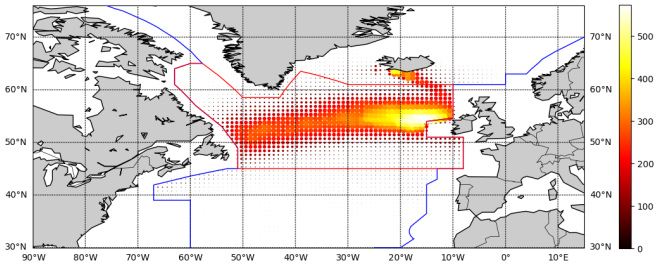

Fig. 5. Conflict locations for the DR scenario for the year of simulation.

TABLE II
Safety indicators for the total year of simulation.

	AR	DR
n_{Conf} [-]	70697	134500
n_{LoS} [-]	45586	100
IS_{max} [-]	1.00	2.66e-1

To get an overview of how the number of conflicts varies over different days, the spread of the daily count is displayed in Figure 6. As daily variations in network and wind are present, a valid comparison between AR and DR samples can only be made by comparing the paired daily differences. This is the difference box plot displayed in the figure and it shows that the DR scenario has a higher number of conflicts on average for all days over the simulated period. This difference in the number of conflicts is significant.

A closer look at the magnitude of the intrusion severity for DR is taken in Figure 7. The majority of the intrusions are well below the 1% limit. Although there are several intrusions (18) above this limit, there is a suspicion that these events can be considered as outliers.

It is of interest to see how the airspace safety behaves for

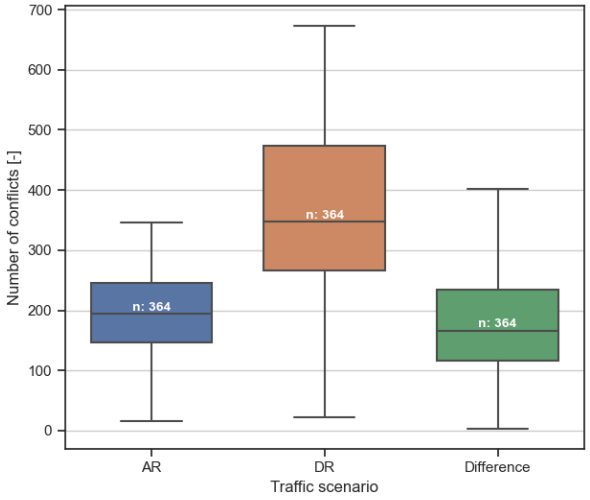

Fig. 6. The number of conflicts per day.

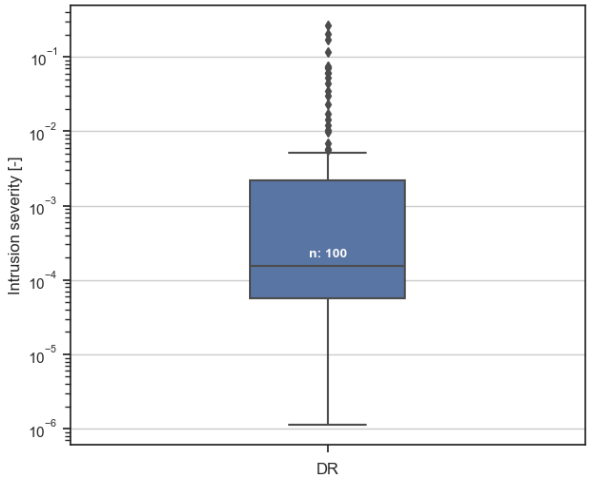

Fig. 7. The intrusion severity for all loss of separations in the DR scenario for the entire year on a logarithmic scale.

the forecasted traffic levels in the FR scenario. In Table III, it is shown that the number of conflicts and the number of LoSs increase. Also, the number of conflicts that result in a LoS is around the same order of magnitude. When looking at the maximum intrusion severity, it is higher for the FR scenario due to the increase in conflicts and LoSs. Out of the seven intrusions, three are only slightly above the 1% level. This indicates that the NAT airspace is not saturated for the FR scenario.

TABLE III
SAFETY INDICATORS FOR THE TOTAL OF THREE SELECTED DAYS.

	DR	FR
n_{Conf} [-]	1670	6549
n_{LoS} [-]	2	7
IS_{max} [-]	1.71e-4	6.84e-2

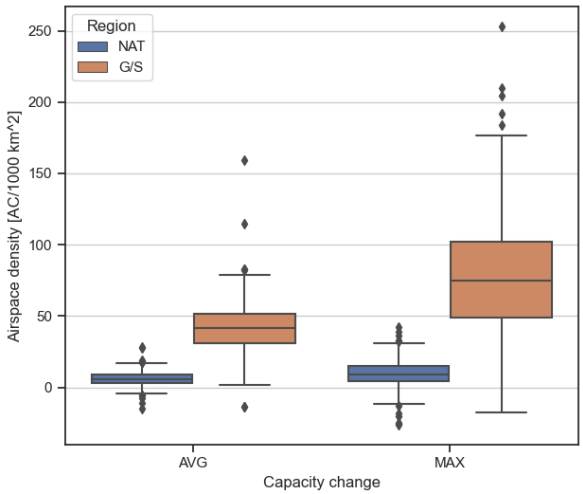

Fig. 8. Change in airspace density for the DR compared to the AR for the NAT and G/S areas, n=364.

B. Capacity

The change in capacity per day for the NAT and G/S areas is displayed in Figure 8. On average, the average and maximum airspace density for the NAT area increase due to an increase in average nominal flight path while the average and the maximum number of aircraft in this area slightly decreases. While a slight density increase for the NAT area is observed when moving to DR, the airspace density within the G/S areas increases more, this is mainly caused by an increase in average and maximum number of aircraft. This indicates that trajectory clusterization for the wind-optimal routes in the DR scenario occurs in these areas, Figure 4 and Figure 5 also support this presumption. The difference in average and maximum airspace density is significant for both the NAT and G/S areas.

The average and maximum traffic densities in the NAT and G/S areas for the DR and FR scenarios are stated in Table IV. Traffic levels are forecasted to increase by 85% in the FR scenario and so do the average traffic densities, approximately. Furthermore, the density ratios between the two areas are compared for the different scenarios. These ratios are susceptible to change over the scenarios if major changes in the network would occur when reassigning departure times whilst creating the FR scenario. As this is not the case, it appears that the FR scenarios represent an appropriate linear extrapolation of the DR network with increased traffic.

TABLE IV
CAPACITY INDICATORS FOR THE DR AND FR SCENARIOS.

	30 Jun 2019		**27 Jul 2019**		**28 Jul 2019**	
	DR	**FR**	**DR**	**FR**	**DR**	**FR**
$\rho_{avg,NAT}$ [-]	106.6	179.1	103.2	192.9	121.2	228.1
$\rho_{avg,G/S}$ [-]	251.5	393.4	206.9	378.2	263.7	424.6
$Ratio_{avg}$	0.42	0.46	0.50	0.51	0.46	0.54
$\rho_{max,NAT}$ [-]	219.1	368.0	227.5	373.1	230.8	420.3
$\rho_{max,G/S}$ [-]	588.0	944.2	555.6	828.1	586.5	944.4
$Ratio_{max}$	0.37	0.39	0.41	0.45	0.39	0.45

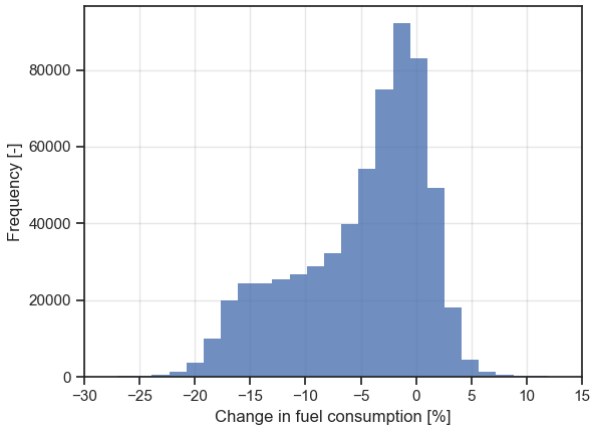

Fig. 9. Distribution of the change in fuel consumption for the DR compared to the AR scenario for all aircraft present in the year of flight data.

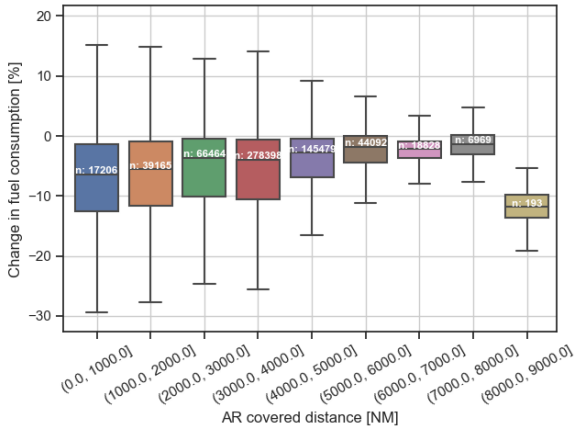

Fig. 10. Change in fuel consumption for different distance ranges.

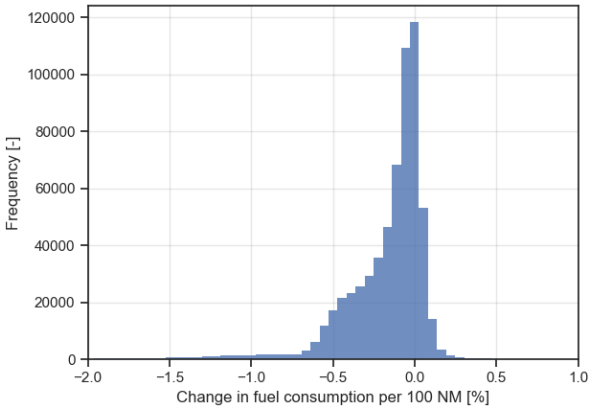

Fig. 11. Distribution of the change in fuel consumption corrected for the AR covered distance.

C. Efficiency

Now, the efficiency improvements in terms of fuel and time for the DR scenario compared to the AR scenario are presented. Both indicators are sampled on a paired basis and the changes in fuel and time are considered to be significant. The change in fuel consumption is the leading efficiency indicator and its distribution is presented in Figure 9. It can be noticed that the highest number of aircraft have a moderate decrease in fuel consumption and the distribution is skewed towards larger fuel savings. As there is a considerable amount of aircraft that experience an increase in fuel consumption, it is of interest to further analyze the results.

To do so, the distribution of the fuel consumption for different distance ranges is displayed in Figure 10. As distance can both decrease or increase for flying WOR, the distance range is taken to be that of the AR scenario. First, it is noticed that the flights that cover a relatively small distance manage to obtain the largest reduction in fuel consumption, apart from the largest distance bin. As WOR becomes beneficial over GCR for distances over 2000 NM, it can be said that the flights that cover a short distance are impacted the most by routing restrictions of the current airspace structure and have the largest optimization potential. Furthermore, it is noticed that the variance decreases for increasing distance. To remove the distance bias from the results, the change in fuel consumption per 100 NM flown is displayed in Figure 11. On average a 0.2% reduction in fuel can be obtained per 100 NM AR when shifting to the DR scenario. However, it is noticed that again an increase in fuel consumption occurs. This indicates that the optimization method indeed does not yield a global optimal trajectory.

The overall efficiency improvement is stated in Table V and a 2.7 tonnes fuel reduction, or a 8-minute flight reduction, on average can be established.

VI. Discussion

This study investigates the benefits of a decentralized, direct routing structure in the North Atlantic airspace. During this research, several simplifications and assumptions have been made. Their absolute effect on the model and the relative effect on the scenario comparison is discussed first. Then, the results of the experiment will be clarified and recommendations for future research are made.

A. Discussion on The Simplifications and Assumptions

The major simplifications and assumptions regarding the flight data, traffic scenario generation, and simulations are discussed here. It discusses the estimated impact on the outcome of the results as well.

1) The Effect of Incomplete and Unavailable Flight Data: According to the literature, at least 730,000 flights should be present in the data set. The data set for the research uses around 620,000 flights that cross the NAT in the simulations. This difference in flights has various reasons. First of all, there is no requirement regarding ADS-B equipment in the NAT. This influence is expected to be limited as these are required in North America and Europe. Then, not all trajectories are fully captured due to limited ADS-B coverage in remote areas. This could result in flights not being present in the data obtained by FR24 or not filtered correctly out of the

TABLE V
EFFICIENCY INDICATORS FOR THE TOTAL YEAR.

	Total Change	**Average Change**	**Relative Change**
Fuel	-1.7 Mt	-2.7 t	-5.1%
Flight time	-9.5 yr	-8.1 min	-1.9%

raw data. Also, Figure 3 shows the start of the COVID-19 pandemic reducing the number of flights. Furthermore, flights that cover a small difference are discarded from the data as these are deemed not representative. Whether a distance is small is determined by the optimization algorithm not being able to construct more than 4 trajectory points via backward propagation. Including more flights is expected to influence all performance indicators. However, the FR scenario shows that around 85% more flights can be handled and airspace is not saturated. Therefore, the approximately 15% of missing flights is not expected to have a large impact on the results.

Besides the missing flights in the data set, data on aircraft mass is unavailable as this is airline-specific information and contributes to their strategic advantages. The way the initial mass is estimated might result in modeling errors during the simulation phase. Aircraft get a mass assigned based on the maximum mass of the specific aircraft type and the covered GCR. If this mass is overestimated, aircraft are not able to climb to the FR24 altitude for some cases. This results in additional fuel consumption. For an underestimation of the initial mass, aircraft cruise at their designated altitude at lower mass, consuming less fuel. For the optimized trajectories, aircraft always cruise at their optimal altitude. Altogether, it is difficult to assess the impact of the mass on the results. However, keeping the initial mass constant for each flight over different scenarios minimizes the impact.

2) The Effect of Trajectory Simplification: All trajectories in the simulation scenarios are reduced with the use of the RDP line simplification algorithm to improve the simulation's computational performance. The impact on the model fidelity is analyzed by simulating a scenario with and without the line simplification for the AR and DR scenarios (no CD&R method is used). Several scenarios for the line simplification algorithm are created with arbitrarily chosen, varying distance dimension factors (ϵ) of 0.001, 0.0015, 0.002, and 0.005, resulting in a total of ten simulation scenarios. Additionally, the assumption that not including all climb and descent points for the DR scenario has a minor influence is validated, adding two more scenarios. The changes in fuel consumption are compared within and across the routing scenarios. Due to the large simulation time for the scenarios without line simplification the comparison is based on a single simulation day, 3 Apr 2019.

The results are stated per routing scenario in Table VI, Table VII. The differences are taken with respect to the scenario without line simplification. Furthermore, the Wilcoxon p-value is stated, indicating significant differences between the sample sets for all distance dimension factors. Hence, applying a trajectory simplification method is undesired as it will affect the fuel consumption results.

TABLE VI
CHANGES IN FUEL CONSUMPTION FOR AR SCENARIOS WITH VARYING DISTANCE DIMENSION FACTORS COMPARED TO NO SIMPLIFICATION.

ϵ	**0.001**	**0.0015**	**0.002**	**0.005**
Actual [tonnes]	-4.93e1	-7.42e1	-8.20e1	-1.13e2
Percentage [%]	-5.51e-2	-8.29e-2	-9.16e-2	-1.26e-1
p-value	0.0000	0.0000	0.0000	0.0000

TABLE VII
CHANGES IN FUEL CONSUMPTION FOR DR SCENARIOS WITH VARYING DISTANCE DIMENSION FACTORS COMPARED TO NO SIMPLIFICATION.

ϵ	**0.001**	**0.0015**	**0.002**	**0.005**
Actual [tonnes]	6.54e2	3.05e3	4.81e3	6.63e3
Percentage [%]	8.06e-1	3.75	5.92	8.16
p-value	0.0000	0.0000	0.0000	0.0000

TABLE VIII
CHANGES IN FUEL CONSUMPTION FOR DR SCENARIOS WITH VARYING DISTANCE DIMENSION FACTORS WITHOUT INCLUDING ALL CLIMB AND DESCENT POINTS COMPARED TO NO SIMPLIFICATION.

ϵ	**0.001**	**0.0015**
Actual [tonnes]	6.85e2	3.08e3
Percentage [%]	8.44e-1	3.80
p-value	0.0000	0.0000

It can be noticed that the fuel consumption reduces for the reduced AR scenarios, while the fuel consumption increases for the reduced DR scenarios. As aircraft fly their GCR between two waypoints in BlueSky, this supports the claim that the actual trajectories are inefficient as they get more efficient when waypoint requirements are relaxed. Vice versa, the expectation of the wind-optimal trajectories being optimal is supported by the fact that the fuel consumption increases when waypoint requirements are relaxed. The divergence of fuel consumption for reduced scenarios makes it of interest to compare the fuel benefits for the different scenarios with equal distance dimension factor Table IX. Furthermore, not including all climb and descent points for the DR has indeed a limited impact for the selected 0.0015 distance dimension factor Table VIII.

TABLE IX
CHANGES IN FUEL CONSUMPTION FOR DR VS. AR SCENARIOS FOR EQUAL DISTANCE DIMENSION FACTORS.

ϵ	**None**	**0.001**	**0.0015**	**0.002**	**0.005**
Actual [tonnes]	-8.17e3	-7.47e3	-5.05e3	-3.29e3	-1.45e3
Percentage [%]	-9.15	-8.37	-5.67	-3.69	-1.62
p-value	0.0000	0.0000	0.0000	0.0000	0.0000

Analyzing the RDP across the routing scenarios shows that the changes in fuel consumption differ significantly, this time it is desired as it compares the AR with the DR scenario. The differences in fuel consumption decrease for increasing distance dimension factors, which is undesirable as this indicates a loss of the explanatory power of the model compared to the

no reduction scenarios. However, this loss is accepted to get a computationally feasible model that validates the benefits of a DR routing structure considering seasonal effects.

3) The Effect of Neglecting SUA in Direct Routing: It should be noted that the AR scenarios already take divergences into account to avoid conflicts/special use airspace (although potentially crossing them in the simulation due to the route simplification), while the DR and FR scenarios do not. Including SUA in the DR and FR would most likely increase the fuel burn as deviations from the optimum trajectory have to be implemented to avoid these areas. The ordered upwind algorithm for horizontal optimization is suited for such applications as it allows for obstacle avoidance by penalizing passage through these areas through adjustment of the speed of the wavefront.

4) The Effect of Different Weather Models: This research uses two different reanalysis data sources of which the differences are assumed to be negligible. This assumption is assessed by making a comparison for a subset of three random days (3 Apr 2019, 19 Jul 2019, and 12 Jan 2020). The grid dimensions for this comparison are set to the extraction region including a margin (170W, 90N, 90E, 10S) with a sparsity of 1x1 degree and pressure levels 100-800 hPa (50 hPa increment). The RMSE for the two wind components is 2.55 m/s for the eastward component u and 2.63 for the northward component v, suggesting a noticeable difference between the two sources. Therefore, six traffic scenarios based on the three previously mentioned days are constructed, an AR and DR one. All six are simulated with two different wind models in BlueSky, yielding a total of 12 simulation scenarios. Based on the differences in fuel consumption for the scenarios, presented in Table X, it is concluded that the assumption of negligible differences between the reanalysis is valid and they can be used interchangeably in the BlueSky simulator.

TABLE X
PERCENTAGE DIFFERENCE IN OVERALL FUEL CONSUMPTION FOR SCENARIOS WITH DIFFERENT REANALYSIS DATA SOURCE (ECMWF/GFS).

	3 Apr	**19 Jul**	**12 Jan**
AR	1.43e-2	3.19e-2	1.76e-2
DR	6.65e-3	1.29e-3	1.01e-2

One disadvantage of the GFS reanalysis data is that data for some days is missing. Using the two different sources results in a situation where trajectories are optimized for wind with the proper reanalysis data, while the scenarios are simulated in BlueSky in absence of the data. The DR and FR scenarios are optimized for wind and, therefore, are expected to be impacted slightly more than the AR scenario. Altogether, 102 out of 2928 files are missing and all scenarios miss the same data, thus the impact is considered to be negligible.

5) The effect of Time Shifts: All required time shifts and their magnitude are computed for the three days with the highest traffic levels. On average 125 time shifts per day are used for the initial deconfliction and their count is displayed inFigure 12. Although this number of shifts is severe, the magnitude is low and the influence on the overall simulation is considered to be negligible.

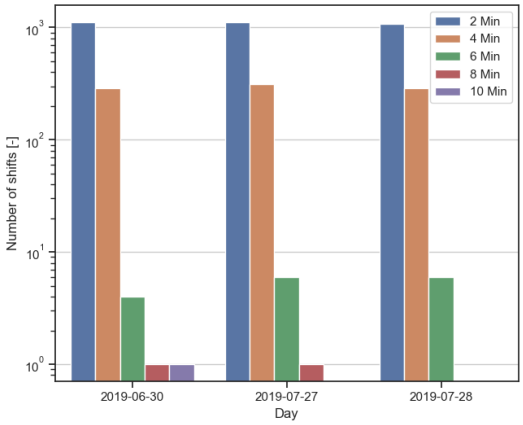

Fig. 12. The initial deconfliction time shift intensity count on a logarithmic scale.

B. Discussion on The Experiment Results

When analyzing the fuel consumption for both the AR and DR scenarios, it is noticed that there are cases for which the fuel consumption increases when flying WOR. It should be emphasized that the decoupling of the vertical and horizontal trajectory optimization methods does not guarantee a global optimum. When an actual trajectory already flies a near-optimal route, it could be the case that the optimized trajectory does not improve (or even decreases) the fuel consumption. A reduction of efficiency could also occur when aircraft do not fly at their reference altitude and a large, disadvantageous wind gradient is present at that location. Besides this, a disadvantage of the grid creation model has been detected of which the impact increases when flights cover shorter distances as they become more sensitive to ”detours” near the origin. The grid positioning around the origin heavily impacts the value function of the expanding front in this region. As the grid positioning is random, a bias in an arbitrary direction may appear here and the ”detour” arises when following the characteristic. This becomes more imminent for short-distance flights and such a situation is displayed in Figure 13). The other side of the spectrum contains flights for which the fuel increase is substantial due to polluted FR24 data of which the majority has been removed from the data during the filtering process. However, not all flights have been filtered out, resulting in cases like displayed in Figure 14.

The impact of both edge cases on the results is expected to be relatively small as the latter is easily detected as an outlier while the first has a small impact due to its short distance. No change in the number of LoSs is detected when outlier trajectories are removed and the change in efficiency is small. No direct effect on the airspace capacity can be derived but it is assumed to be negligible as the number of impacted flights is small.

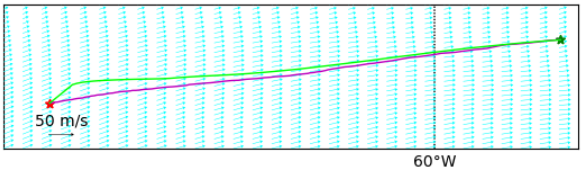

Fig. 13. Example of short distance flight where the actual trajectory (magenta) covers a more efficient route than the optimized one (lime).

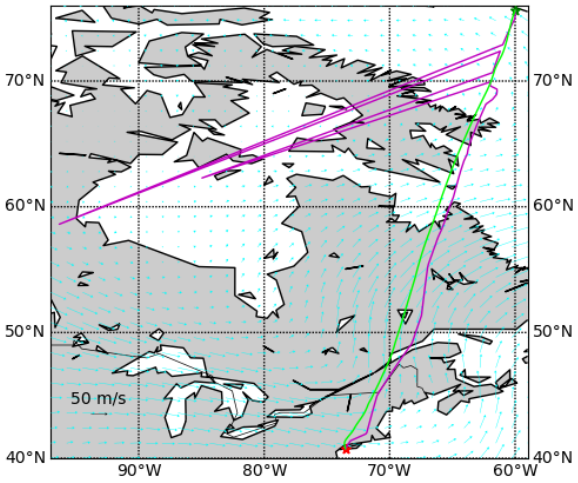

Fig. 14. Actual (magenta) and optimized (lime) trajectories with polluted actual trajectory data.

C. Recommendations

Overall, the DR scenario performed better than the AR scenario and the DR scenario showed to be robust for forecasted increases in traffic levels. The assumptions made for this research influence the results up to some extent and some recommendations are made to improve the overall model fidelity.

A major step in improving the model can be accomplished by taking SUA into account for the DR and FR scenarios. Currently, model bias likely arises as SUA are incorporated in the AR scenario up to some extent. Another feature that could increase the model fidelity is including ADS-B noise. Real-life ADS-B data contains position noise and viable decentralized airspace can only be obtained when noise does not result in additional LoSs. Also, performing simulations in BlueSky with turbulence potentially reduces the number of LoSs and maximum intrusion severity as this avoids certain ambiguous edge cases with the MVP algorithm. The same is likely to be accomplished when simulating with ADS-B noise. Additionally, previous research shows that incorporating ADS-B noise has a minor effect on the MVP safety performance [41]. Therefore, adding noise to the simulation could be the additional step that proves that implementing a decentralized, wind-optimal routing structure in the North Atlantic region could be accomplished without a single safety violation.

Besides increasing the model fidelity, it could be of interest to research the integration of free-routing airspace with ATC. As free-routing airspace is likely to be implemented stage-wise as regions near airports are heavily constrained, a smooth transition should be guaranteed. One way to research this is by taking airport location and orientation into account in the simulation.

Furthermore, improvements in the wind-optimal routing algorithms can be researched. Potentially, algorithms that produce global optimums yield even greater fuel reduction. Another approach could be to take the specific location (including altitude) of jet streams into account and take advantage of these.

VII. Conclusion

This article presents the findings of a study investigating the benefits of a decentralized, wind-optimal routing structure in the North Atlantic airspace for a year of flight data. It addresses the routing inefficiencies imposed by the current organized tracks systems routing structure. This research aims to show that optimizing trajectories under the influence of winds while solving conflicts in a decentralized way results in a reduction of flight time and emissions while preserving safe airspace operations. Also, it researches the robustness of the airspace to forecasted traffic growth. Two simulation setups have been constructed to do so.

An initial simulation experiment has been conducted to compare the actual routes to wind-optimal routes after both have been reduced with a line simplification algorithm. The modified voltage potential conflict resolution method is used for self-separation by solving conflicts tactically. Flying wind-optimal routes has no significant influence on the airspace capacity, although an increase of capacity in the Gander and Shanwick flight information regions indicates a clusterization of trajectories. Nevertheless, the number of severe loss of separations (18 with an intrusion severity above 1%) over the one-year simulation period is small and the result shows to be promising as the most severe intrusion still assures 734 ft vertical and/or 3.67 NM horizontal separation. On average, a 5.1% fuel reduction or 1.9% time reduction has been established for the new routing structure, yielding significant savings for this busy oceanic airspace.

Additionally, a second simulation to research the robustness of the wind-optimal routing structure has been generated. The future routing scenario is constructed by adding dummy flights to the simulation based on the current network. As a result, the airspace density scales roughly linearly with the number of flights added to the simulation. No indications of the airspace being saturated are deducted as the number of conflicts that result in a loss of separation remain approximately constant and only three loss of separations that slightly exceed the 1% limit are encountered. Overall, the future network is prone to several uncertainties including but not limited to demographics, governance, innovations, and customer demand. Only limited conclusions for the future direct routing structure can be drawn as it is merely an extrapolation of the current circumstances.

Altogether, this research shows that the implementation of a wind-optimal, decentralized routing structure in the North Atlantic airspace is a promising structure to increase efficiency while maintaining safe separations. It shows the industry that a short-term reduction of fuel and operational costs can be accomplished by just operational improvements.

REFERENCES

[1] O. Rodionova, M. Sbihi, D. Delahaye, and M. Mongeau, "Optimization of aicraft trajectories in north atlantic oceanic airspace," 2012.

[2] E. A. Irvine, B. J. Hoskins, K. P. Shine, R. W. Lunnon, and C. Froemming, "Characterizing north atlantic weather patterns for climate-optimal aircraft routing," *Meteorological Applications*, vol. 20, no. 1, pp. 80–93, 2013.

[3] ICAO, *North Atlantic Operations and Airspace Manual*. International Civil Aviation Organisation, 92522 Neuilly-sur-Seine CEDEX, France, 1 ed., Jan 2020.

[4] B. Sridhar, N. Y. Chen, K. N. Hok, O. Rodionova, D. Delahaye, and F. Linke, "Strategic planning of efficient oceanic flights," 2015.

[5] N. SPG, *NAT Systems Planning Group - Appendix M NAT Traffic Forecast*. ICAO, EUR/NAT Office, 55 ed., 2019.

[6] S. Gössling and A. Humpe, "The global scale, distribution and growth of aviation: Implications for climate change," *Global Environmental Change*, vol. 65, p. 102194, 2020.

[7] J. M. Hoekstra, R. N. van Gent, and R. C. Ruigrok, "Designing for safety: The 'free flight' air traffic management concept," *Reliability Engineering & System Safety*, vol. 75, no. 2, pp. 215–232, 2002.

[8] L. Jacolin and R. Stengel, "Evaluation of a cooperative air traffic management model using principled negotiation between intelligent agents," in *Guidance, Navigation, and Control Conference and Exhibit*, p. 4103, 1998.

[9] O. Rodionova, M. Sbihi, D. Delahaye, and M. Mongeau, "North atlantic aircraft trajectory optimization," *IEEE Transactions on Intelligent Transportation Systems*, vol. 15, no. 5, pp. 2202–2212, 2014.

[10] O. Rodionova, D. Delahaye, B. Sridhar, and H. K. Ng, "Deconflicting wind-optimal aircraft trajectories in north atlantic oceanic airspace," 2016.

[11] O. Rodionova, B. Sridhar, and H. K. Ng, "Conflict resolution for wind-optimal aircraft trajectories in north atlantic oceanic airspace with wind uncertainties," in *2016 IEEE/AIAA 35th Digital Avionics Systems Conference (DASC)*, pp. 1–10, IEEE, 2016.

[12] M. Hagström and A. Lennartsson, "Aircraft navigation," *Encyclopedia of Aerospace Engineering*, 2010.

[13] ICAO, *Regional Supplementary Procedures*. International Civil Aviation Organisation, 999 University Street, Montréal, Quebec, Canada, 5 ed., 2008.

[14] P. Koch, H. Wernli, and H. C. Davies, "An event-based jet-stream climatology and typology," *International Journal of Climatology: A Journal of the Royal Meteorological Society*, vol. 26, no. 3, pp. 283–301, 2006.

[15] H. David, *Conflict-free Direct Routing in European Airspace*. Eurocontrol, 91222 Bretigny-Sur-Orge Cedex, France, report no, 308 ed., 1997.

[16] M. S. Eby, "A self-organizational approach for resolving air traffic conflicts.," *The Lincoln Laboratory Journal*, 1994.

[17] S. Magill, "Effect of direct routing on air traffic control capacity," *2nd USA/Europe Air Traffic Management R&D Seminar*, 1998.

[18] M. R. Jardin, "Analytical relationships between conflict counts and air-traffic density," *Journal of guidance, control, and dynamics*, vol. 28, no. 6, pp. 1150–1156, 2005.

[19] K. Bilimoria, K. Sheth, H. Lee, and S. Grabbe, "Performance evaluation of airborne separation assurance in free flight," *AIAA Guidance, Navigation and Control Conference*, 2000.

[20] E. Sunil, J. Hoekstra, J. Ellerbroek, F. Bussink, A. Vidosavljevic, D. Delahaye, and R. Aalmoes, "The influence of traffic structure on airspace capacity," 2016.

[21] H. Q. Lee and K. D. Bilimoria, "Properties of air traffic conflicts for free and structured routing," in *AIAA Guidance, Navigation, and Control Conference and Exhibit*, p. 4051, 2001.

[22] J. Hoekstra, R. Van Gent, and R. Ruigrok, "Conceptual design of free flight with airborne separation assurance," p. 4239, 1998.

[23] M. Ribeiro, J. Ellerbroek, and J. Hoekstra, "Review of conflict resolution methods for manned and unmanned aviation," *Aerospace*, vol. 7, no. 6, p. 79, 2020.

[24] W. Schaberg, "A decentralized recovery method for air traffic conflicts," 2020.

[25] E. M. Rantanen, J. Yang, and S. Yin, "Comparison of pilots' and controllers' conflict resolution maneuver preferences," in *Proceedings of the Human Factors and Ergonomics Society Annual Meeting*, vol. 50, pp. 16–19, Sage Publications Sage CA: Los Angeles, CA, 2006.

[26] C. A. Wells, P. D. Williams, N. K. Nichols, D. Kalise, and I. Poll, "Reducing transatlantic flight emissions by fuel-optimised routing," 2021.

[27] H. K. Ng, B. Sridhar, and S. Grabbe, "A practical approach for optimizing aircraft trajectories in winds," in *2012 IEEE/AIAA 31st Digital Avionics Systems Conference (DASC)*, pp. 3D6–1, IEEE, 2012.

[28] J.-H. Kim, W. N. Chan, B. Sridhar, and R. D. Sharman, "Combined winds and turbulence prediction system for automated air-traffic management applications," *Journal of Applied Meteorology and Climatology*, vol. 54, no. 4, pp. 766–784, 2015.

[29] M. R. Jardin and A. E. Bryson Jr, "Neighboring optimal aircraft guidance in winds," *Journal of Guidance, Control, and Dynamics*, vol. 24, no. 4, pp. 710–715, 2001.

[30] E. E. Centre, *User Manual for the Base of Aircraft Data (BADA) Revision 3.12*. Eurocontrol, Centre de Bois des Bordes, B.P. 15, F-91222 Bretigny-sur-Orge CEDEX France, 3.12 ed., 2014.

[31] F. Cheng and J. Gulding, "Computing wind-optimal routes for flight performance benchmarking," in *16th AIAA Aviation Technology, Integration, and Operations Conference*, p. 4361, 2016.

[32] B. Girardet, L. Lapasset, D. Delahaye, C. Rabut, and Y. Brenier, "Generating optimal aircraft trajectories with respect to weather conditions," 2013.

[33] B. Girardet, L. Lapasset, D. Delahaye, and C. Rabut, "Wind-optimal path planning: Application to aircraft trajectories," in *2014 13th International Conference on Control Automation Robotics & Vision (ICARCV)*, pp. 1403–1408, IEEE, 2014.

[34] J. P. Snyder, "Map projections-a working manual," 1987.

[35] J. M. Hoekstra and J. Ellerbroek, "Bluesky atc simulator project: An open data and open source approach," in *Proceedings of the 7th International Conference on Research in Air Transportation*, vol. 131, p. 132, FAA/Eurocontrol USA/Europe, 2016.

[36] I. Metz, J. Hoekstra, J. Ellerbroek, and D. Kügler, "Aircraft performance for open air traffic simulations," in *AIAA Modeling and Simulation Technologies Conference*, p. 3522, 2016.

[37] J. Sun, J. Ellerbroek, and J. Hoekstra, "Flight extraction and phase identification for large automatic dependent surveillance–broadcast datasets," *Journal of Aerospace Information Systems*, vol. 14, no. 10, pp. 566–572, 2017.

[38] F. Wilcoxon, "Individual comparisons by ranking methods," *Biometrics Bulletin*, vol. 1, pp. 80–83, 1945.

[39] R. B. d'Agostino, "An omnibus test of normality for moderate and large size samples," *Biometrika*, vol. 58, no. 2, pp. 341–348, 1971.

[40] R. D'AGOSTINO and E. S. Pearson, "Tests for departure from normality.," *Biometrika*, vol. 60, no. 3, pp. 613–622, 1973.

[41] T. Langejan, E. Sunil, J. Ellerbroek, and J. Hoekstra, "Effect of ads-b characteristics on airborne conflict detection and resolution," *6th SESAR Innovation Days (SID)*, 2016.

Part II

Appendices

Appendix A

Conflict Detection and Resolution Experiment

A conflict detection and resolution experiment is conducted to determine what resolution domain and settings are preferred for this research. The experiment is twofold as first the best performing resolution domain is selected before deciding on the appropriate resolution settings in BlueSky. This experiment uses the same DR scenario with optimized and simplified trajectories as specified previously. It is conducted on a reduced data set of three randomly selected days with variations in the day of week and time of year. The data of 3 April 2019, 19 July 2019, and 12 January 2020 is used. No statistical tests are performed on the safety and stability results due to the low statistical power when only including three data points.

A-1 Resolution Domain

On a tactical level, conflicts can be avoided by performing a maneuver in the vertical (climb/descent), lateral (turn), and longitudinal (speed) direction, [11]. In general, pilots have a preference for solving conflicts in the vertical domain due to the rapid result (shape of the protected zone with a 5NM radius and 1000 ft altitude) and lower cognitive workload. Previous work has shown that airspace with a high traffic density remains manageable for a direct routing structure in combination with the MVP algorithm. The goal of this experiment is to see how the MVP behaves for different resolution domains under the wind-optimal routing structure in the North Atlantic airspace. The aim is to find the most fuel-efficient resolution domain while maintaining safe separation and stability. Furthermore, the results are used to determine if a strategic deconfliction method is required. It is expected that the vertical resolution domain gives the best performance in terms of efficiency, safety, and stability due to the shape of the PZ and no strategic deconfliction method is required.

All indicators for the different performance criteria, apart from the airspace stability, have been discussed. Solving conflicts could result in secondary conflicts that destabilize the airspace, especially in high traffic densities. Therefore, the stability of the airspace is assessed by the number of secondary conflicts. This is measured by the Domino Effect Parameter (DEP) as described in Equation 5-2. $S1$ presents the set of all conflicts without resolution and $S2$ the set of conflicts with resolution, for identical scenarios. The three regions in the Venn diagram, displayed in Figure 5-1, can be identified as the stabilizing effect ($R1$), the common conflicts ($R2$), and the destabilizing effect ($R3$) [1, 12].

$$DEP = \frac{R3 - R1}{S1} = \frac{S2}{S1} - 1 \tag{A-1}$$

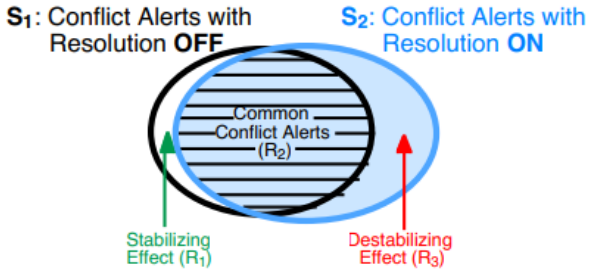

Figure A-1: Venn diagram of the DEP [1].

The research domains that will be researched are the vertical, lateral, and horizontal ones. The vertical resolution domain allows for an altitude action by changing the vertical speed, the lateral domain allows for a heading change only, and the horizontal domain allows for both a speed and heading change. This results in three simulation scenarios with the resolution method set to either domain. For each simulation, the number of conflicts, losses of separation, intrusion severity, and fuel consumption are logged. To determine the Domino Effect Parameter (DEP), a fourth scenario is created without any conflict resolution method resulting in 4 scenarios per day (12 simulations). All but the fuel consumption are computed for just the North Atlantic region as well, as these parameters are not representative outside the NAT due to the absence of other traffic. The conflict detection parameters are set to a protected zone radius of 5 NM, altitude of 1000 ft, a look-ahead time of 300 seconds. A resolution factor of 1.05 is used in BlueSky. Furthermore, initial masses are kept constant for each aircraft.

The simulation is conducted with the use of the BlueSky Air Traffic Management (ATM) simulator. One day of traffic built-up is used in advance to guarantee representative traffic levels during the eastbound OTS hours. The safety and stability results are logged and compared over a 24 hour period for the NAT region only, starting after the traffic built-up. The fuel consumption is logged over a 72 hour (day-1, day considered, day+1) period and the fuel consumption is compared for the entire trajectory for all flights that are present in the simulation on the considered day.

The results of the experiment are stated in Table A-1, Table A-2, and Table A-3. Although only the NAT region is considered to be of interest (stated within brackets),

the performance indicators in the whole simulation region are indicated as well to be able to identify potential modeling errors. First, the performance indicators for the entire simulation region are assessed. When looking at the number of conflicts, it can be seen that these increase when a resolution method is put into place for most cases. The lateral domain has the worst stability performance, while the vertical and horizontal perform better. For the first and third day, the number of conflicts even decrease when using a vertical or horizontal resolution method. Generally, the horizontal resolution domain results in the least amounts of losses of separations and the lowest intrusion severity. When considering the fuel consumption difference for the different resolution domains compared to the no resolution domain, all differences are considered to be significant according to the Wilcoxon signed-rank test, with no resolution as the base case. Overall, the fuel consumption increases when using a resolution method as aircraft have to diverge from their local optimal trajectory to avoid a conflict.

A more detailed overview of the changes in fuel consumption for the different resolution domains compared to the no resolution scenario is displayed in Figure A-2. This shows that the vertical resolution domain has strong variations in fuel consumption in both directions due to the independence of wind on the vertical optimization domain. The lateral and horizontal domains show more moderate variations, predominantly in the positive direction (with exception of some outliers). The frequent decreases in fuel consumption when applying a vertical resolution domain once more confirms that the trajectories are not optimized globally. When diverting vertically, an aircraft ends up at a non-optimal altitude for the aircraft's performance characteristics. However, more beneficial winds at that altitude could compensate for that, or even decrease the fuel consumption.

When only considering the performance indicators (except for the fuel consumption) within the North Atlantic region, it is noticed that no noteworthy losses of separation occur when using the horizontal resolution domain. No clear effect can be deducted from the changes in the number of conflicts and the DEP for the specific region.

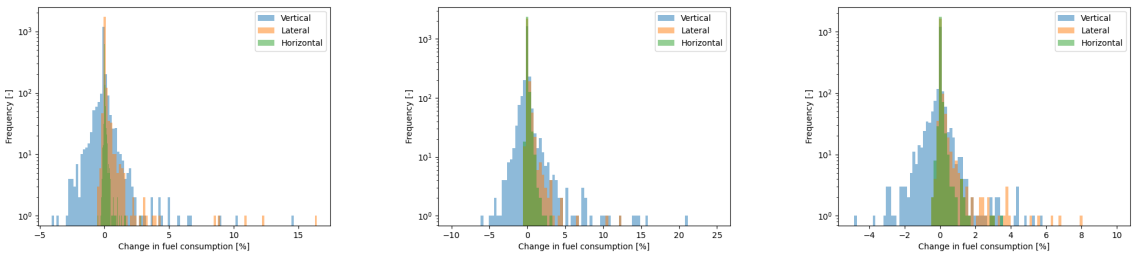

(a) Percentage change for 3 Apr 2019. **(b)** Percentage change for 19 Jul 2019. **(c)** Percentage change for 12 Jan 2020.

Figure A-2: Percentage change in fuel consumption for the vertical, lateral, and horizontal resolution domain compared to the no resolution case on a logarithmic scale.

Although the horizontal resolution domain does not have the best fuel efficiency, the overall separation safety is of such importance that this is concluded to be the preferred resolution domain for this research. The tactical resolution method has satisfactory

Table A-1: Performance indicators per resolution domain for the entire (NAT) simulation region, 3 April 2019.

	None	**Vertical**	**Lateral**	**Horizontal**
n_{Conf} [-]	1869 (683)	1853 (581)	3474 (1200)	1786 (602)
n_{LoS} [-]	506 (222)	2 (0)	6 (5)	1 (0)
IS_{max} [-]	0.937 (0.911)	0.289 (-)	0.179 (0.179)	0.075 (-)
DEP [-]	- (-)	-8.56e-3 (-1.49e-1)	8.59e-1 (7.57e-1)	-4.44e-2 (-1.19e-1)
m_f [t] (p-value)	1.070e5	1.070e5 (0.0000)	1.071e5 (0.0000)	1.071e5 (0.0000)

Table A-2: Performance indicators per resolution domain for the entire (NAT) simulation region, 19 July 2019.

	None	**Vertical**	**Lateral**	**Horizontal**
n_{Conf} [-]	2246 (705)	2293 (587)	4997 (2140)	2264 (657)
n_{LoS} [-]	597 (233)	0 (0)	21 (9)	2 (0)
IS_{max} [-]	0.983 (0.945)	- (-)	0.295 (0.150)	0.040 (-)
DEP [-]	- (-)	2.09e-2 (-1.67e-1)	1.22 (2.04)	8.01e-3 (-6.81e-2)
m_f [t] (p-value)	1.278e5	1.279e5 (0.0000)	1.280e5 (0.0000)	1.279e5 (0.0000)

Table A-3: Performance indicators per resolution domain for the entire (NAT) simulation region, 12 January 2020.

	None	**Vertical**	**Lateral**	**Horizontal**
n_{Conf} [-]	1340 (427)	1181 (328)	2690 (927)	1257 (366)
n_{LoS} [-]	389 (162)	2 (0)	12 (8)	0 (0)
IS_{max} [-]	0.946 (0.934)	0.242 (-)	0.253 (0.253)	- (-)
DEP [-]	- (-)	-1.19e-1 (-2.32e-1)	1.01 (1.17)	-6.19e-2 (-1.43e-1)
m_f [t] (p-value)	1.018e5	1.018e5 (0.0000)	1.019e5 (0.0000)	1.019e5 (0.0000)

results and no strategic deconfliction method (apart from the initial deconfliction for BlueSky spawning purposes) will be implemented.

A-2 BlueSky Resolution Factor

In the BlueSky Air Traffic Management simulator, a resolution factor in both the horizontal and vertical domain can be set for the MVP. This resolution factor increases the radius and height of the protected zone for the resolution method only (leaving that of the detection method intact) and can be seen as a safety margin for the required velocity actions. A safety margin might be desired due to round-off errors, response inertia (due to the simulation time step-ASAS update interval differences), turbulence & ADS-B noise, and aircraft dynamics. However, increasing the resolution factor results in fuel consumption inefficiencies and possibly affects the resolution capability of the MVP algorithm in high-density airspace.

To research the influence of this parameter, the optimized trajectories with previously selected trajectory simplification and resolution domain methods are simulated. The standard resolution factor of 1.05 is compared to resolution factors of 1.10, 1.15, and

1.20. Both the horizontal and vertical resolution factors are kept equal. The DEP is not evaluated as no representative scenario without conflict resolution is simulated. The significance of the difference in fuel consumption is determined with the standard resolution as the base case.

Table A-4: Performance indicators for different resolution factors for the entire (NAT) simulation region at April 3rd 2019.

	1.05 (Standard)	**1.10**	**1.15**	**1.20**
n_{Conf} [-]	1786 (602)	1651 (567)	1580 (560)	1538 (523)
n_{LoS} [-]	1 (0)	0 (0)	2 (0)	1 (0)
IS_{max} [-]	0.074 (-)	- (-)	0.118 (-)	0.029 (-)
m_f [t] (p-value)	1.120e5	1.120e5 (0.0008)	1.120e5 (0.0000)	1.120e5 (0.0000)

Table A-5: Performance indicators for different resolution factors for the entire (NAT) simulation region at July 19th 2019.

	1.05 (Standard)	**1.10**	**1.15**	**1.20**
n_{Conf} [-]	2264 (657)	2195 (645)	2084 (632)	1975 (579)
n_{LoS} [-]	2 (0)	0 (0)	1 (1)	0 (0)
IS_{max} [-]	0.040 (-)	- (-)	0.000 (0.000)	- (-)
m_f [t] (p-value)	1.319e5	1.319e5 (0.0000)	1.319e5 (0.0000)	1.319e5 (0.0000)

Table A-6: Performance indicators for different resolution factors for the entire (NAT) simulation region at January 12th 2020.

	1.05 (Standard)	**1.10**	**1.15**	**1.20**
n_{Conf} [-]	1257 (366)	1185 (336)	1159 (325)	1108 (323)
n_{LoS} [-]	0 (0)	1 (0)	1 (0)	1 (0)
IS_{max} [-]	- (-)	0.048 (-)	0.055 (-)	0.044 (-)
m_f [t] (p-value)	1.052e5	1.052e5 (0.0000)	1.052e5 (0.0000)	1.052e5 (0.0000)

When going over the results, it is noticed that the resolution factor has very little impact on the overall routing efficiency (fuel consumed). Furthermore, the number of conflicts decreases for increasing resolution factor. All cases have a LoS with a severe intrusion severity. Only looking at the North Atlantic region (the region of interest for LoSs), all resolutions factors appear to perform sufficiently when looking at the intrusion severity. Therefore, the standard resolution factor of 1.05 is used for the conflict resolution method in BlueSky.

Appendix B

Trajectory Simplification

This appendix precedes *the effect of the trajectory simplification* in the discussion. It elaborates upon different trajectory simplification methods that are tested to reduce the number of waypoints passed to BlueSky and speed up the simulation process. First, the simplified trajectories (both the actual and optimized scenarios) are compared to the no simplification scenario. Then, the difference between the actual and optimized equivalents is analyzed. This comparison only uses data of April 3rd, 2019 due to the large simulation time of the no simplification scenarios.

First, multiple scenarios are constructed from different trajectory simplification algorithms, with the base scenario being the no simplification one. A promising line simplification method is the Ramer-Douglas-Peucker (RDP) algorithm[1]. This method is applied in multiple setups with a variation in flight phase incorporation. The first is the 3D Ramer-Douglas-Peucker (RDP) algorithm on the lat/lon/alt dimensions with distance dimension ϵ set to 0.001, including every waypoint identified within the climb or descent phase. Then, a similar approach is taken without incorporating every climb or descent waypoint. The latter is solely done for the optimized trajectories as these follow the BlueSky climb and descent logic and are expected to be influenced less by the absence of these waypoints. At last, a simplification method with a threshold function is used with thresholds lat/lon=0.5 deg, alt=500 ft, CAS=10 kts.

The actual and percentage difference in fuel consumption between the base scenario and the other scenarios for the actual and optimized trajectories are stated in Table B-1 and Table B-2, respectively. These are compared to see which simplification method approaches the base scenario best and to see how the fuel consumption changes for different scenarios. Then, the actual and optimized equivalent scenarios are compared and stated in Table B-3 to decide which method most accurately approaches the differences between the actual and optimized base scenarios. It is tested if the differences between the samples are significant at the 5% significance level. The p-value is stated in the tables.

[1] https://github.com/mourner/simplify-js.git, Oct 2021

Table B-1: Changes in fuel consumption for the AR scenario simplification methods compared to the no simplification scenario.

Method	RDP	Threshold
Actual [tonnes]	-4.94e1	-9.49e1
Percentage [%]	-5.51e-2	-1.06e-1
p-value	0.0000	0.0000

Table B-2: Changes in fuel consumption for the DR scenario simplification methods compared to the no simplification scenario.

Method	RDP	RDP No CL/DE	Threshold
Actual [tonnes]	6.55e2	6.86e2	2.73e2
Percentage [%]	8.05e-1	8.43e-1	3.36e-1
p-value	0.0000	0.0000	0.0000

Looking at the results of the tables above, it can be seen that the fuel consumption of the simplified trajectories differs significantly from that of the no simplification scenarios. Hence, applying a scenario simplification method is undesired as it will affect the fuel consumption results. Out of the used methods, the threshold simplification method appears to perform better on average than the RDP simplification method in terms of fuel consumption. The effects of including all climb and descent waypoints for the RDP simplified optimized trajectories has little effect, as expected, due to the BlueSky climb and descent logic.

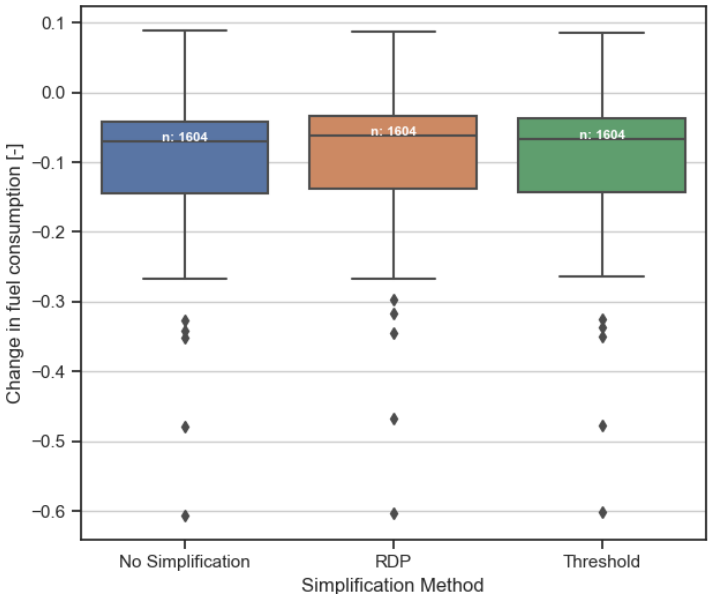

Figure B-1: Change in fuel consumption for the optimized vs actual trajectory pairs.

First, the difference per flight is researched for the different simplification methods in Figure B-1. Looking at the no simplification case, possible outliers are detected outside the lower whisker and a closer look is taken at these flights. All flights out of

the lower whisker turn out to contain polluted data, these outliers are removed from the data. With the outliers removed and negative improvements assessed, the overall improvements in fuel consumption are stated in Table B-3.

Table B-3: Changes in fuel consumption for DR vs. AR scenarios for equivalent simplification methods.

	None	**RDP**	**Threshold**
Actual difference [tonnes]	-8.17e3	-7.47e3	-7.80e3
Percent difference [%]	-9.15	-8.37	-8.75
Wilcoxon p-value	0.000	0.0000	0.0000

When assessing these differences in Table B-3 it can be seen that by flying wind-optimal routes the total fuel consumption can be reduced by 9.15%. For all simplification methods, the change in fuel consumption is significantly different. It can again be noticed that the threshold simplification method performs slightly better than the RDP method. However, the simulation time of the base scenarios is such that an extensive simplification is needed to keep the simulation of a year of flight data feasible. As the RDP significantly cuts down on simulation time compared to the threshold simplification and it only further changes the results by 0.38 percent point, the RDP simplification method is selected.

Appendix C

Scenario File Example

An example of a scenario file to load flights in BlueSky is presented in this appendix. Some remarks about the scenario file:

- The conflict detection parameters are already defined in BlueSky and are not required to be re-stated.
- The SETMASS and LOGMASS commands are part of the performance logger and become available when calling this logger.
- The first waypoint has to restate the creation location of the aircraft. This is due to an irregularity in BlueSky that makes it difficult to perform proper initial deconfliction, namely: Flights that have a first waypoint altitude higher than their creation altitude start at their first waypoint altitude, while flights that have a first waypoint altitude lower than their creation altitude start at their creation altitude.
- The speed should be indicated in either the CAS [kts] or the Mach number depending on the altitude (above or below Mach transition altitude).
- No DEST is defined, instead, a DEL command is included at the last waypoint to avoid out of area descent when near-destination resolutions cause path deviations.

Command lines of scenario file	**Explanation**
# Set simulation parameters for flights	Header for simulation settings
00:00:00.00>DATE 3, 4, 2019	Start of simulation (day, month, year)
00:00:00.00>TRAILS OFF	Turn off trails
00:00:00.00>SWRAD LABEL	Hide aircraft labels
00:00:00.00>SWRAD VOR	Hide navigation beacons
00:00:00.00>SWRAD APT	Hide airports
# Conflict resolution	Header for CD&R settings
00:00:00.00>NOISE ON	Turn on turbulence and ADS-B noise
00:00:00.00>CDMETHOD CStateBased	Define CD method
00:00:00.00>RESO MVP	Define CR method
00:00:00.00>RMETHH ON	Define CR domain
# Plugins	Header to load plugins
00:00:00.00>AREA 14.0, -166.0, 90.0, 86.0, 60000, 1500	Define deletion area (lat, lon, lat, lon, alt, alt)
00:00:00.00>PLUGINS LOAD PERFLOG	Load performance logger
00:00:00.00>PLUGINS LOAD WINDGFS	Load wind field data plugin
00:00:00.00>IMPL WINDSIM WINDGFS	Implement wind plugin in simulation
00:00:00.00>WINDGFS 15.00, -165.00, 90.00, 85.00, 2019, 4, 3, 0	Define wind plugin area (lat, lat, lon, lon) and starting time (year, month, day, hour)
00:00:00.00>FF	Fast forward the simulation
# Create flights and start simulation	Header for trajectory loading
00:00:00.00>CRE 537253102, B744, 44.818, -66.1589, 38.0, 37025.0, 0.84	Create aircraft (type, lat, lon, hdg, alt, spd)
00:00:00.00>SETMASS 537253102, 374855	Set initial mass (AC ID, mass [kg])
00:00:00.00>ADDWPT 537253102, 44.818, -66.1589, 37025.0, 0.84	Add initial waypoint (AC ID, lat, lon, alt, spd), equal to create location
00:00:00.00>ADDWPT 537253102, 45.0982, -65.853, 33952.0, 0.84	Add waypoint (AC ID, lat, lon, alt, spd)
⋮	Add multiple intermediate waypoints
00:00:00.00>ADDWPT 537253102, 51.6259, -0.5096, 7740.0, 310.0	Add final wypt (AC ID, lat, lon, alt, spd)
00:00:00.00>LNAV 537253102 ON	Turn on lateral navigation of AC
00:00:00.00>VNAV 537253102 ON	Turn on vertical navigation of AC
00:00:00.00>AT 537253102, 537253102036 DO LOGMASS 537253102	Log mass of AC at waypoint X (AC ID, AC ID + wypt, cmd, AC ID)
00:00:00.00>AT 537253102, 537253102036 DO DEL 537253102	Delete AC at waypoint X (AC ID, AC ID + wypt, cmd, AC ID)

Table C-1: Scenario file example

Appendix D

Wind Model Comparison

Two different reanalysis data sources are used for this research. Here, the results for the comparison between the two models are presented.

	RMSE East-comp (u) [m/s]			**RMSE North-comp (v) [m/s]**		
Time of day	**3 Apr**	**19 Jul**	**12 Jan**	**3 Apr**	**19 Jul**	**12 Jan**
00:00	2.2621	1.8718	2.1419	2.1563	1.8207	2.0307
03:00	3.3217	2.6281	3.4847	3.4757	2.7023	3.7885
06:00	2.1099	1.9199	2.1257	2.0103	1.8768	1.9927
09:00	3.2311	2.5612	3.4026	3.4554	2.6690	3.6261
12:00	1.9300	1.9700	2.0881	1.9088	2.0103	1.9774
15:00	3.0991	2.5836	3.3737	3.4220	2.7547	3.5798
18:00	1.8695	2.1221	2.0202	1.8563	2.2231	1.9306
21:00	3.0131	2.6897	3.3255	3.3779	2.8480	3.5276

Table D-1: RMSE for the East- and Northward wind components for the analyzed region, described by (170W, 90N, 90E, 10S) with a sparsity of 1x1 degree and pressure levels 100-800 hPa (50 hPa increment).

	3 Apr	**19 Jul**	**12 Jan**
Actual scenarios	1.43e-2	3.19e-2	1.76e-2
Optimized scenarios	6.65e-3	1.29e-3	1.01e-2

Table D-2: Percentage difference in overall fuel consumption for BlueSky simulation scenarios with different reanalysis data source (ECMWF/GFS).

Appendix E

BlueSky Adjustments

This appendix describes the noteworthy modifications and actions that have been taken to BlueSky and the MVP algorithm to reduce the number of edge cases that lead to conflicts and losses of separations. Small adjustments are not discussed but can be found in GitHub[1]. The modifications are discussed per BlueSky module.

Modified Voltage Potential module (mvp.py)

Incorporation of the 2 criteria recovery method.

A new function is implemented in the MVP algorithm to determine if the recovery phase of a conflict can be started. The old method is based on passing the closest point of approach. The new 2 criteria method is based on two intruder states, the one at the start of the conflict and the current state. This method is implemented in line with the findings in W. Schaberg's thesis [13].

Added a VS stop when aircraft are climbing/descending in each other's PZ.

Aircraft that are within each other's horizontal PZ but not in each other's vertical PZ were at risk of loss of separation due to autopilot behavior at waypoints. For instance, when an aircraft at a lower altitude starts to climb due to the next waypoint constraint, it climbs directly into the other aircraft's vertical PZ causing a LoS. In general, this behavior is adequately captured in the MVP algorithm, except for the case that one or more aircraft are at/near their maximum altitude and have no/little more room to climb. One way to avoid this is by taking a margin into account when setting the optimal cruise altitude. However, due to the BlueSky fastest possible climb/descent logic, this approach gets complex when few waypoints are present. The next waypoint altitude could be higher than the maximum altitude for the current mass, resulting in the aircraft still flying at maximum altitude. The preferred solution is to determine if a conflict pair is within their horizontal PZ and potentially within their vertical PZ at the next time step. The latter is calculated based on the vertical speed and altitude of both the ownship and intruder and ASAS time step.

[1] git@github.com:ninyes/bluesky.git

Generalized the performance limits check.
The performance limits are now set with the use of the bs.traf.perf.limits function which has an implementation in both the OpenAP and BADA performance files. The old implementation contained an error as the ground speed is capped by a minimum and maximum calibrated airspeed and is not suitable for the BADA performance implementation. As the capped performance returns a true airspeed and no ground speed is required for the remainder of the MVP, the true airspeed is returned. Not incorporating winds in the return speed results in incompatibility with other CR modules. However, applying multiple GS/TAS and TAS/GS conversions resulted in singularities at some often encountered angles in North Atlantic flight. This results in losses of separations when one or more aircraft are near their maximum velocity and the aircraft that has to slow down by a velocity delta computed by MVP is slowed down less due to the singularities. Simply increasing the resolution factor did not solve this issue. The improvement of the model performance of the chosen solution is preferred over the decrease in modularity of the CR implementation.

Autopilot or Airborne Separation Assurance Systems module (aporasas.py)

Removed GS/TAS conversion.
In line with the issue addressed above, the conversion from ground speed to true airspeed when wind fields are incorporated is removed from this module.

BADA Performance module (perfbada.py)

Changed the Mach number input to calculate the performance limits.
The Mach number input of the calclimits function was simply the current Mach number taken from bs.traf.M. When this number was slightly above the limit set by MMO (Maximum Mach Operating speed), for instance, caused by an altitude change, the velocity would automatically be set to the MMO. Even if the desired velocity by MVP was well below this number, leaving no room for a velocity decrease in conflict resolution. Therefore, this input is changed to a function of the current ownship altitude and the desired true airspeed (given by either the AP or ASAS).

Part III

Preliminary Report

Chapter 1

Introduction

Ever-growing customer demand and an increasing incentive to reduce aviation climate impact challenge the sectors' current standards. One way aviation impacts the environment is by in-flight emissions. The North Atlantic corridor contributes 6.5% of total aviation emissions, of which 97% are above an altitude of 7 km [14]. The International Civil Aviation Organization (ICAO) expects traffic in the North Atlantic region to almost double in the coming twenty years, making the problem even more imminent. Besides this significant contribution to emissions, flights crossing the North Atlantic region are structure by the Organized Track System, also known as "highways in the sky" to guarantee safe separation. This system has emerged due to Air Traffic Control (ATC) limitations in remote areas and facilitates inefficient routing [15]. Two ways to reduce emissions are either by technological advancements or operational improvements. The latter yields the highest short-term benefits and is promising for the North Atlantic region.

Previous research addressing inefficiencies in the North Atlantic region mainly focuses on adjusting the structure of the tracks by decreasing separation standards and/or allow for along-track rerouting [16]. Furthermore, research has focused on investigating the benefits of wind-optimal routing combined with a strategic deconflicting method [17]. General research on airspace restructuring often focuses on introducing the free flight concept [7] as this provides a safe and efficient airspace structure. As surveillance, communication, and navigation methods have improved over the past years, the free-flight concept has become viable. With aviation expected to grow and sector densities to increase, the workload of the Air Traffic Controller (ATCo) will increase. Free flight shifts control from ATC to the flight deck, reducing this workload and Air Traffic Management (ATM) costs. This shift allows for maximizing behavior instead of satisficing behavior [18], improving the overall efficiency.

This research will look into possible operational improvements by allowing free flight in the North Atlantic region. It will investigate the benefits of wind-optimal routing in the North Atlantic airspace by implementing a decentralized, direct routing structure.

Crucial for the feasibility of the free flight principle in the North Atlantic area is self-separation assurance. A system has to be implemented to allow for safe separation. Furthermore, the efficiency of the trajectories above the North Atlantic should be improved by allowing for optimization on the individual level. Flying the shortest distance does not guarantee time- or fuel-optimal trajectories, and an optimization strategy has to be selected to make overall routing more efficient.

A thorough review of the relevant literature is conducted. This provides background information on routing structures in the North Atlantic region. First, an overview is given on how the current airspace structure in general, and particularly in the North Atlantic region, has emerged. This also includes further elaboration upon the concepts of free flight and direct routing. Then, an overview of common conflict detection and resolution methods is presented. A difference between strategic and tactical methods is made. Furthermore, the issue of trajectory optimization is addressed. At last, different ways to assess the airspace performance are addressed. Based on the literature study, a thesis framework and methodology are composed along with some concluding remarks.

Chapter 2

Airspace

Aviation is a heavily regulated transportation sector with a major focus on safety. It is therefore of importance to have a thorough understanding of the current systems and structures before these can be challenged with new concepts. This chapter elaborates upon the relevant airspace concepts.

First, the current airspace structure is explained by discussing the history, the current layout, and the role of Air Traffic Control (ATC). Then, special attention is paid to the structure of the North Atlantic corridor connecting Europe and North America. At last, the concept of free flight/direct routing is elaborated upon.

2-1 Airspace Structure

This section explains the current day airspace and its layout. First, its emergence is discussed and the different sectors of the airspace are elaborated upon to establish a general overview of the role of ATC. After this, special attention is paid to the North Atlantic region and oceanic airspace in general.

2-1-1 History

In the early days of aviation, navigation was performed similar to naval navigation, with maps and compasses. After traffic increased, a more structured way of coordinating and planning became necessary [19] to handle the complex situation and safely separate aircraft. This resulted in a centralized control approach through ATC. This approach was made possible with the emergence of more advanced navigation systems, such as radar and navigation beacons. The increased intervention of ATC reduced the freedom of pilots to fly their preferred routes as they had to fly predefined routes. These routes consist of a series of waypoints. To assure safe separation and smooth airport services by the human controllers the airspace is structured into layers and sectors.

2-1-2 Airspace Layout and The Role of Air Traffic Control

A broader overview of the sectors and layers is established to understand how ATC is connected with these areas. The sectors and layers are discussed in a top-down manner.

The first layer broadly divides the airspace into navigational regions that divide the world into eight zones, Figure 2-1. These regions are divided in such a way for regulatory purposes as each region requires its supplementary procedures stated in [2]. For this research, the North American Region (NAM), North Atlantic Region (NAT), European Region (EUR) are considered to be most interesting. Besides these, the Caribbean Region (CAR) and Middle East Region (MID) might be of interest.

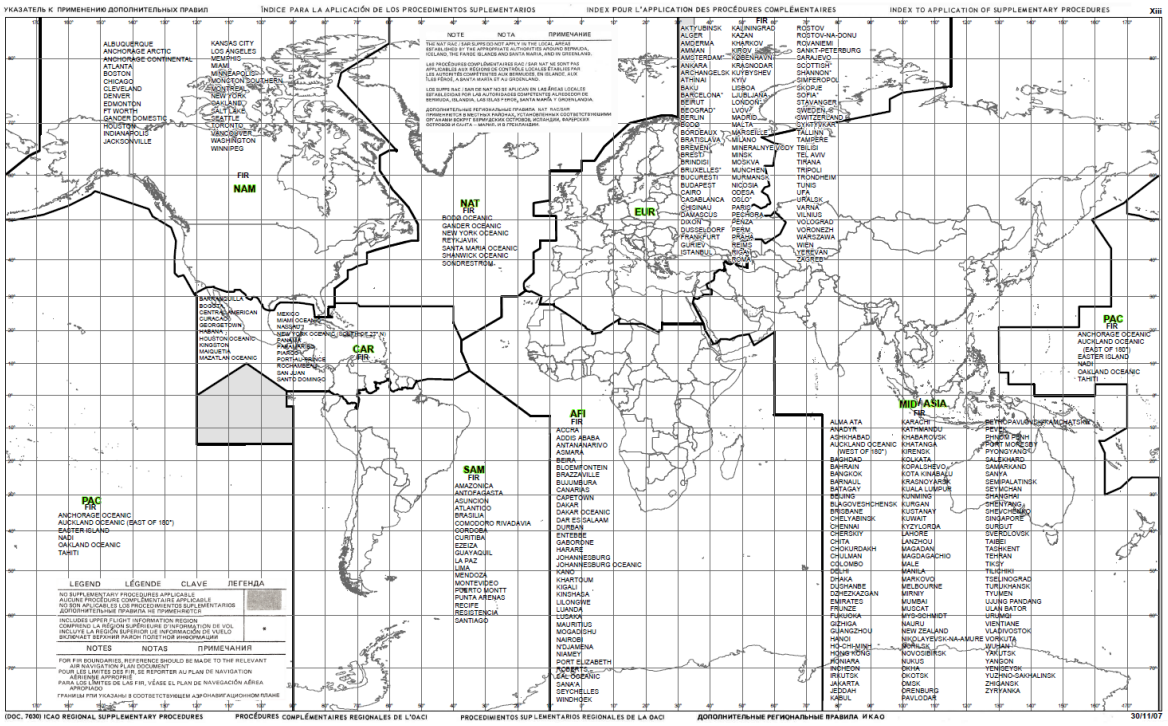

Figure 2-1: The navigation regions with their flight information regions according to ICAO [2].

Each navigational region is divided into a multitude of Flight Information Region (FIR) [2] [3] due to politics (countries like to control their airspace), technology (radar has limited coverage), and governance (Air Traffic Services (ATS)/ATC have the resources to only serve a limited region). The FIRs are mostly shaped by a countries borders, but not limited to this as countries might share a FIR and large countries may have multiple FIRs. As this thesis mainly targets the NAT, its FIRs are displayed in Figure 2-2. The FIR is divided into controlled, uncontrolled, and special-use airspace of which the first require ATC.

The traffic in the controlled areas is guided by several ATC entities. Looking at Figure 2-3, it can be seen that the airspace is divided into an upper and lower airspace. As traffic usually is less complex in the upper airspace, Upper Airspace Control (UAC) might control the upper airspace over multiple FIRs. The overall role of UAC is to

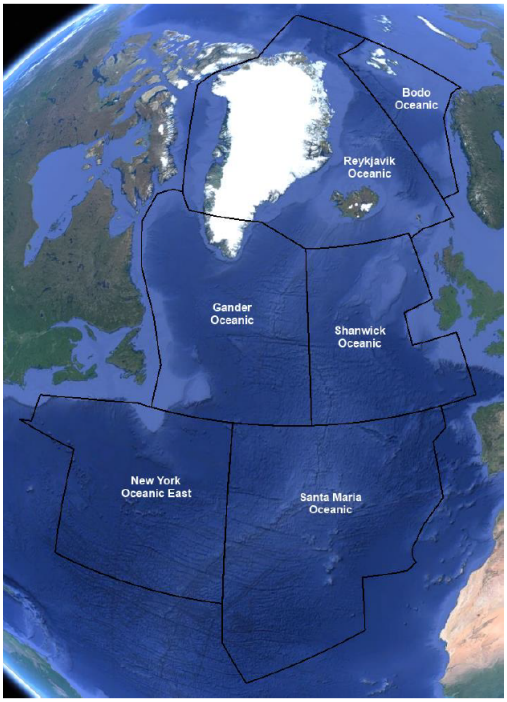

Figure 2-2: The high level airspace flight information regions in the North Atlantic navigation region [3].

safely separate aircraft and perform en-route guidance from sector entry to sector exit.

When having a closer look at the controlled FIR lower airspace, it can be seen that this can be divided into Control Areas (CTA), Terminal Control Area (TMA), and Control Zones (CTR) which are usually located around airports. The CTA is controlled by Area Control (ACC), the TMA is controlled by Approach Control (APP) and the CTR is controlled by Tower Control (TWR). The task of these controllers is to safely separate aircraft and perform the guidance around the airport in an efficient manner. Routes around airports can be divided into Standard Instrument Departures (SID) and Standard Arrival Routes (STAR) which connect the en-route to the terminal phase. These routes are predefined to reduce the controller workload and comply with noise regulations around airports and they depend on weather and runway conditions.

At last, there are regions indicated as Special Use Airspace (SUA). Commercial flights in these regions might be restricted or prohibited. The reasons vary from noise constraints for cities to military reasons like war zones. These areas cause inefficiencies as aircraft have to take a detour and/or the airspace gets congested.

As mentioned in subsection 2-1-1, over the years more structures have been put to place for ATC to deal with the complexity. It holds for all areas mentioned above that aircraft have to obey ATC orders unless there is an imminent danger appointed by the prevention systems Traffic Alert and Collision Avoidance System (TCAS). This has come at the cost of overall efficiency as aircraft can not use their most optimal route in most cases.

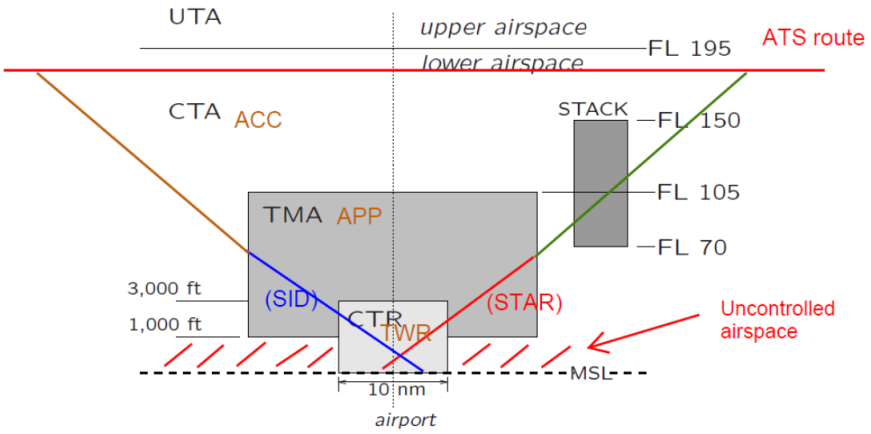

Figure 2-3: The controlled airspace structure in the FIR around airports [4].

All these air services have to be paid for. Therefore, each entity charges a fee to each aircraft passing based on its flown distance and weight. Some airlines base their strategic advantage on reducing these costs as they fly to cheaper airspace. Of course, this could affect the overall fuel consumption and its corresponding emissions.

Overall it can be beneficial to get rid of ATC in some sectors to increase the airspace capacity [20]. This can be achieved by using modern-day technology. It can be argued that the decoupled ATC structure might be beneficial when implementing the direct routing principle in a single sector, as it can be nicely integrated into the other existing ATC entities without modifying them. This gives a conceptual perspective for the implementation in the short run.

2-1-3 North Atlantic Track System

The airspace of special interest is the North Atlantic region. This airspace is the busiest oceanic airspace in the world connecting Europe and North America [21]. In 2017, approximately 730,000 aircraft crossed the North Atlantic. Most areas above the Atlantic are remote areas which make Direct Controller Pilot Communications (DCPC) and ATS surveillance unavailable, [3]. To assure safe separation, a different system was created that is called the Organized Track System (OTS). These tracks assure reduced vertical separation throughout the ICAO NAT (1000 ft), longitudinal separation is defined by clock minutes and there is a standard lateral separation distance of 60 NM, which is one degree latitude. Most aircraft fly within the economically viable FL290-410 region, therefore the flight levels associated with the OTS are FL310 to FL400, [2] [16].

The routes which the aircraft crossing this region follow are predefined. These tracks support a westbound flow departing from Europe in the US morning (day flight) and eastbound flow departing from the US in the US evening (night flight). This results from time zone differences, passenger demand, and airport noise restrictions. There are several constraints to the capacity of the airspace: the horizontal separation distance, vertical separation distance, and a limited economical height band (FL310-400). A

system of organized tracks is constructed to accommodate as many flights as possible. Minimum time tracks are established to accommodate as many flights as possible within the major flows (pressure systems and jet streams). There is a day-to-day variation of the weather phenomena and flight plans, hence, a day-to-day variation of the tracks. This changing system is what is called the OTS. An example of the location on the map and a textual example are displayed in Figure 2-4 and Figure 2-5, respectively. Deviation from the OTS is possible if a flight remains clear of OTS and ATC makes sure that these flights do not interfere, which can lead to substantial deviations. About half of all flights crossing the North Atlantic follow the NAT-OTS [3] (8.1.7).

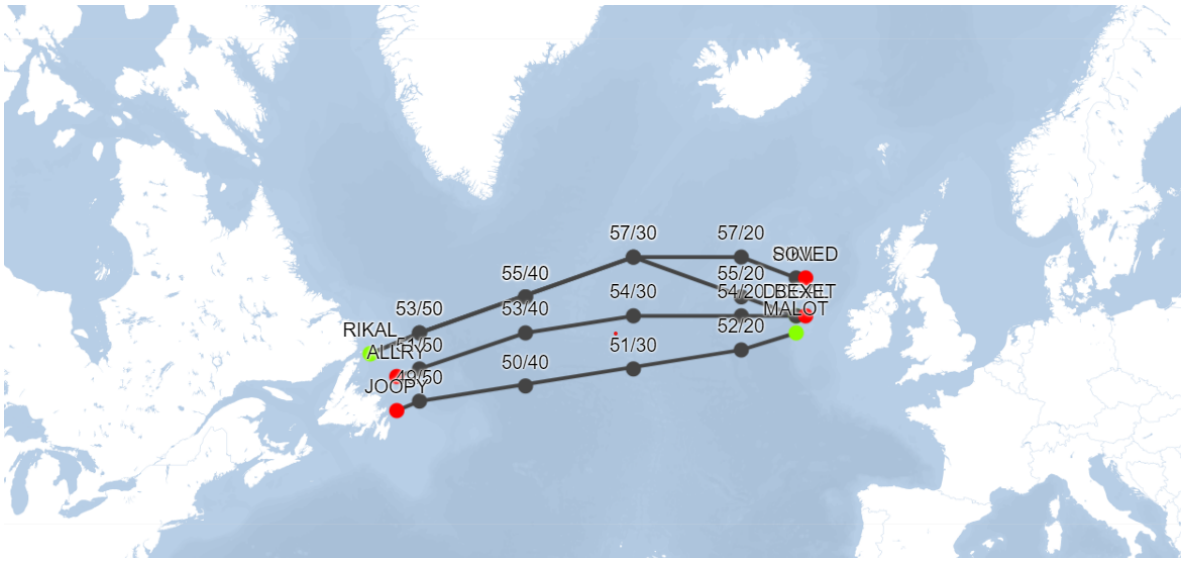

Figure 2-4: North Atlantic Organized Track System (NAT-OTS) locations for 5 and 6 Jan 2021 displayed on a map[1].

Track	Valid From	Valid To	Route	East Levels	West Levels
A	04 Jan 1130 UTC	04 Jan 1900 UTC	DOGAL 54/20 54/30 53/40 51/50 ALLRY		350 370 390
A	05 Jan 1130 UTC	05 Jan 1900 UTC	MALOT 52/20 51/30 50/40 49/50 JOOPY		350 370 390
Z	06 Jan 0100 UTC	06 Jan 0800 UTC	RIKAL 53/50 55/40 57/30 55/20 DOGAL BEXET	320 340 360 380 400	
Z	05 Jan 0100 UTC	05 Jan 0800 UTC	RIKAL 53/50 55/40 57/30 57/20 PIKIL SOVED	320 340 360 380 400	

Figure 2-5: Textual NAT-OTS location information for 5 and 6 Jan 2021[1].

As mentioned above, the OTS is constructed based on airlines' preferred routes (distributed as Preferred Route Message (PRM)) and stays clear of SUA. All these individually filed routes take weather systems into account up to a certain extend (to their standards). Together, all flight plans are used to produce a basic minimum time track. The eastbound OTS is produced by Gander Oceanic Control and the westbound is produced by Shanwick Oceanic Control.

If justified by suspected traffic demand, additional tracks are established to connect EUR with CAR, the Iberian peninsula, and NAM. These can differ slightly from the core tracks. They may cross the OTS by Flight Level (FL) and do not always extend coast-out to coast-in. Additionally, there can be routing structures for flights arriving

[1] https://flightplandatabase.com/nav/tracks, Jan 2021.

and departing from Reykjavik airport. Route structures for flights between the Iberian peninsula and Northern Europe. Between the Azores and Portuguese mainland, and some more [3].

The NAT's are published as a Notice to Airman (NOTAM) according to Track Message Identification (TMI) (Julian calendar). It consists of an entry and exit waypoint, 4 intermediate coordinates, and multiple flight levels as can be seen in Figure 2-4 and Figure 2-5. Multiple tracks may be established during periods of high demand. These are labeled alphabetically, starting at A for the most southern westbound track and Z for the most northern eastbound track.

Future Traffic Forecast for the NAT region

According to the International Civil Aviation Organization (ICAO) [5], the peak week travel frequency above the North Atlantic will continue to grow in the coming decades with a predicted average of 2.9%. This projection is displayed in Figure 2-6 and the projected increase in North Atlantic Travel complements the incentive to look for a more efficient way for aviation above the North Atlantic. Note that the current COVID-19 setback is not taken into account in this forecast and the mid-term impact is still considered to be unknown. However, it is expected that aviation will bounce back based on previous crises [22].

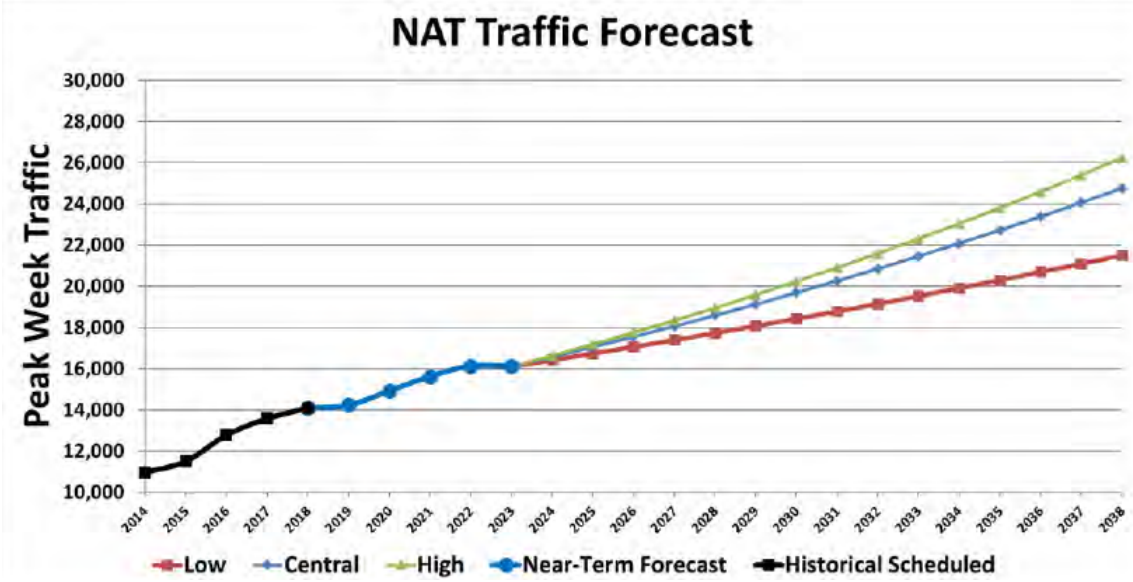

Figure 2-6: NAT peak week traffic forecast [5].

Future Structure of the NAT region

As the demand for the OTS is forecasted to increase, research is performed to increase the airspace capacity and reduce the overall flight time. The main areas of interest focus on either modification of the current OTS or airspace restructuring. Modification is mostly performed by reducing separation standards or implementing a rerouting

approach along the tracks, while restructuring focuses on new trajectory optimization and conflict resolution techniques to reduce the overall number of conflicts.

In [16], it is shown that the total flight duration and congestion level can be reduced within the current OTS framework. This is done by reducing the separation standards, allow for rerouting within the OTS, and taking oceanic winds into account. A similar approach with a different resolution method has been taken in [21].

Another approach outside the scope of the current OTS is taken in [17]. This approach uses wind-optimal trajectories to find individual optimal routes after which a strategic conflict resolution method is applied to reduce congestion clusters and obtain much less congested trajectory sets. This reduces the workload on the tactical conflict resolution stage. A similar approach that takes wind uncertainties into account is taken in [23].

2-1-4 Characteristics of the North-Atlantic Airspace

Altogether, some general characteristics relevant in the North Atlantic region can be stated. First, the weather-related characteristics are mentioned. Then, the routing characteristics are stated.

Weather Characteristics

As mentioned above, weather conditions impact the location of the OTS. In general, weather has a substantial impact on aviation. Think of the massive delays caused by thunderstorms, snowstorms, or volcanic eruptions and it becomes prevalent that weather can have a significant negative impact. However, weather can also positively impact aviation by designing routes that efficiently use tailwinds. Some of these weather systems are subjected to seasonal variations. Altogether, it can be said that aviation can benefit from a more thorough understanding of weather systems and the incorporation of weather data in trajectory prediction algorithms.

This research is particularly interested in the weather systems in the North Atlantic region. The polar jet stream plays a significant role in this region. The location of the jet stream differs over time and seasonal patterns can be witnessed, stronger and more south during winter and vice versa during summer [24]. The overall location of the jet stream justifies the westbound tracks being located more to the south and the eastbound tracks more to the north.

Routing Characteristics

First of all, aircraft operate at both cruise altitude and speed. This constrains the problem as any deviation from this optimum results in inefficiencies. Therefore, airlines prefer to operate under these conditions. Also, aircraft fly in a predefined track at constant altitude and speed in the current OTS. As aircraft lose weight, their altitude increases throughout the flight to remain in their optimal cruise condition. The urge to follow such tracks results in inefficiencies as at most a staged climb can be performed instead of a continuous climb. Furthermore, aircraft mainly fly in parallel along the

tracks due to their structure. Even if there are no tracks in place, aircraft are expected to mainly fly in near parallel. The conflicts are likely to be in the shallow angle region or head-on (large angle). This has to be taken into account when designing for conflict detection and resolution methods.

2-2 The Free Flight Concept

As mentioned in subsection 2-1-1, over the course of years aviation got more structured and has moved away from the free flight principle. Routes are determined by fixed waypoints to cope with centralized ATC. This structuring was especially necessary to safely separate aircraft in remote oceanic areas where very limited ATC coverage is available. However, more advanced navigation and commercial satellite navigation systems have emerged. Therefore, the possibility presents itself to shift control back from ATC to the flight deck to remove the limitations of Air Traffic Controller (ATCo) workload (capacity limit, ATC costs) and drastically reduce their numbers [25]. This sparked research into the field of free flight which shows that this concept can have several advantages over the fixed routing structure.

One of the advantages of free flight airspace is that the airspace capacity could be increased [26]. This can be explained by two mechanisms. The first is a result of the reduced flight time of aircraft. The second is caused by a more evenly spreading of aircraft throughout the airspace as they are not bounded by fixed structures anymore [20]. However, some research shows that free flight could decrease the airspace capacity for high levels of traffic density due to the conflict chain reaction property [27]. This possible drawback is a result of solving conflicts in an unstructured manner. Resolved conflicts cause one or multiple new conflicts and the system destabilizes [28].

Another major advantage is airspace efficiency. The free-flight concept brings great possibilities to the overall efficiency of aviation as aircraft have the freedom to optimize their vertical and horizontal flight trajectory so that they can fly their desired optimal routes [26]. This would mean greater full efficiency and a reduction in the overall flight time. When not just looking at free flight and fully structured routing, but at multiple levels of structuring, it can be said that there appears to be a negative correlation between the level of structuring and the overall efficiency [12]. However, the same principle mentioned for the airspace capacity holds. When traffic density levels become too high, the efficiency benefits can no longer be realized [27].

For the same reason that the airspace capacity increases for the free flight case, an increased spreading of flights, it can be argued that safety increases. When the number of conflicts of structured routing and free flight is compared, it can be said that free routing increases the safety as fewer conflicts are counted [12] [29]. Furthermore, the cockpit crew experiences the free-flight scenario as safer compared to the ATC situation on a subjective scale [7]. This lays an important foundation as the human perception in the cockpit of the free-flight concept is of utmost importance as control shifts in that direction. As safety is the primary concern in aviation, safe separation has to be guaranteed in the free-flight concept to make it implementable. With the use of

Automatic Dependent Surveillance-Broadcast (ADS-B) data, promising conflict detection and resolution methods have been developed which are discussed in Appendix 4.

Direct Routing

When the free flight concept emerges, commercial aircraft aim at flying their most optimal route in both the vertical and horizontal direction to reduce cost and flight time. This concept is called direct routing. The trajectory optimization part of the direct routing approach can be implemented in several ways discussed in Appendix 3.

Current initiatives that look into improving current airspace structures with the use of modern technologies as ADS-B are the Single European Sky ATM Research (SESAR) and its US counterpart, Next Generation Air Transportation System (NextGen). These initiatives look into implementing direct routing in parts of the airspace as well. Over the past couple of years free route airspace, that allows for direct routing, has been implemented in several parts of the European upper airspace and it has been proven to reduce the en-route flight distance according to Eurocontrol.

Chapter 3

Trajectory Optimization

Trajectory optimization for aviation is widely researched and believed to result in immediate, low-cost, low-risk, and significant fuel reductions [30]. These reductions are required to meet the set goal by International Civil Aviation Organization (ICAO) to improve the fuel efficiency of international aviation by 2% annually [31]. By shifting the responsibility of separation to the flight deck and work towards a decentralized airspace, opportunities to increase routing performance arise. This approach is promising for future implementation as airlines' and aircraft tend to seek for maximizing behavior to improve their competitive advantage [18].

This chapter discusses several trajectory optimization methods in multiple dimensions. Both general methods and methods specifically applied to the North Atlantic region in previous research are discussed. First, models to describe aircraft motion are discussed together with optimization objectives and optimization horizons. Then, optimization methods in the vertical and horizontal domains are elaborated upon.

3-1 Preliminaries

Before trajectory optimization methods are discussed in detail, some preliminaries are discussed. First, it is discussed how the dynamics of aircraft are modeled. Then, different optimization targets are elaborated upon before discussing the optimization horizon of the trajectories.

3-1-1 Aircraft Dynamics

The concept of flight trajectories is closely related to the dynamics of the body in aerial motion [32]. The models considered to describe these bodies are focused on fixed-wing aircraft. Two main models to describe aircraft dynamics are the rigid body and point-mass model. Rigid body models are fundamental for the study of transition maneuvers

and the analysis of dynamic stability and control. Therefore, they have been adopted in some trajectory optimization studies. In general, they are considered to be unsuitable for the trajectory calculations on medium to long time intervals due to the high number of states, the complexity of the problem and the sensitivity to numerical instabilities [33]. Point-mass models tend to perform better for trajectory calculations and these are discussed below.

For point-mass models, all aspects regarding rotational dynamics are discarded resulting in three degrees of freedom expressed along the coordinate axes of the body frame. Such models can involve either a constant or variable mass. As mass is considered to vary throughout the flight, the latter is stated in Equation 3-1. This model is taken from Springer Fundamentals of Airplane Flight Mechanics [34].

$$\begin{cases} \dot{v}_{lon} = \frac{g}{W}(T\cos\epsilon - D - W\sin\gamma) \\ \dot{\gamma} = \frac{g}{vW}\cdot[(T\sin\epsilon + L)\cos\mu - W\cos\gamma] \\ \dot{\chi} = \frac{g}{vW}\cdot\frac{(T\sin\epsilon+L)\sin\mu}{\cos\gamma} \\ \dot{\phi} = \frac{v\cos\gamma\sin\chi+v_{w_\varphi}}{R_E+z} \\ \dot{\theta} = \frac{v\cos\gamma\cos\chi+v_{w_\theta}}{(R_E+z)\cos\phi} \\ \dot{z} = v\sin\gamma + v_{w_z} \\ \dot{m} = -f \end{cases} \tag{3-1}$$

In these equations, the following variables for the angles are used. γ is the flight path angle [rad], χ is the track angle [rad], ϵ is the thrust angle of attack [rad], μ is the bank angle [rad]. These basic equations can be subjected to restrictions on the flight profile in the horizontal and/or vertical plane.

3-1-2 Optimization Objective

When optimizing an aircraft trajectory, the optimization objective has to be specified. This objective can consist of either a single or multiple elements. The objective is what the optimal trajectory minimizes for. Often used optimization objectives are regarding fuel/time/emissions minimization. A reduction in flight time implies a reduction in fuel consumption when flying at constant velocity [30], hence emissions are reduced. However, it is necessary to realize that fuel-optimized routes are not necessarily climate-optimized routes. Flying climate optimized routes could reduce North Atlantic aviation climate impact by 10% while increasing fuel consumption by 1%. When formulating a research goal, it is important to select the right optimization objective and set the right assumptions.

Furthermore, additional external factors that (in)directly pose restrictions on the objective can be incorporated. These factors are mostly weather and obstacle related. For instance, the presence of jet streams in the North Atlantic region could be taken into account. Convergence problems due to nonlinearities around these jet streams may arise and have to be accounted for [35]. Another design criteria could be to avoid convective areas to prevent turbulence causing an uncomfortable customer experience

and in extreme cases aircraft damage. These areas have been modeled and added to the cost function in previous research [36]. This shows that the timing of optimal trajectory diversion is of importance as it can be beneficial to wait for some time to divert from the Wind-Optimal Route (WOR) when weather information is more precise. At last, Special Use Airspace (SUA) could be incorporated in the model as these areas have to be avoided as well.

3-1-3 Optimization Horizon

Trajectories can be optimized at various stages before or during a flight. These stages are displayed in Figure 3-1 from far in advance (left) to final moment (right) [32].

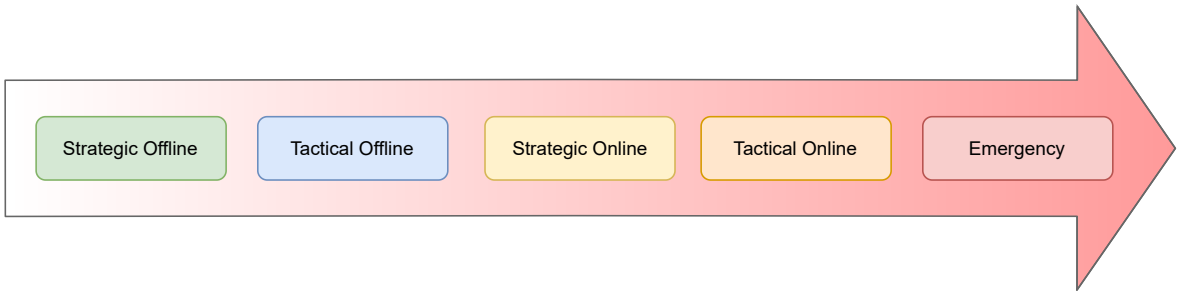

Figure 3-1: Chronological operational time frame for trajectory optimization methods.

The overall dominant trade-off for trajectory optimization methods in the strategic domain is the one between computational time and routing efficiency. Flights are susceptible to stochastic weather behavior and delays which are more difficult to capture far in advance. These uncertainties negatively affect the efficiency and result in sub-optimal trajectories. However, this longer available time allows for more computational time which could be used to employ more accurate methods in more extensive search domains, increasing the efficiency. In the tactical domain, uncertainties are of lesser concern, but solutions have to be calculated in (near) real-time, resulting in sub-optimal trajectories.

3-2 Trajectory Optimization Methods

Trajectory optimization can be performed in both the horizontal and vertical domain. Vertical optimization schemes are employed to determine optimal vertical profiles during the climb, cruise, and descent phase. Horizontal optimization is employed to determine optimal horizontal profiles in presence of weather and obstacles. These optimizations goals are considered to be weakly coupled [37] and often considered separately to reduce the overall model complexity and increase the computational performance. Optimization methods and general assumptions for the vertical and horizontal flight profile are discussed in subsection 3-2-1 and subsection 3-2-2, respectively.

The airspace in which trajectory optimization is performed can broadly be split into two parts. The first part is the region around the airports. As mentioned in subsection 2-1-2, trajectories in this area are mainly constraint by Standard Instrument Departures (SID) and Standard Arrival Routes (STAR). These routes are optimized based on runway orientation, noise requirements, flow management requirements, and surrounding obstacles. These routes are within the Terminal Control Area (TMA) which is anywhere between Mean Sea Level (MSL) to $\pm$10,000 ft. The second part is the Control Areas (CTA) and Upper Control Area (UTA) combined. These are the areas where trajectories are optimized based on the filed flight plans.

3-2-1 Vertical Flight Profile

Early research on trajectory optimization mainly targeted the vertical flight profile (altitude and speed) [32]. This vertical flight profile can be divided into three phases; climb, cruise, and descent. Each of the three phases requires a different optimization approach as described below. Vertical optimization is mainly a function of aircraft aerodynamics, engine performance, and vertical wind gradients [37]. For conventional jet aircraft, weight is not constant over time. Due to fuel consumption by the engines, aircraft weight decreases.

Climb and Descent

As mentioned above, the climb and descent phase below 10,000 ft are constraint by SID and STAR. Therefore, climb and descend operations above this altitude are considered.

First, climb operations are considered. Optimal climb can be considered for multiple optimization criteria; time, fuel, distance, and noise. Constructing vertical flight profiles based on the different criteria can be complex as they depend on weather conditions, individual aircraft performance, and initial weight. Most methods are based on the maximum energy state [38]. In reality, aircraft climb at constant Indicated Airspeed (IAS) during the first part and constant Mach number during the second part of the climb phase. This can be implemented with the use of the Base of Aircraft Data (BADA) model [10]. According to that, the climb phase above 10,000 ft can be split up into two parts; the part from 10,000 ft to the Mach transition altitude and the climb above the Mach transition altitude. One should keep in mind that climbing with constant IAS results in an increasing True Airspeed (TAS).

Now looking at descend operations, different optimality conditions can be considered. Time optimal descend is capped by structural limitations, while fuel optimal descend is limited by the gliding performance. Emission and noise optimality is fairly similar to fuel optimality as engines are operated in idle conditions. Both ends of the spectrum are somewhat unrealistic optimization conditions and require aircraft-specific knowledge. An equal approach as described above can be taken for the descend phase with the use of the BADA model. Descend is split up into two parts for altitudes above 10,000 ft by the Mach transition altitude.

Cruise Flight

The cruise phase makes up a large part of the total fuel consumption for long-haul flights crossing the Atlantic. This means savings in fuel consumption during cruise lead to high overall savings. Jet aircraft can have several design strategies for the cruise phase; maximum endurance (minimum fuel flow), maximum range, and minimum fuel for a given range (maximize the specific range). In general, the maximum specific range is obtained by keeping airspeed constant while weight decreases. Therefore, altitude increases during cruise flight. In practice, this results in a step climb to a higher flight level cleared by Air Traffic Control (ATC). When shifting control to the flight deck, step climb could be improved to a gradual climb. Besides keeping a constant speed, an often-used design assumption is to keep the cruise altitude constant.

First, the case of constant cruise speed is discussed. A commonly used method is to establish the minimum-time or minimum-fuel vertical trajectories with the use of the energy-state approximation [38]. For this method, the constant cruise speed is assumed to calculate the cruise altitude with a minimum fuel burn rate. Then the vertical profile along-track based on the aircraft weight and true airspeed is optimized.

This vertical optimization method has previously been applied in combination with the BADA model for wind-optimal trajectories [35]. It requires the fuel consumption equations in subsection 5-2-3 and the drag and lift coefficient equations in subsection 5-2-2. The optimal cruise altitude is derived by taking the first-order variation of the fuel flow rate with respect to the cruise altitude to zero. This results in a optimal altitude equation for the troposphere (Equation 3-2) and tropopause (Equation 3-3).

$$h_{opt} = \left[1 - e^{\frac{-f(m,V_{TAS})K_T R_{gas}}{2(g+K_T R_{gas})\rho_{0,ISA}^2}}\right]\left(\frac{1000T_{0,ISA}}{6.5}\right) \tag{3-2}$$

$$h_{opt} = \frac{-f\left(m, V_{TAS}\right) R_{gas} T_{trop,ISA}}{2g{\rho_{trop,ISA}}^2} + 11000 \tag{3-3}$$

$$f\left(m, V_{TAS}\right) = \ln\left(\frac{4m^2 g^2 C_{D2}}{S^2 V_{TAS}^4 C_{D0}}\right) \tag{3-4}$$

These equations result in the optimal cruise altitudes for atmospheric constants, aircraft-dependent aerodynamic drag coefficients, aircraft mass, and airspeed. When a certain thrust margin should not be exceeded, this has to be included in the model. The thrust margin is incorporated to assure a predefined rate of climb at the optimal cruise altitude [39]. To cope with regulations or allow for a predefined level of computational complexity, the optimal cruise altitude can be set according to a set of flyable altitudes h_{opt}^{Legal} by use of Equation 3-5.

$$h_{opt}^{legal}(t) = \min_{h^{Legal}}\left\{\left|h_{opt}(t) - h^{Legal}\right|\right\} \tag{3-5}$$

Secondly, the constant altitude assumption is elaborated upon. Keeping altitude constant requires little to no vertical optimization (only for the climb and descent phase) and does not add to the fidelity of the model. However, it is commonly used as it simplifies the horizontal optimization process. The minimum-time trajectory is fuel-optimal for aircraft cruising at constant altitude [15]. This minimum-time trajectory is determined by a horizontal flight profile optimization method which is elaborated upon in the next section.

3-2-2 Horizontal Flight Profile

Nowadays, more research is performed on the optimization of the horizontal flight profile. Flight plans provide ATC with the airlines' route preference. This route is based on existing waypoints that aircraft have to follow and actual routes can deviate from this due to congestion levels and safe separation. Due to the current aircraft structure, these routes are not the shortest paths from origin to destination, denoted as the Great Circle Route (GCR). Although the GCR is the shortest, it is not always the most efficient and fastest route when taking external factors like winds, convective areas, and jet streams into account. An active area of research is the computation of WOR. Taking the presence of winds into account yields a higher than 1% benefit on average fuel consumption for routes over 2000 nm (3700 km) distance [40]. As can be seen in Figure 7-10, most flights crossing the North Atlantic region cover a distance larger than this.

Aircraft horizontal trajectories can be optimized on the individual level or considering multiple aircraft at the same time. Even with today's computers, this results in a computationally heavy task for only two agents [41], therefore only individual optimization is considered. Current trajectory optimization methods are formulated as optimal control or as geometric and heuristic methods. The ones formulated as optimal control problems can be categorized as indirect problems (boundary value problem based on calculus of variations), direct problems (Non-Linear Programming (NLP)), a hybridization, and heuristic problems (simulated annealing, evolutionary algorithms, etc.) [32]. Two trajectory optimization methods for wind-optimal routes that are formulated as optimal control problems and often encountered in literature are elaborated upon below.

Wind-Optimal Extremals

The first method to be assessed regarding minimum-time paths is based on the problem addressed by Zermelo in 1930 [42]. This problem is reduced from a two-point boundary value problem to an initial value problem that can be solved by collocation methods or interpolation techniques. The main drawback of such algorithms is to find a good initial condition. The algorithm searches for optimal solutions by combining calculus of variations and dynamic programming. The target is the minimization of a cost function that consist of one or several components (Equation 3-6) [35]. This optimization cost function can be reduced to a time component only or extended by a cost coefficient for specific emissions and/or penalty areas [43] [36]. The aircraft's equations of motion

and mass at constant altitude and speed are described by Equation 3-7, Equation 3-8, and Equation 3-9.

$$J = \int_{t_0}^{t_f} \left[C_t + C_f f(m, h, V) \right] dt \tag{3-6}$$

$$\dot{\phi} = \frac{V \cos\psi + u(\phi, \theta, h)}{R \cos\theta} \tag{3-7}$$

$$\dot{\theta} = \frac{V \sin\psi + v(\phi, \theta, h)}{R} \tag{3-8}$$

$$\dot{m} = -f \tag{3-9}$$

The travel time is minimized by determining an optimal aircraft heading that yields the minimum-time trajectory in winds. Pontryagin's Minimum Principle is applied to determine the control input ψ to minimize the cost function. This results in the optimal heading stated in Equation 3-10, with F_{wind} being the aircraft heading dynamics in response to winds (Equation 3-11).

$$\dot{\psi} = \frac{-F_{\text{wind}}\left(\psi, \phi, \theta, u, v\right)}{R \cos\theta} \tag{3-10}$$

$$\begin{aligned} F_{\text{wind}}\left(\psi, \phi, \theta, u, v\right) = \Big[& -\sin\psi\cos\psi \tfrac{\partial u(\phi,\theta,h)}{\partial \phi} + \cos^2\psi \sin\theta u(\phi, \theta, h) \\ & + \cos^2\psi\cos\theta \tfrac{\partial u(\phi,\theta,h)}{\partial \theta} - \tfrac{\partial(\phi,\theta,h)}{\partial \phi} + \sin\psi\cos\psi\sin\theta v(\phi, \theta, h) \\ & + \cos\psi\sin\psi\cos\theta \tfrac{\partial(\phi,\theta,h)}{\partial \theta} + V\cos\psi\sin\theta + \cos^2\psi \tfrac{\partial(\phi,\theta,h)}{\partial \phi} \Big] \end{aligned} \tag{3-11}$$

Different approaches using this principle have been taken. One approach optimizes trajectory segments based on cost-to-go associated with extremals generated by forward and backward integration of the dynamical equations for optimal heading and aircraft motion in various points in the airspace along them [35]. Cost-to-go can be determined for any point in the covered airspace with the use of Delaunay triangulation and interpolation techniques using the points on the extremals. In the case of constant altitude during cruise, the minimum-time trajectory is specified by integrating the above equations from origin to destination. A climb or descent process can be mimicked by applying multiple step climbs. The optimal trajectory is computed by combining the wind-optimal extremals on the different altitudes.

A similar approach has been taken to optimize trajectories in the North Atlantic region [15] before applying strategic deconfliction. The total fuel savings depend on aircraft type, origin-destination and weather, but is estimated to be between 3 to 5%. This is approximated to result in a saving of around 200 million dollars annually.

Another approach using the principle is discussed in [30]. The cost function solely exists of a time component and a bisection method is applied to the initial heading angle to

reduce the computational time. This results in an estimated 2.1% fuel savings during the winter period.

When the climate impact is included in the cost function as suggested above, contrails and emissions of CO, HC, and NO_x are taken into account. Fuel burn is shown to be reduced anywhere between 4 to 8% and a reduction of 105 to 135 minutes of contrail formation can be established [43].

Ordered Upwind by Girardet

Another trajectory optimization method is based on a Dijkstra like Ordered Upwind algorithm [6], [44]. This method assumes constant true airspeed and constant altitude yielding the following equations of motion (Equation 3-12) with heading angle θ, aircraft speed V_a, and wind components $W_x(x, y)$ (Eastward) and $W_y(x, y)$ (Northward).

$$\begin{cases} \dot{x}(t) = V_a \sin(\theta(t)) + W_x(x, y) \\ \dot{y}(t) = V_a \cos(\theta(t)) + W_y(x, y) \end{cases} \tag{3-12}$$

The controlled parameter is the optimal heading angle θ and this should be chosen to minimize the total travel time. The optimization problem is written in Equation 3-13. Setting the control variable to a unit vector, the optimization model reduces to Equation 3-14.

$$\begin{cases} \min\limits_{\theta} & (t_f - t_0) \\ \text{s.t.} & \dot{x}(t) = V_a \sin(\theta(t)) + W_x \\ & \dot{y}(t) = V_a \cos(\theta(t)) + W_y \\ & (x\,(t_0)\,, y\,(t_0)) = (x_0, y_0) \\ & (x\,(t_f)\,, y\,(t_f)) = (x_f, y_f) \end{cases} \tag{3-13}$$

$$\begin{cases} \min\limits_{\mathbf{a} \in A} & (t_f - t_0) \\ \text{s.t.} & \dot{\mathrm{X}} = f(\mathrm{X}(t), \mathbf{a}(t)) \\ & \mathrm{X}\,(t_0) = \mathrm{X}_0 \text{ and } \mathrm{X}\,(t_f) = \mathrm{X}_f \end{cases} \tag{3-14}$$

This problem is a standard formulation of the optimal control problem and it is solved by writing it in the Hamilton-Jacobi form. The Hamilton-Jacobi equation can be seen as a front expansion problem and the optimal path problem is written as a front expansion problem where the speed of the wavefront $F(X, n)$ depends on the speed of the mobile $f(X, a)$ (Equation 3-15). The direction $\mathbf{n}$ is the outward unit vector normal to the front at point X and $u(X)$ represents the minimum time to reach the endpoint. The optimal path is designed by following the characteristics of the Hamilton-Jacobi PDE from the departure point to the arrival point.

$$F(\mathrm{X}, \mathbf{n}) = \max_{\mathbf{a} \in \mathbb{A}} \{-\mathbf{n} \cdot f(\mathbf{X}, \mathbf{a})\} \tag{3-15}$$

The Ordered Upwind algorithm is developed to approximate this solution. In order to compute the value function u, a 2D non-regular triangular mesh is considered as displayed in Figure 3-2. All the mesh point belong to one of the following classes as can be seen in the figure: *Accepted* are the points where the function u has been computed, *Considered* is the set of points where an estimate v of u has been computed but not frozen, and *Far* is the set of points where an estimate has not been computed yet. Furthermore, the subset of accepted points that are adjacent to the considered points are defined as the *AcceptedFront* and the line segments between these points are denoted as *AF*.

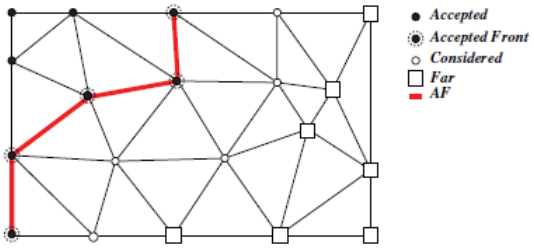

Figure 3-2: The mesh points and labelling of the Ordered Upwind algorithm [6].

This algorithm that assesses the mess points and moves them into different classes is highly efficient since it avoids iterations by carefully using the information on the characteristic directions of the Partial Differential Equation (PDE) and constructing the value function $u(X)$ gradually using the previous smaller values of $u(X)$ along the characteristic.

To implement obstacle avoidance, the speed of propagation is modified. The wavefront is slowed down in areas to be avoided, which penalizes the value function u by increasing it. A map of penalty values is created as a function of the obstacles slowing down the wavefront by $(1-\xi)\,F(X,n)$, with ξ between 0 and ξ_{max} smaller than 1.

The Ordered Upwind algorithm works on a Cartesian grid and the sphericity of Earth has to be taken into account to increase the fidelity. Simply projecting the points on a sphere into a plane is insufficient to use the algorithm as the projections cause a distortion in shapes, areas, and/or distances. Therefore, some steps to get a working algorithm are addressed [6]. First, the Lambert Conformal Conic Projection is applied of which the equations are stated in [45]. Then, the scale factor m is applied to give the distortion of the projection in the area of interest denoted by the distance on the map projection divided by the distance on the sphere. For a triangulation, the geodesic is approximated by a straight line and the distance between the points is corrected for by the scale factor. The aircraft speed has to be modified and the wind speed has to be projected on the map. At last, the optimal trajectory is built by solving for Equation 3-16. To get the trajectory on a sphere, a reverse Lambert Conformal Conic Projection is applied. This method yields a time reduction of 1.9% for routes of 25 minutes [44] and 2.9% for routes of 315 minutes [6] compared to their GCR.

$$\frac{d\mathrm{X}}{dt} = -mV_a \frac{\nabla u(\mathrm{X})}{\|\nabla u(\mathrm{X})\|} + Wp(\mathrm{X}) \tag{3-16}$$

This method can be extended in the three-dimensional domain by advancing altitude as the wavefront propagates, yielding a sub-optimal result as the local optimum direction is determined. The optimal trajectory is computed by following the characteristic direction. Another approach could be to compute wind-optimal trajectories at several altitudes and determine the optimal trajectory by connecting segments of these individual ones. A global optimum can be reached by computing a multitude of trajectories for advancing altitude and time. However, this is considered to be computationally expensive.

Altogether, several papers focus on trajectory optimization in the North Atlantic airspace. An overall aim is to increase the airspace capacity and to reduce flight time and emissions. Different approaches have been taken to achieve this. Generally, papers look at different route optimization strategies in terms of cost functions (subsection 3-1-2) and optimization methods (section 3-2). Overall, fast-time simulations are used for validation purposes.

Chapter 4

Conflict Detection and Resolution

Conflict Detection and Resolution (CD&R) methods have and will always be in place to safely guide aircraft through airspace. Currently, Air Traffic Control (ATC) is commissioned with the task to safely separate aircraft and their instructions have to be obeyed by pilots unless there is an imminent threat indicated by one of the on-board systems (Traffic Alert and Collision Avoidance System (TCAS)/Ground Proximity Warning System (GPWS)) [8]. Decentralizing ATC by shifting control to the flight deck to allow for direct routing is solely possible when a well-functioning CD&R method is in place.

Therefore, this chapter discusses some of the relevant characteristics and several methods. The relevant factors which define the airspace environment are discussed in section 4-1. Then, both tactical and strategic resolution methods will be elaborated upon in subsection 4-2-1 and subsection 4-2-2, respectively.

4-1 Preliminaries

To successfully prevent conflicts from happening, the characteristics of conflicts have been widely studied. Overall, a conflict can be divided into three phases: a detection, resolution, and recovery phase. According to Ribeiro [8], methods can be reviewed according to ten characteristics of which not all are equally relevant to the direct routing case. The level of surveillance, the level of intent, and the avoidance planning strategies are discussed below. A time horizon for CD&R methods is displayed in Figure 4-1.

4-1-1 Conflict Detection

As mentioned above, the first phase is detecting a conflict. To do so, it has to be defined what a conflict is. A conflict occurs when the Airborne Separation Assurance

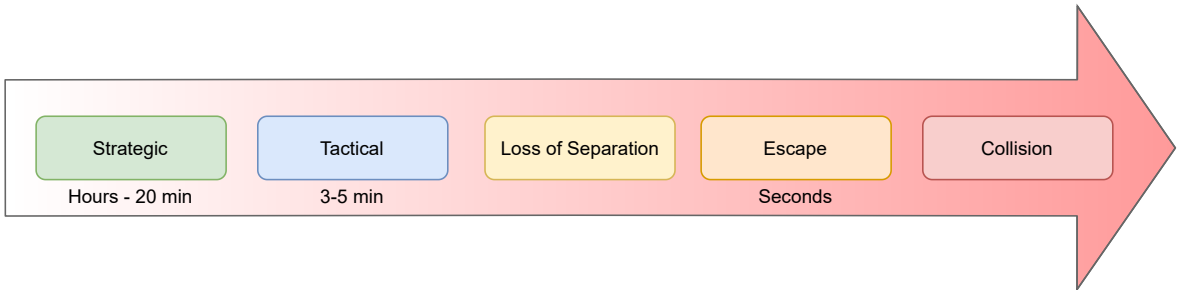

Figure 4-1: Time line for conflict detection and resolution methods.

System (ASAS) detects a predicted Loss of Separation (LoS) or intrusion. This happens when an intruder enters the protected zone of the ownship [46]. This protected zone is a disk-shaped area, usually of 5 NM radius and a 1000 ft height above and below the aircraft [47]. When aircraft have an even closer encounter within a radius of 0.1 NM height of 100 ft, this is called a Near Mid-Air Collision (NMAC). Altogether, this leaves two conflict detection parameters susceptible to change, the protected zone volume (primarily the separation distance in terms of the radius) and the look-ahead time. Not all aircraft are within a relevant range as all aircraft are susceptible to uncertainties regarding their trajectory and these increase with the distance to the ownship. Therefore, a look-ahead time or distance is set to determine the relevant potential intruders.

Level of Intent

Now the definition of a conflict has been clarified above, the different ways to consider an aircraft's trajectory propagation are discussed to elaborate upon the look-ahead parameter of the conflict. This trajectory propagation can be determined by different levels of intent information. As an overall rule, it can be taken that a higher level of intent adds complexity to the conflict detection system. The different levels of intent are stated below of which the first is considered to be state-based trajectory propagation.

- No intent (just position extrapolated with the velocity vector)
- Mode control panel intent (include autopilot information)
- The next trajectory change point.
- A set of upcoming trajectory change points.
- The complete flight plan (as stored in the flight management system)

According to [7], the first level of intent (no intent) will better suit in a direct routing environment than in an airway-like routing structure as aircraft are likely to maneuver less due to flying direct routes. This level of intent is beneficial as it is easy to implement and transparent to the crew at the cost of missing longer look-ahead conflicts.

4-1-2 Centralized versus Decentralized

Currently, aircraft operate in a hybrid environment where they mainly rely on ATC (centralized) for separation unless there is a LoS and TCAS overrules ATC (decentralized). However, overall it can be said that the current ATC system is a centralized one that is decentralized by moving towards direct routing. This means that each aircraft is responsible for safe separation and conflict handling. By shifting the responsibility of separation to the flight deck, the nature of the incentive is changing. Where ATC has the main priority to safely separate aircraft, aircraft will focus on the reduction of cost (trajectory optimization). Airlines and aircraft tend to show maximizing behavior, while ATC shows satisficing behavior [18]. This fundamental difference has to be accounted for when shifting to a decentralized surveillance domain. To operate with a distributed dependent surveillance system, all aircraft have to be equipped accordingly (Automatic Dependent Surveillance-Broadcast (ADS-B), TCAS, ASAS) [8].

This shift is promising regarding benefits of environmental impact (decrease in fuel consumption), airline operations (reduction in flight time), and relaxation of Air Traffic Controller (ATCo) workload limitations and some additional ones already discussed in section 2-2.

However, a negative result of the decentralization might be a decrease in airspace stability. This effect is measured according to the Domino Effect Parameter (DEP) as elaborated upon in section 2-2.

4-1-3 Conflict Resolution

After a future conflict is detected, it has to be resolved to avoid a LoS. Conflicts can be resolved in several ways. Conflicts can be resolved on a different time scale ranging from pre-departure deconflicting up to escape maneuvers only seconds before a collision occurs. Three different stages of avoidance planning can be identified as displayed in Figure 4-1. When a maneuver is employed with more than 20 minutes till LoS it is a strategic one, a maneuver from 20 minutes till LoS is a tactical one, and any maneuver from LoS till collision is called an escape [8]. As a LoS is to be avoided at all times and a proven system is already in place TCAS, the area of focus lays within the strategic and tactical avoidance planning.

As one may notice, there is a trade-off between the used level of intent and the relevance of an early resolution maneuver. Performing a strategic maneuver hours in advance requires a high level of intent. A disadvantage of such early maneuvers is the increased level of uncertainty caused by delays and weather events. Furthermore, a relatively large detour arises from an early maneuver, which negatively affects the efficiency and might require a recovery phase. This recovery is usually not necessary for tactical maneuvers as deviations are relatively minor [8].

4-2 Conflict Detection and Resolution Methods

This section provides actual conflict detection and resolution methods. First, tactical methods are discussed before discussing strategic methods. For the remainder of this chapter, strategic methods imply methods deployed during the pre-flight phase. Before the methods are discussed, the detection and resolution domains and criteria for the tactical and strategical resolution methods are stated.

4-2-1 Tactical Conflict Detection and Resolution Methods

The use of a tactical resolution method is necessary in absence of ATC to avoid a LoS and several tactical methods are discussed. On a tactical level, conflicts can be avoided by performing a maneuver in the vertical (climb/descent), lateral (turn), and longitudinal (speed) direction [11]. Pilots have a preference for performing conflict resolution in the vertical domain, followed by longitudinal and lateral maneuvers.

To be in line with this research, a tactical resolution method has to meet several criteria. A solution has to be generated fast and efficiently, to be used in online applications. Also, a method has to yield a robust solution with some level of redundancy in case of failure aboard one aircraft. To comply with both criteria above, a negotiation method is not recommended as there is a chance of a deadlock [8]. Furthermore, the resolution has to be route, fuel, and time-efficient. This section will discuss two tactical CD&R methods often encountered in literature.

Modified Voltage Potential

First of all, the Modified Voltage Potential (MVP) is discussed. This method is based on Eby's self-organizational algorithm [26]. The method is explained via the drawing displayed in Figure 4-2. When a conflict is detected by the detection module, the resolution module uses the predicted future position of both the intruder and ownship at the moment of minimum distance [7]. The detection module can use either intent information or the currently expected track based on the extrapolation of the states. The minimum distance vector is used to compute an avoidance vector which consists of a speed and/or heading change to stay out of the intruder's protected zone and it is the shortest way out of conflict. In the case of multiple conflicts, the resolution vectors are summed for each conflict pair. The resolution method assumes the intruder not to maneuver to avoid the conflict which results in a fail-safe system as the avoidance vector will point in the opposite direction due to the geometry of the conflict. This also implies that no negotiation or communication is required. The MVP yields a route efficient solution as conflicts can be solved in both the horizontal and vertical domain. Furthermore, the algorithm is computationally efficient, hence, suitable for online implementation. A look-ahead time of 5 minutes ensures sufficient time to identify and solve the conflict.

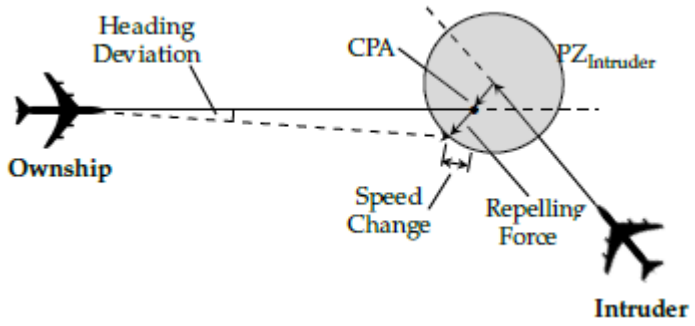

Figure 4-2: Modified Voltage Potential resolution [7] [8].

Velocity Obstacle

Another conflict resolution method is the solution space, which is based on a combination of the Velocity Obstacles (VO) theory and kinematic constraints. A VO is defined as the set of all velocity vectors of a moving agent which will result in a LoS [48]. The solution space consists of a set of conflict-free and conflicting velocity vectors. Figure 4-3 shows the visual representation of the VO. The VO of multiple intruders can be combined and displayed on the Solution Space Diagram (SSD) of the ownship (Figure 4-3b) [49]. This presents the reachable combination of speed and heading. Conflict resolution methods are used to select the heading and/or speed changes from this reachable set. The main benefits are its simple geometric representation and the possibility of taking the union to avoid multiple obstacles.

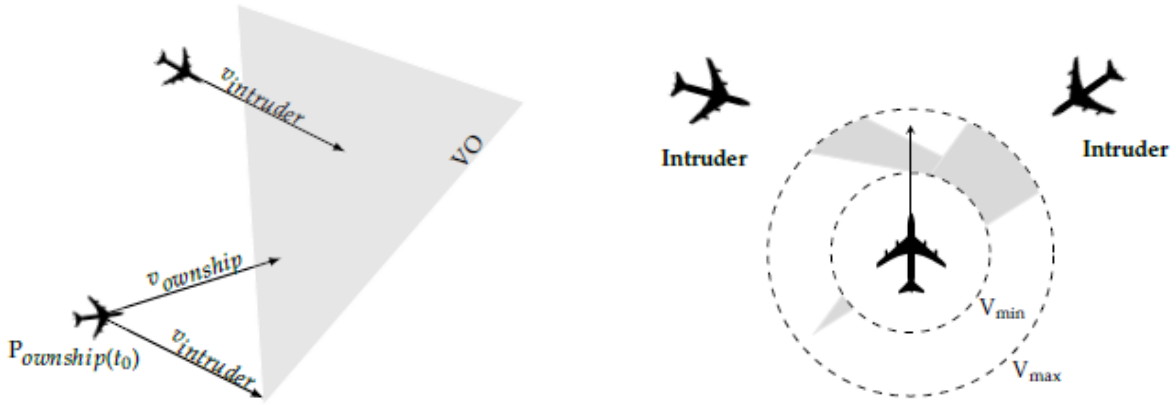

(a) VO in absolute velocity plane [8].

(b) SSD resolution. [8] [49].

Figure 4-3: Velocity Obstacles solution space.

In general, pilots prefer to solve conflicts in the vertical domain over lateral and longitudinal maneuvers when under time pressure [11] as vertical maneuvers have a rapid result (due to disk-shaped protected zone) and have a lower cognitive workload. Furthermore, complex dual-axis maneuvers tend to be avoided. As control is shifted towards the flight deck, it is relevant to take this into account for applying a tactical resolution method.

4-2-2 Strategic Conflict Detection and Resolution Methods

When the traffic density in an airspace is high, it might result in a situation where tactical conflict resolution increases the number of total conflicts (section 2-2). This could pose a risk to the overall safety and result in a situation where the overall efficiency is significantly reduced. The chance of a situation like this happening could be reduced by applying strategic deconflicting. A criterion of such a method is to keep the overall efficiency high. The goal of strategic deconflicting is to align flight plans to identify potential conflicts during the pre-departure phase. Conflicts can be avoided by modifying trajectories in space (shape, flight level, airspeed, or a combination) and time (departure time shifts). Both are susceptible to operational limitations. Aircraft are limited by airport restrictions regarding departure and arrival, which imposes a cap on time shifts. Trajectory modification is limited by reasonable routing time. The deconflicting process is often based on simulated annealing or evolutionary algorithms.

Before elaborating upon the different methods, it is important to keep in mind that a strategic deconflicting method is related to the trajectory optimization method. To be able to identify conflicts and deconflict trajectories, the trajectories have to be known upfront. It might be that different optimization methods result in a different amount/structure of conflicts and that conflict clusters emerge in the area of interest. Therefore, some strategic deconflicting methods might be more suitable than others as they deal with these clusters differently. Furthermore, different conflict types appear to behave differently in changing wind fields [23]. Continuous conflicts that persist over a large portion of the flight are not significantly affected by wind changes and are more likely to be found between the same trajectories on different days. Spot conflicts are heavily affected by winds and are seldom repeated from one day to another.

Evolutionary Algorithm

Methods based on a search heuristic inspired by the evolution theory are called evolutionary algorithms. For this method, an initial population is created and the fitness of each individual is assessed. A fitness function is used to assure that a configuration without conflicts has a better fitness than configurations with conflicts. Individuals are selected and reproduced according to their adaptation. A part of the population is crossed to generate new children which replace the parents in the population. A certain percentage of children undergo mutation to enlarge the gene pool. This process stops after a certain termination criteria or a maximum number of generations is reached.

In the case of strategic deconfliction, a cluster-based approach is taken to optimize each cluster in combination with a genetic algorithm [50]. The optimization function for each cluster is subjected to the following criteria; all separation between aircraft has to be ensured, minimize the number of delays, minimize the number of maneuvers and aircraft undergoing maneuvers, and minimize the duration of the maneuvers. The fitness represents a configuration of maneuvers and a "Stochastic Reminder Without Replacement" selection technique is used. Mutations consist of a change in maneuver configurations of an aircraft in a cluster. This process stores the best-performing individuals to make sure that they are not lost during the crossover or mutation phase. In

general, genetic algorithms have difficulty solving large conflict clusters. This has been solved with the use of a partially separable structure of the fitness function. Overall, this genetic algorithm has been able to solve all conflicts in the French airspace within reasonable computation time (26-55 min) for 7540 flights.

Another approach uses an evolutionary algorithm in combination with a sliding forecast time window model to limit the problem size and increase the reactiveness to uncertainties [51]. This method solely solves conflicts by delaying flights and is, therefore, more of a ground-holding problem. Setting a time window of 30 minutes resolves all conflicts by delaying around one-fifth of all aircraft with a mean delay of 7 minutes and a maximum delay of 87 minutes. A drawback is the large computational time of 21584 seconds for 8693 flights over a day. The mean delay and computational time increase even further for an increasing time window.

Constraint Programming

The same problem has been solved with a constraint programming strategy [51] [52]. This method has a similar approach as the one mentioned above which is of the ground holding problem form. The constraints of the model are computed based on couples of conflicting points. A search strategy based on a branch and bound algorithm is applied to find the optimal solution for the minimization of the maximum allocated delay while keeping the overall delay low. This method yields a mean and maximum delay of 4 and 88 minutes, respectively, for a time window of 90 minutes and a computational time of 2096 seconds.

Simulated Annealing

Several methods based on simulated annealing in combination with other algorithms have been used for strategic deconfliction. Simulated annealing is a metaheuristic from thermodynamics theory as it imitates the annealing process of metal involving heating followed by an iterative process of controlled cooling [17]. In short, a current solution is established by counting the number of conflicts. A deterministic or random scheme is employed to modify one or more trajectories after which the total number of conflicts is determined. If this is less than the current solution, the new solution is adopted as the current solution. If this is not the case, the solution is accepted or rejected with a probability given by the simulated annealing scheme. When the maximum number of iterations is reached at a temperature $Temp$, the temperature is decreased according to a predefined scheme until a final temperature is reached. This process is stated in (Equation 4-1), where z_c is the current solution, z' is the new solution, and C_t gives the number of conflicts for the specific solution.

$$p\left(z_c \rightarrow z', Temp\right) = \begin{cases} 1, & \text{if} \quad C_t\left(z'\right) < C_t(z_c) \\ \exp\left(\frac{C_t(z_c) - C_t(z')}{Temp}\right), & \text{if} \quad C_t\left(z'\right) \geq C_t(z_c) \end{cases} \tag{4-1}$$

This process is combined with several methods to improve performance. For instance, flights are preprocessed with a sliding window algorithm [53]. The method in this paper is restricted by the current North Atlantic Organized Track System (NAT-OTS). It orders flights according to the entry time in the routing structure and creates sub-problems to be solved by the simulated annealing algorithm, which is constrained by solutions from previous time windows. The simulated annealing uses a probabilistic approach for the modification domain with the following order; longitudinal maneuver, entry/exit point, delay, and flight level change. This process has been applied to the North Atlantic region, resulting in a near 100% reduction of conflicts for around 350 flights taking around 45 minutes.

Another approach used in combination with simulated annealing is local search [15] [54]. It has been shown that this can reduce the computational time by a factor of ten for small traffic instances (around 4000 flights) with respect to classical simulated annealing methods. During each iteration, the algorithm selects at random whether to use simulated annealing, the local search, or both methods consecutively. A local

search is applied to narrow the trajectory modification process to conflicting trajectories and incorporate logic into solving them. In this case, the logic starts by modifying particular trajectories, then interacting trajectories, and finally a combination of the previous methods. This method has been applied to the North Atlantic region [15]. The conflicts are resolved by changing the departure time, followed by a slight modification of the trajectory shape to minimize the fuel increase. As departure time shifts are relatively small (maximum of 30 minutes) compared to changes in the wind field, the wind field is assumed not to change for small deviations in departure time. Making this a relatively straightforward choice for conflict resolution.

Research has been performed on the effectiveness of different modification methods within the simulated annealing framework [17]. The following modifications have been compared: time modification (T), shape modification (S), and time + shape modification (T+S). A shape modification is performed with the use of a smooth function (Equation 4-2), where b^f is drawn from the domain [-1,1] and Y is a predefined maximal deviation function. The modification domain for time + shape modification has been researched as well. For this, modifications over the North Atlantic only (T+S) and the whole trajectory have been assessed (T+Sc). Overall it turns out that the biggest conflict reduction for modification within the North Atlantic region is obtained by (T+Sc). However, eliminating all conflicts by trajectory modification comes at a cost for trajectory length and cruising time. A maximum shape modification rate of 2% results in a mean time increase of 0.5% to 2%. Penalizing trajectory deviations decreases the mean time increase.

$$y = \xi(x) = b^f Y \left(cos(2\pi x - \pi) + 1\right) \tag{4-2}$$

All together, strategic and tactical methods can be used separately and next to each other. These methods can be solved on different time intervals and resolution domains. Some methods may be more suitable for certain trajectory optimization methods than others and this has to be kept in mind.

Chapter 5

Performance Assessment

This chapter discusses the performance assessment required to compare different scenarios. First, multiple performance criteria are discussed. Then, the performance model to measure fuel consumption is elaborated upon. At last, a flight phase identification method separate from the one incorporated in Base of Aircraft Data (BADA) is described. This might be useful when creating scenarios.

5-1 Performance Indicators

In general, there are several indicators to assess the performance of an airspace. These are used to compare different airspace structures and conflict detection and resolution methods in Air Traffic Management (ATM) research. Generally, the airspace performance is assessed based on the following criteria; safety, stability, capacity, and efficiency. For each of these criteria, a framework is established with their performance indicators which are discussed below. One can notice that some performance indicators are used for multiple criteria. A more detailed definition of a conflict can be found in subsection 4-1-1.

5-1-1 Safety

The first and most important criterion is safety, which is a measure of separation performance. The most frequently used indicators are stated in Table 5-1. This incorporates indicators that impose a direct risk on safety like the Loss of Separation (LoS) and indicators that impose an indirect risk on safety like airspace stability. As most indicators speak for themselves and the stability is discussed below, it leaves the intensity of an intrusion ($Int_{severity}$) to be discussed. Equation 5-1 describes this, where I_H and I_V are the horizontal and vertical intrusions that are normalized with respect to the

corresponding minimum separation requirements, while $t_{0_{int}}$ and $t_{1_{int}}$ are the start and end time of an intrusion [12].

$$Int_{severity} = \max_{t_{0_{int}} - t_{1_{int}}} [min\left(I_H(t), I_V(t)\right)] \tag{5-1}$$

Table 5-1: Performance indicators for airspace safety.

Indicator	Measure	Reference
Loss of separation (ASAS)	Number of intrusions in X NM radius	[7]
Time of loss of separation	Intrusion time	[7] , [29]
Severity of intrusion	Intesity	[12]
Secondary conflicts	Conflicts created by resolution (DEP)	[8], [12]
Escape	Number of times TCAS is required to prevent a collision	[8]

5-1-2 Stability

The airspace stability assessment mostly consists of indicators of conflict count which are presented in Table 5-3. Another way of assessing stability is by looking at the number of secondary conflicts, measured by the Domino Effect Parameter (DEP). This parameter is visualized with the use of the Venn diagram in Figure 5-1. $S1$ presents the set of all conflicts without resolutions and $S2$ the set of conflicts with resolutions, for identical scenarios. The three regions in the Venn diagram can be identified as the stabilizing effect ($R1 = S1/S2$), the common conflicts ($R2 = S1 \cup S2$), and the destabilizing effect ($R3 = S2/S1$). The actual DEP is defined by Equation 5-2 [1] [12].

$$DEP = \frac{R3 - R1}{S1} = \frac{S2}{S1} - 1 \tag{5-2}$$

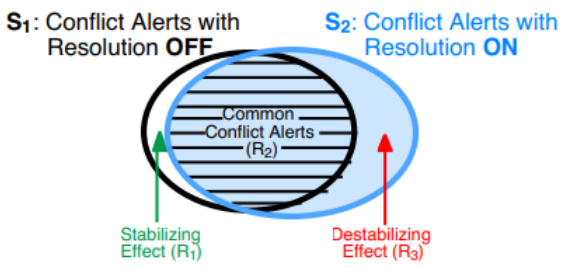

Figure 5-1: Venn diagram of the Domino Effect Parameter (DEP) [1].

Table 5-2: Performance indicators for airspace stability.

Indicator	Measure	Reference
Secondary conflicts	Conflicts created by resolution (DEP)	[8], [1], [12]
Conflict count (total/over time/per number of aircraft)	Number of conflicts in predefined region	[29]
Encounter angle	Distributed by segments 0-180	[29]
Altitude rates	Distributed by FL	[29]
Conflict time	Distributed by time	[29]
Distribution of conflict intrusion (hor/vert/comb)	Loss of Separation (LoS) to collision	[29]

5-1-3 Capacity

Next, the airspace capacity category is discussed and the indicators are stated in Table 5-3. Each airspace has a maximum capacity, just like a road has one. When it reaches this maximum capacity it can be said that the airspace is saturated. There are possibilities to structure airspace in a different way to increase this capacity. The indicators stated below have different purposes. The first two indicators are actual airspace capacity measures, while the final two indicators are supportive measures to research the mechanisms which cause the airspace capacity to change. The traffic density (ρ_{AC}) can be calculated by Equation 5-3. Where N_{AC} is the number of aircraft, A is the airspace area, Δt is the time interval over which the conflicts are counted, V_{avg} is the average aircraft speed, and L_{path} is the average nominal path distance of the aircraft in the simulation space.

$$\rho_{AC} = \frac{N_{AC}}{A\Delta t(V_{avg}/L_{path})} \tag{5-3}$$

Table 5-3: Performance indicators for airspace capacity.

Indicator	Measure	Reference
Traffic density	Number of flights per simulation region	[27]
Controller workload	Amount of work that can safely be assigned to ATCo	[20]
Separation threshold	Separation between aircraft pairs	[20]
Relative Track Angles	Angle between trajectories of interacting aircraft pairs	[20]

5-1-4 Efficiency

At last, the efficiency of the airspace is discussed. When talking about airspace efficiency, this means the overall efficiency of all aircraft involved. Case by case deviations may be possible and an overall improvement does not mean that the efficiency of each individual is improved. The assessment indicators are stated in Table 5-4 and most indicators are closely related. The time, emission, and fuel performance are discussed in further detail.

Table 5-4: Performance indicators for airspace efficiency.

Indicator	**Measure**	**Reference**
Travelled distance	NM	[27]
Travelled time	Hrs	[26]
Delay time	Hrs	[50]
Burned fuel	Tonnes	[26]
GWP	Tonnes CO_2 equivalence	[43]
Work done	Thrust and displacement	[12]

Time Performance

An initial performance indicator for airspace efficiency is the total flight time. A measure of efficiency is the time it takes aircraft to transport their customers/cargo from origin to destination. This is part of their network strategy as the fastest routes increase overall customer satisfaction and make it more likely for individuals to become frequent customers.

The total flight times of different scenarios can be compared in various ways. One possibility is to compare the average and overall flight times. This is a good measure for comparing changes in the overall efficiency of the system. However, it might be that some flights are more heavily influenced by the change of scenario than others. Therefore, the deviations over the whole flight time spectrum have to be assessed and compared between the different scenarios. Maximum deviations need to be compared and large maximum deviations need to be avoided. This because a bias in optimization preference has to be avoided.

Furthermore, an improvement in departure delays can be assessed. Delays are costly as airlines have to pay their crew, might lose future customers, and in some cases have to compensate their passengers. These delays become more of interest if strategic deconflicting operations are performed. An overall optimization criterion is that delays should be minimized. The overall and average delays can be assessed to measure the overall efficiency. To get a more detailed overview, deviations over the whole delay spectrum have to be assessed and the maximum deviations should be compared for the same reasons as mentioned above.

Emission Performance

Emissions are related to the fuel consumption of aircraft and an improvement in overall consumption is likely to positively impact the overall emissions. However, the composition of emission products depends on external factors of the outdoor environment such as temperatures and humidity. A way of reducing climate impact is by avoiding these areas to reduce the overall emission impact while this might increase the flight time and CO_2 emissions. For instance, by flying through regions that are less sensitive to contrail formation. This optimizes for Global Warming Potential GWP instead of fuel consumption.

A detailed overview of the influence of the different products and by-products is not the scope of this research. Standard relations between fuel, combustion products, and emissions may be used to determine the GWP impact. The emission performance can be expressed in total saved tonnes of CO_2 equivalent to give a rough estimation.

Fuel Performance

Reducing fuel consumption is of interest as this has a direct economical benefit for airlines and there will be an incentive to implement such findings. Similar to the time performance, the overall fuel consumption is a good measure of the efficiency of the system. However, it is important to investigate the whole spectrum to see if

some flights are more heavily impacted than others. If there are routes that have a structural disadvantage, it might be that airlines do not want to cooperate as they lose any competitive advantage.

5-2 Fuel Performance Modeling

Several performance models can be used to measure fuel performance. An often-used model is the Base of Aircraft Data (BADA). BADA is developed by Eurocontrol to model aircraft performance. It contains performance and operating procedure coefficients for 438 different aircraft types. These are used to calculate thrust, drag, and fuel flow and nominal cruise, climb, and descent speeds.

A promising open-source competitor for the BADA model has been developed by TU Delft and is called OpenAP [55]. It contains fewer aircraft, but all that frequently cross the North Atlantic region. Relevant differences become more prevalent at lower altitudes due to different ways of thrust modeling. BADA models fuel flow based on thrust and speed, while OpenAP models it with thrust and altitude. The OpenAP model appears to have better results for a specific analysis performed on the Cessna Citation II. However, this model is still under development and its performance has been validated at cruise levels of 10,000 ft, while commercial aircraft cruise at altitudes above 30,000 ft.

As a BADA 3.12 license is available at the TU Delft, this model is used and the fuel computations are based on this [10].

5-2-1 Preliminaries

Before discussing the thrust and fuel consumption calculations, some preliminary assumptions regarding the atmospheric model and aircraft mass for these calculations are discussed.

Atmospheric Model

Aircraft performance is influenced by weather conditions. Air density, temperature, and wind affect the aircraft performance through engine operations and directly. This affects the fuel consumption. Therefore, International Standard Atmosphere (ISA) is assumed for all scenarios. This simplifies calculations between different measures of velocity and altitude. Automatic Dependent Surveillance-Broadcast (ADS-B) data provides ground speed and altitude above sea level. As described in subsection 5-2-2, the calculation of the thrust requires the true airspeed V_{TAS}. This is defined as the ground speed influenced by wind speed (V_{ground} - V_{wind}). Calibrated airspeed V_{CAS} is used as well and this can be computed with the use of ISA, altitude, and V_{TAS}. As aircraft experience real non-ISA conditions, these may exceed the maximum levels based on the ISA. This could result in modeling errors.

Aircraft Mass

One of an airlines' competitive features is the aircraft mass. this information is not disclosed in ADS-B data and provided to third parties. Therefore, a model has to be developed to determine the initial mass. When the initial mass has been determined, the en-route mass reduction can be estimated with the use of the fuel flow. BADA uses masses that are taken from the aircraft manufacturer. BADA defines the Maximum Take-Off Weight (MTOW), Operational Empty Weight (OEW), the maximum payload ($W_{payload}$), and a reference mass (roughly 70% of the weight between the minimum and maximum mass) [56]. The weights are related by Equation 5-4.

$$W_{MTO} = W_{OE} + W_{payload} + W_{fuel} \tag{5-4}$$

The reference mass is used to calculate the varying speeds for varying mass according to Equation 5-5.

$$V = V_{ref}\sqrt{\frac{m}{m_{ref}}} \tag{5-5}$$

To accurately estimate the fuel consumption, the estimate of the initial mass is of importance. BADA provides a range of mass levels from $1.2 \cdot m_{min}$ to m_{max} and a nominal mass m_{ref}. To account for uncertainties, initial masses can be determined based on a probability distribution. Each aircraft is assigned a mass drawn from a normal distribution. As most flights crossing the North Atlantic cover relatively large distances, it is assumed that the aircraft's initial weights are rather high. Therefore, the mean is set to be the average of the nominal and maximum mass and the difference between the maximum and the mean is set to two standard deviations. All drawn initial weights are capped by the limits, this way they are between $1.2 \cdot m_{min}$ and m_{max} and the majority (around 95%) lies within m_{ref} and m_{max}.

Furthermore, only the part of the flight trajectories above FL100 is considered. Aircraft use fuel during the initial mission segments and the mass fractions are taken as defined by Roskam I [9]. Commercial aircraft are assumed to match the transport jet type and the mass fractions are stated in Table 5-5.

Table 5-5: Transport jet mass fractions for generic mission segments based on Roskam I [9].

Airplane type	Engine start, warm-up	Taxi	Take-off	Climb	Descent	Landing, taxi, shut-down
Transport jets	0.990	0.990	0.995	0.980	0.990	0.992

With this information at hand, the initial mass of the to be optimized trajectory can be determined by drawing a mass from the normal distribution as stated above and multiplying it with the mass fractions for the *engine start, warm-up*, *taxi*, *take-off*, and *climb* segments. FL100 roughly is one-third of the total climb phase, therefore, the initial mass is multiplied with one-third of the climb mass fraction. As wind-optimal routes are more efficient than the actual routes, less fuel is required. This might result

in a lower required initial mass. However, one could argue that airlines account for this reduction in fuel consumption by adding more payload weight to increase revenues. Altogether, flights are assigned the same initial mass for the actual and wind-optimal routes.

5-2-2 Thrust Calculation

Now the methods for deciding on the initial mass have been explained above, the change of mass over time has to be modeled. This is done by computing the fuel consumption (subsection 5-2-3) for which the thrust has to be modeled first. All commercial aircraft crossing the North Atlantic are equipped with jet engines. The thrust in BADA is modeled based on the total energy model (Equation 5-6).

$$(T - D)V_{TAS} = mg\frac{dh}{dt} + mV_{TAS}\frac{dV_{TAS}}{dt} \tag{5-6}$$

This can be simplified by rewriting the equation and include the terms for total drag and the drag and lift coefficients. This is done in Equation 5-7. The drag coefficient is a function of the lift coefficient under different conditions. The lift coefficient (Equation 5-8) can be modeled this way as the lift is assumed to equal weight for quasi-rectilinear, symmetric flight (this can be assumed for all phases).

$$T = \frac{mg}{V_{TAS}}\frac{dh}{dt} + m\frac{dV_{TAS}}{dt} + \frac{C_D\rho V_{TAS}^2 S}{2} \tag{5-7}$$

$$C_L = \frac{2mg}{\rho V_{TAS}^2 S} \tag{5-8}$$

This equation can be used to model the thrust in different flight phases, which are presented below.

Thrust during Climb

For the take-off and climb phase, the engines are often operated in (near) maximum thrust setting. The simplified energy model can be used with the drag coefficient set to cruise settings (Equation 5-9).

$$C_D = C_{D0,CR} + C_{D2,CR}C_L^2 \tag{5-9}$$

When the calculated thrust exceeds the maximum thrust, Equation 5-10 should be used. This equation has to be corrected for temperature deviations from standard atmosphere according to Equation 5-11. The change in effective thrust (ΔT_{eff}) can be described by ΔT_{eff} - $C_{Tc,4}$, where $\Delta T_{eff} C_{Tc,5}$ is between 0.0 and 0.4, and $C_{Tc,5}$ is larger than zero.

$$(T_{maxclimb})_{ISA} = C_{Tc,1} \times \left(1 - \frac{H_p}{C_{Tc,2}} + C_{Tc,3} \times H_p^2\right) \tag{5-10}$$

$$T_{maxclimb} = (T_{maxclimb})_{ISA} \times (1 - C_{Tc,5} \cdot \Delta T_{eff}) \tag{5-11}$$

Thrust during Cruise

During the cruise phase, aircraft are assumed to be in steady, symmetric flight as small deviations are relatively small and can be neglected. The thrust is considered to equal the total drag, Equation 5-12. The drag coefficient C_D is that for cruise conditions as stated in Equation 5-9.

$$T_{cruise} = \frac{\rho V_{TAS}^2 S C_D}{2} \tag{5-12}$$

The maximum thrust in cruise condition can be calculated with Equation 5-13 and is a ratio of the maximum climb thrust.

$$T_{cr_{max}} = C_{Tcr} T_{maxclimb} \tag{5-13}$$

Thrust during Descent

Descent operations can be divided into low and high altitude phases. For the low altitude phase, there exist three configurations; the cruise, approach, and landing configuration. All equations are ratios of the maximum climb thrust as stated below.

$$T_{des,high} = C_{T_{des,high}} T_{maxclimb} \tag{5-14}$$

$$T_{des,low} = C_{T_{des,low}} T_{maxclimb} \tag{5-15}$$

$$T_{des,app} = C_{T_{des,app}} T_{maxclimb} \tag{5-16}$$

$$T_{des,ldg} = C_{T_{des,ldg}} T_{maxclimb} \tag{5-17}$$

For the approach and landing configuration, the drag coefficients can be described by Equation 5-18 and Equation 5-19, respectively.

$$C_D = C_{D0,AP} + C_{D2,AP} C_L^2 \tag{5-18}$$

$$C_D = C_{D0,LDG} + C_{D0,\Delta LDG} + C_{D2,LDG} C_L^2 \tag{5-19}$$

All coefficients used above are described in Table 5-6.

Table 5-6: The thrust coefficient used in the BADA model [10].

Symbols	Description	Unit
$C_{D0,CR}$	Parasitic drag coefficient (cruise)	[-]
$C_{D2,CR}$	Induced drag coefficient (cruise)	[-]
$C_{D0,AP}$	Parasitic drag coefficient (approach)	[-]
$C_{D2,AP}$	Induced drag coefficient (approach)	[-]
$C_{D0,LDG}$	Parasitic drag coefficient (landing)	[-]
$C_{D0,\Delta LDG}$	Parasitic drag coefficient (landing gear)	[-]
$C_{D2,LDG}$	Induced drag coefficient (landing)	[-]
$C_{Tc,1}$	1^{st} max. climb thrust coefficient	[N]
$C_{Tc,2}$	2^{nd} max. climb thrust coefficient	[ft]
$C_{Tc,3}$	3^{rd} max. climb thrust coefficient	[1/ft^2]
$C_{Tc,4}$	4^{th} max. climb thrust coefficient	[K]
$C_{Tc,5}$	5^{th} max. climb thrust coefficient	[1/K]
$C_{T_{des,high}}$	High altitude descent thrust coefficient	[-]
$C_{T_{des,low}}$	Low altitude descent thrust coefficient	[-]
$C_{T_{des,app}}$	Approach thrust coefficient	[-]
$C_{T_{des,ldg}}$	Landing thrust coefficient	[-]
C_{Tcr}	Maximum cruise thrust coefficient	0.95

5-2-3 Fuel Consumption

Now the thrust is calculated according to the equations above, the fuel consumption can be determined with the fuel flow. The fuel flow depends on the thrust level and flight phase. For jet engines, the thrust specific fuel consumption (η [kg/(min $\cdot$ kN)]) is specified as a function of true airspeed (Equation 5-20) and used to calculate the nominal fuel flow, f_{nom} (Equation 5-21).

$$\eta = C_{f1}\left(1 + \frac{V_{TAS}}{C_{f2}}\right) \tag{5-20}$$

$$f_{nom} = \eta T \tag{5-21}$$

These equations are used during all flight phases except for cruise and idle descent. To get the fuel flow for cruise flight f_{cr}, a cruise fuel flow factor C_{fcr} is used (Equation 5-22).

$$f_{cr} = \eta T C_{fcr} \tag{5-22}$$

For idle descent, the minimum fuel flow (f_{min} is computed based on the geopotential pressure height (Equation 5-23). This idle thrust stops when the aircraft goes into the approach and landing phase, for which the maximum of the nominal fuel flow and minimum fuel flow is used as displayed in Equation 5-24.

$$f_{min} = C_{f3}\left(1 - \frac{H_p}{C_{f4}}\right) \tag{5-23}$$

$$f_{app/ldg} = MAX\left(f_{nom}, f_{min}\right) \tag{5-24}$$

With the fuel flow during each phase known, the total fuel consumption can be calculated by taking the integral over time Equation 5-25.

$$FC_{tot} = \int_{t_0}^{t_{final}} f dt \tag{5-25}$$

Table 5-7: The fuel coefficient used in the BADA model [10].

Symbols	Description	Unit
C_{f1}	1^{st} thrust specific fuel consumption coefficient	[kg/(min · kN)]
C_{f2}	2^{nd} thrust specific fuel consumption coefficient	[kts]
C_{f3}	1^{st} descent fuel flow coefficient	[kg/min]
C_{f4}	2^{nd} descent fuel flow coefficient	[ft]
C_{fcr}	Cruise fuel flow correction coefficient	[-]

5-3 Flight Phase Identification

Predominantly, the vertical but to some extent the horizontal flight profile are divided into several phases. To be able to calculate the fuel usage, the thrust during different phases has to be calculated. These flight phases seem somewhat arbitrary to humans, but require logic to be identified by a computer. The phase of the aircraft has to be determined based on the available ADS-B data. Deterministic logic can be used to process the flight data. However, large deviations in flight procedures are making it difficult to do so. Therefore, fuzzy logic is used for flight phase identification [57]. Fuzzy logic makes use of membership functions to determine the degree of truth for different features. Mostly Gaussian functions are used, but Z-shaped and S-shaped membership functions are used as well. These functions can take any value between 0 and 1. The phase is determined based on three different inputs (altitude, rate of climb, and ground speed). The following relationships are used to identify the correct flight phase (Equation 5-26). These functions should be read such that a high altitude, high ground speed, and no rate of climb indicate that a flight is in the cruise phase. As this research only takes flights above FL100 into account, the first relationship is irrelevant.

$$if \quad H_{gnd} \wedge V_{lo} \wedge RoC_0 \quad then\ Ground \tag{5-26a}$$
$$if \quad H_{lo} \wedge V_{mid} \wedge RoC_+ \quad then\ Climb \tag{5-26b}$$
$$if \quad H_{hi} \wedge V_{hi} \wedge RoC_0 \quad then\ Cruise \tag{5-26c}$$
$$if \quad H_{lo} \wedge V_{mid} \wedge RoC_- \quad then\ Descent \tag{5-26d}$$
$$if \quad H_{lo} \wedge V_{mid} \wedge RoC_0 \quad then\ Level\ flight \tag{5-26e}$$

An example of membership functions is displayed in Figure 5-2. Using these for phase identification of a flight from JFK to LHR results in an accurate approximation (Figure 5-3). The figure displays both the horizontal and vertical flight profiles with proper phase identification for each data point. Some faulty data is present at the end of the flight data resulting in a *NA* qualification. This is no reason for concern as this predominantly occurs below FL100.

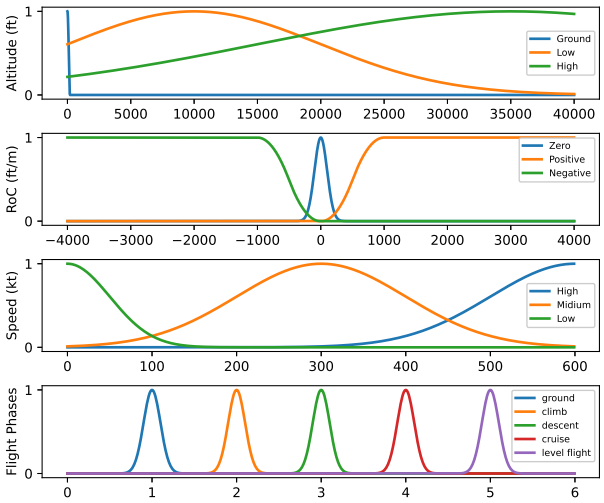

Figure 5-2: Membership functions for altitude, speed, and RoC range.

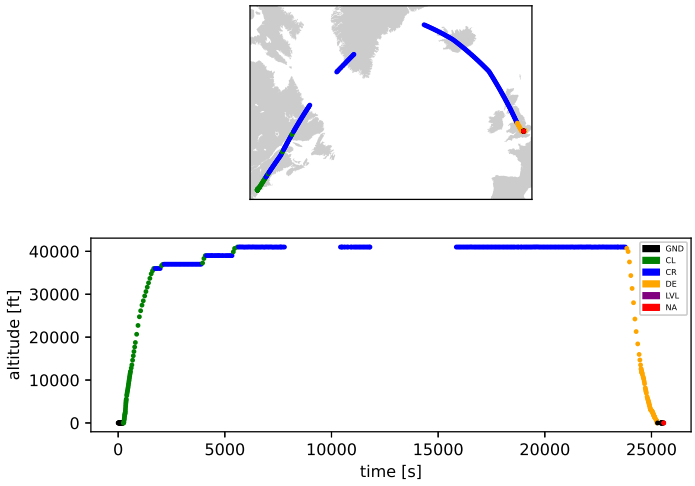

Figure 5-3: Flight phases identification in the horizontal and vertical domain for a flight from JFK to LHR.

Chapter 6

Thesis Framework

This chapter elaborates upon the problem statement. First, the research question, subquestions, and objectives are defined. Based on this objective, several research activities are stated. Then the research scope is clearly defined by stating assumptions to further demarcate the research.

6-1 Problem Statement

The literature study shows that previous research in the field of North Atlantic trajectory optimization in the presence of winds has been performed. These studies mainly consist of an individual wind-optimal trajectory optimization approach to reduce the overall fuel usage and an optional strategic deconfliction method to guarantee safety by reducing or eliminating the number of conflicts.

To the best of the author's knowledge, a research gap appears in the field of direct routing in the North Atlantic region. Optimizing trajectories on the individual level and taking a decentralized, tactical conflict resolution approach. Therefore, the following research question for this master thesis is proposed:

What are the benefits of direct routing in the North Atlantic region compared to the current routing structure in terms of efficiency, safety, and capacity?

This research question can be broken down into the following subquestions.

1. How much fuel/time can be saved by implementing direct routing in the North Atlantic region?

2. Is direct routing in the North Atlantic region safe according to the current separation standards?

To define the scope of the thesis, the research objective is stated below:

The research objective is to compare a direct routing scenario in the North Atlantic region with the current Air Traffic Management (ATM) routing structure and assess its benefits by simulating a year of real flight data.

To answer the research (sub)question and to ensure completion of the research objective, several research activities are defined:

Activity 1
Data collection, prepossessing, and analysis.
The main data of interest is the data obtained from FlightRadar24. This flight data contains all flights in the extraction region (90N, 165W, 15N, 85E). It has to be filtered for flights that cross the North Atlantic region. An analysis of this data is performed to determine whether the chosen extraction region sufficiently covers the majority of flights or any adjustments to the extraction region are required. Additionally, navigational data on airports, flight information regions, and North Atlantic Track System are collected.

Activity 2
Perform a preliminary study on the horizontal trajectory optimization method and run an experiment.
Two suitable horizontal optimization methods in presence of winds that are frequently used in literature are implemented and their route and computational efficiency are assessed. A single origin-destination pair (in both directions) shall be used for the performance assessment. An additional analysis will be performed for the best-performing method on three different days. This, to determine the overall efficiency and to determine the number of conflicts. A large number of conflicts will require research in strategic deconfliction methods. Even though conflicts at current traffic levels can be solved by tactical conflict resolution, there is no guarantee that this will be the case for increasing traffic levels. At last, it is investigated if a single altitude optimized horizontal trajectory is a sufficient representation for varying altitudes.

Activity 3
Run an experiment on the effectiveness of the tactical conflict detection and resolution method for different resolution domains.
This research activity relates to the second subquestion. With the trajectory optimization method chosen, a tactical conflict detection and resolution method is incorporated. It is investigated which tactical resolution domain performs best under the Wind-Optimal Route (WOR) routing structure. Conflicts are solved in the horizontal domain or the vertical domain. The different resolution domains will be assessed by comparing efficiency, safety, and stability. Three days of traffic are simulated in BlueSky to account for different weather and traffic conditions.

Activity 4
Propose a suitable strategic conflict detection and resolution method.
On top of the tactical conflict detection and resolution method, a strategic one might be required. If the outcome of research activity 3 shows that the tactical method is not successful in solving all conflicts and this results in Loss of Separation (LoS), measures have to be taken to make sure they do get solved. The strategic conflict detection and resolution method that will be used in this case is discussed in this research activity. Furthermore, the dynamics between the tactical and strategic methods are discussed.

Activity 5
Simulate the direct routing and current scenario in BlueSky.
This activity is the main goal of the research. The current ATM routing scenario is compared to the direct routing scenario over a simulation period of a year. This allows for a comparison in overall fuel consumption, safety, and capacity.

Activity 6
Simulate a future direct routing scenario in BlueSky.
This activity is performed when there is time left and aims at answering the following research subquestion: Will direct routing in the North Atlantic region remain safe with increasing traffic? To research the sensitivity of the direct routing scenario to the predicted future growth in aviation in the North Atlantic region, a third scenario is simulated. This scenario consists of flights in the direct routing scenario of the previous research activity with dummy flights added to the peak weak traffic level forecasted by International Civil Aviation Organization (ICAO). The three days that contain most flights crossing the North Atlantic are selected to be compared to the direct routing scenario for safety and capacity.

The order and relations of the research activities are displayed in a flowchart in Figure 6-1.

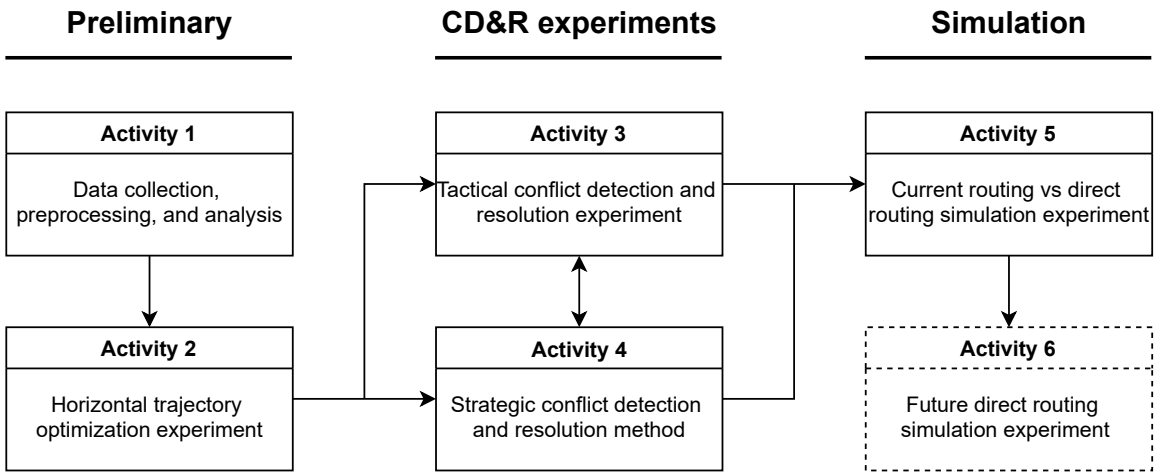

Figure 6-1: A flowchart of the research approach.

6-2 Research Scope

With the research objective and activities defined above, the research is narrowed down by further defining the research scope. This is done by defining a set of assumptions.

All commercial aircraft are equipped with Automatic Dependent Surveillance-Broadcast (ADS-B)
All aircraft crossing the North Atlantic region are equipped with ADS-B and are, therefore, (up to some extend) captured by FlightRadar24. This is plausible as all commercial aircraft are required to be ADS-B equipped in Europe and the US as of 2020. Not all aircraft are tracked by satellite in remote areas, but at least some part of the flight is captured when they are entering or exiting the North Atlantic region. Furthermore, fully functioning ADS-B equipment for conflict detection and resolution is assumed.

Only commercial airlines are taken into account
Predominantly commercial aircraft are considered to make use of the organized track system. Therefore, these flights are expected to benefit most from a direct routing structure compared to any private/military activity.

Horizontal trajectory optimization is most suited above FL100
Trajectories below this level are already optimized regarding airport constraints (runway locations, flow optimization, noise, etc.). Therefore, only the part of the trajectory above this level is taken into account for the scenarios. This means that the initial coordinate used for trajectory optimization is set to be the location where an aircraft reaches FL100 first and the final coordinate where an aircraft reaches it last.

The trajectory within the extraction region is optimized
The trajectory within the extraction region is completely optimized taking wind into account, not just the part in the North Atlantic region. Trajectories of flights crossing the North Atlantic region with origin and/or destination outside the extraction region will only be optimized within the extraction region. The start/endpoint of the trajectory optimization is/are taken as the entry/exit point of the planned flight in the extraction region.

Wind fields are constant over a 3 hr interval
To reduce the wind data size, wind reanalysis data is extracted every three hours. During those hours, it is assumed not to vary for the trajectory optimization and simulation processes.

Standard conflict detection settings are used
The conflict detection settings are set to the standard ones in BlueSky. This means that a state-based method is used with a look-ahead time of 5 minutes. The protective zone of an aircraft is defined by a horizontal and vertical separation of 5 NM and 1000 ft, respectively.

MVP assumes intruder not to maneuver to avoid conflict
This assumption assures that the avoidance vector of the ownship and intruder will always point in opposite direction and that no negotiation is needed. This way a fail-safe conflict resolution is established.

International Standard Atmosphere (ISA) is assumed
For both the current routing scenario and direct routing scenario ISA is assumed. This simplifies conversions between different measures of velocity and altitude. The flight performance (including speed and altitude) in BlueSky is capped based on ISA (BADA). FlightRadar24 provides actual data on speed and altitude levels that may exceed maximum levels based on ISA. This could result in modeling errors when simulating in BlueSky.

Aircraft initial weight is assumed to random
The initial mass is drawn from a normal distribution specified by BADA weights. Fuel fractions are used to get the start weight at FL100.

Quasi-rectilinear, symmetric flight
Quasi-rectilinear, symmetric flight is assumed for all flight phases. This way lift is assumed to equal weight and the lift coefficient can be computed. This lift coefficient is used to calculate the thrust and with this the fuel consumption.

Undefined aircraft types are assumed to be B747.
All aircraft of which the type is not defined in the performance data will be considered to be of the B747 family as this is in line with the BlueSky simulator. This is done to make sure that the performance limits of all aircraft in the simulation are defined.

The airspace is not managed by Air Traffic Control (ATC) in the direct routing scenario
The direct routing scenario represents a decentralized approach in which pilots solve conflicts themselves en-route. No ATC is involved to direct aircraft along a route or to intervene if conflicts are at hand.

Only flights crossing the North Atlantic region are taken into consideration.
Flights in the extraction region that do not cross the North Atlantic region are not taken into account. They do not affect the trajectory generation or conflict detection and resolution and are not present in any simulations.

Airspace fees do not vary.
Charges for passing different Flight Information Region (FIR) are assumed to be equal. Therefore, airlines will not have the incentive to prolong their routes through more cost-efficient airspace.

6-3 Tools

This research will make use of Automatic Dependent Surveillance-Broadcast (ADS-B) provided by FlightRadar24[1]. All aircraft crossing the North Atlantic region are assumed to be equipped with ADS-B and, therefore, captured in this data set.

To extract wind data, two prominent sources can be used. The first is the National Oceanic and Atmospheric Administration (NOAA) and provides an aviation weather forecast and historic weather data with limited access. Its European counterpart, the

[1] https://www.flightradar24.com/

European Centre for Medium-Range Weather Forecast (ECMWF) provides more extensive historic data which can be handled with a Python-based Application Programming Interface (API) and is the preferred source. Another weather-related tool that might be used is the Convective Weather Avoidance Model (CWAM) by the National Aeronautics and Space Administration (NASA). This might be useful as regions of heavy turbulence are encountered near jet streams (the so-called Clear Air Turbulence (CAT) regions).

All computations and modeling is performed in python 3.X. Python is open-source, therefore, many packages are available and platforms like ECMWF provide easy-to-use APIs. Furthermore, the simulation tool that is used runs on Python. This tool, BlueSky, is an open-source, open-data air traffic management simulation tool developed by TUDelft [58]. Performance modeling in BlueSky based on BADA is validated [59]. The used hardware is a HP ZBook 15 2014, 2.40GHz Quad-Core Intel i7-4700MQ, 16GB RAM.

6-4 Project Planning

The following planning is made to structure the research. The thesis is divided into four phases. A more elaborate project planning is presented in Appendix C.

6-4-1 Phase 1

- Perform literature study
- Define research topic
- Data collection
- Select research tools

6-4-2 Phase 2

- Perform initial data preprocessing and analysis
- Perform preliminary research
- Define problem statement
- Write preliminary report and research plan

6-4-3 Phase 3

- Pre-process all data and create optimized trajectories
- Perform experiment on tactical CD&R
- Select strategic CD&R
- Run all simulations and log results

6-4-4 Phase 4

- Analysis and discussion of results
- Write research paper
- Presentation and defence

Chapter 7

Methodology

The goal of this thesis is to compare two scenarios by performing a simulation over a one-year period. The base scenario, also the current scenario, is the situation in presence of the current, centralized Air Traffic Control (ATC) routing structure. This scenario is created by using Automatic Dependent Surveillance-Broadcast (ADS-B) flight data from FlightRadar24. A comparison of efficiency, safety, and capacity is made with a decentralized, direct routing scenario. If there is time left, a future scenario for forecasted traffic increase is simulated.

Before these scenarios can be compared, the direct routing scenario has to be established according to steps presented in the flowchart in section 6-1. This chapter provides the methodology for the steps in the flowchart. First, collecting, preprocessing, and analysis of flight data are discussed together with some additional data requirements. Then, the trajectory construction process both in the horizontal and vertical domain is elaborated upon. Using this information, the methodology of the tactical and strategic CD&R experiments is discussed. Before the main simulation can be performed, the flight performance methodology is stated. At last, the method for the simulation phase is provided.

7-1 Data Collection, Preprocessing, and Analysis

Real flight data is required to develop the scenarios. This data will be used to construct the direct routing scenario and the current scenario for validation purposes. The flight data has to be preprocessed and analyzed before it can be used properly. This section will elaborate upon the flight data structure, the preprocessing, and the analysis. Additionally, data required besides flight data is discussed.

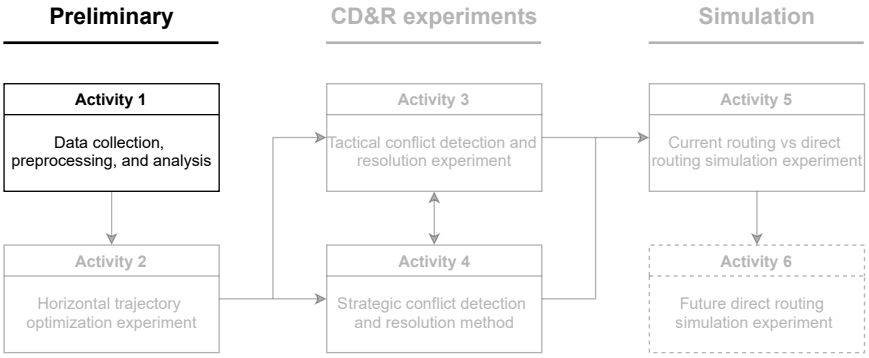

Figure 7-1: Corresponding phase of the thesis flowchart.

7-1-1 Flight Data Structure

To construct the current scenario for validation, position data is required. For the development of the direct routing scenario, data on origin and departure is required. Global aviation has seen a significant decrease since the start of the COVID-19 pandemic and the impact of this event on future aviation remains unsure. However, organizations like International Air Transport Association (IATA) and Eurocontrol expect aviation to recover after which growth is possible. This, in combination with the fact that scenarios of higher traffic density are more of interest in terms of conflict avoidance and potential savings, results in the use of data of the pre-COVID period. A year of flight data is provided by Flightradar24[1] for the period of April 1^{st} 2019 till March 31^{st} 2020. The extraction region is displayed in Figure 7-2 and Figure 7-3 and covers a region from 15°N-90°N by 165°W-85°E. This region has been selected based on a trade-off between capturing as many flights crossing the North Atlantic and limiting the total amount of data. Most flights crossing the North Atlantic connect North America with Europe and, North America with the Gulf states. The analytical justification of this choice is given in subsection 7-1-3.

The data of FlightRadar24 is gathered with the use of a worldwide system of over 20,000 ADS-B receivers. These receivers are operated by volunteering civilians and FlightRadar24 itself. Aircraft receive position data from a Global Navigation Satellite System (GNSS) source. This information, and much more, is transmitted via a digital data link and picked up by ADS-B receivers in the FlightRadar24 network. ADS-B has the advantage over radar in that it gives a better (near-)ground coverage. ADS-B equipment is not yet required in the North Atlantic region [3]. However, as of 2020, ADS-B equipment for commercial aircraft is required in Europe (commission regulation No 1207/2011 [60]) and the US (Federal regulations 14 CFR 91.225 and 14 CFR 91.227 [61]). In theory, nearly all aircraft crossing the North Atlantic will be equipped with ADS-B.

The data of interest consists of some basic flight data (origin/destination, ac type, flight id) and position data. The position data is updated at a dynamic frequency of 5-60 seconds, depending on the significance of the changes in position data. The data has

[1] https://www.flightradar24.com

Figure 7-2: The extraction region in a planar representation.

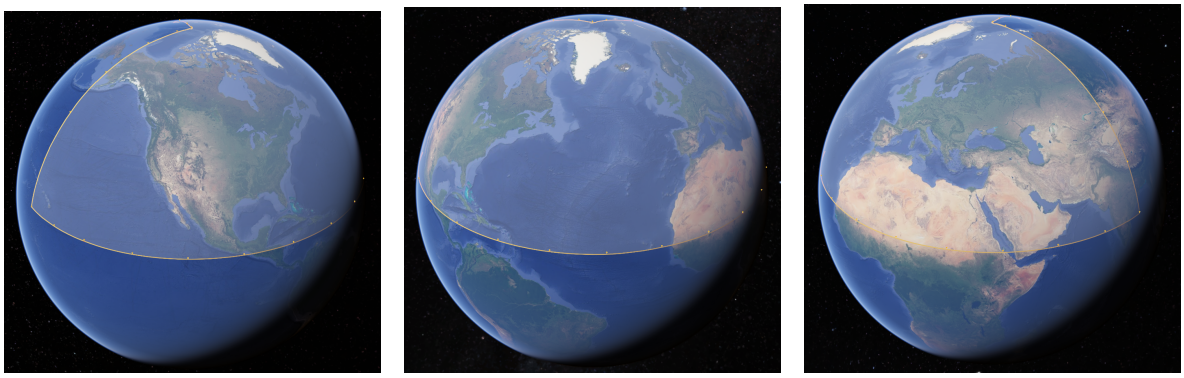

Figure 7-3: The extraction region in a spherical earth representation.

been supplied in several formats. Each UTC-based day consists of a Flights, Positions, and Environmental Management System (EMS) data file. Information of interest in these files is presented in Table 7-1 and Table 7-2.

7-1-2 Data Preprocessing

The received data is already ordered by day. Each day consists of ordered timestamp data per aircraft. No further filtering regarding aircraft position data grouping is required. However, what requires filtering is extracting the flights crossing the North Atlantic region. This will be done by looking at which flights contain position data of which the coordinates are within the assessed region. The position data should contain at least 3 coordinates per flight within the North Atlantic Region (NAT) Flight Information Region (FIR) to filter out outliers/faulty data. Aircraft that include position data within the region but have an origin and destination on the same continent are removed. Furthermore, position data can be captured and split over two consecutive UTC days in the data set. These flights have to be merged to obtain the full flight

Table 7-1: "Flights" data file.

Name	Definition
Flight_{id}	Unique decimal identifier for the flight leg (assigned by FR24)
Equipment	ICAO aircraft designator, mapped from address
Schd_{from}	IATA code for scheduled departure airport
Schd_{to}	IATA code for scheduled arrival airport
Real_{to}	IATA code for actual arrival airport (when diverted)

Table 7-2: "Positions" data file.

Variable	Definition	Unit
Snapshot_{id}	Time of position update	[s]
Altitude	Height above sea level	[ft]
Heading	True heading	[deg]
Latitude	Floating point	[°]
Longitude	Floating point	[°]
Speed	Ground speed	[kts]

trajectory.

This preprocessing has been performed on a reduced data set of three days to perform an initial analysis (subsection 7-1-3). The merging step to obtain the full flight trajectory during the initial analysis is only performed in one way (from the specified UTC day to its neighboring days) as this is sufficient as three non-neighboring days for the initial analysis are used. The days for the initial analysis are selected at random while taking a variation of the day of week and time of year into account. This resulted in using the data of 03 April 2019, 19 July 2019, and 12 January 2020.

7-1-3 Data Analysis

With the data preprocessed, an initial analysis on a subset of the obtained data as mentioned in subsection 7-1-2 is conducted. Mainly, the flight data is assessed to justify the size of the chosen extraction region. Besides this, the quality of the data and the characteristics of the trajectories and aircraft are discussed.

In the most optimal scenario, all flights are within the extraction region such that the complete trajectory of each flight is known. A downside of enlarging the extraction region is the large amount of data to handle, adding both time by downloading from the FlightRadar24 servers and processing the data. Therefore, the extraction region stated in subsection 7-1-1 has been chosen.

First of all, the continent pairs of aircraft crossing the North Atlantic region are assessed. The continent pairs of the three days combined are displayed in Figure 7-4 and the per day continent pairs are displayed in Figure 7-5. Both are visualized in absolute values and percentages. The percentage variations between the days appear to be negligible. Therefore, further analysis is performed on the total set. Looking at the

graphs, by far most flights have Europe (EU) and North America (NAM) as origin and destination and vice versa. These continents are largely within the specified extraction region. Other continent pairs with a substantial contribution are Asia (AS) - North America (NAM) and Europe (EU) - South America (SA). Asia and South America are largely and entirely, respectively, outside the extraction region. Further analysis is required to detect the part of the trajectories of these flights that are outside the extraction region and their significance. When assessing the least represented continent pairs, it turns out that the NAM-SA pair can be discarded and the AF-EU and AS-EU pairs apart from entries from Iceland (IS ISO country) are not relevant to the problem and can be discarded as well. The result of these operations can be seen in Figure 7-6.

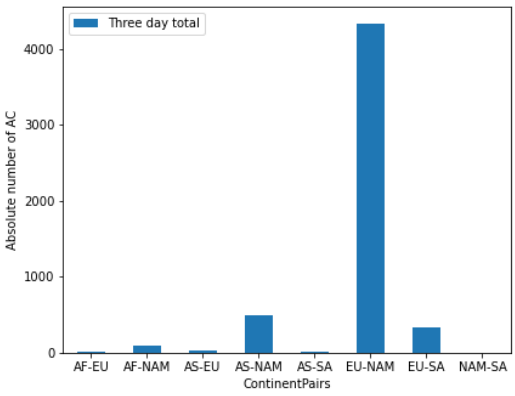

(a) The total number of continent pairs over a three day period.

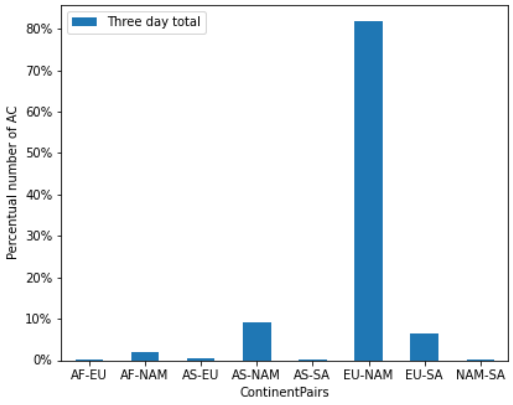

(b) The percentage of continent pairs over a three day period.

Figure 7-4: The total continent pairs for three random days.

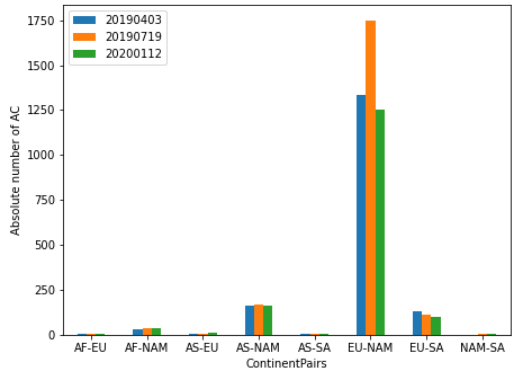

(a) The number of continent pairs per day.

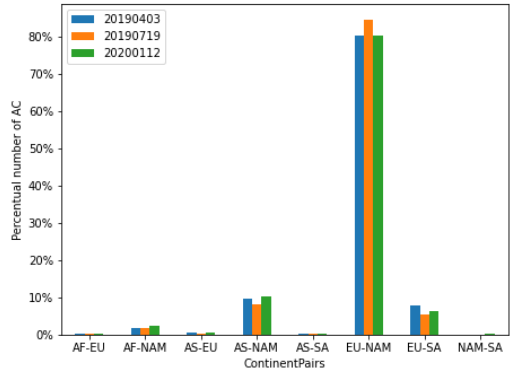

(b) The percentage of continent pairs per day.

Figure 7-5: The continent pairs per day for three random days.

Now the potential relevant flights that cross the NAT FIR have been examined by continent pairs, they will be assessed by their origin and destination airport coordinates.

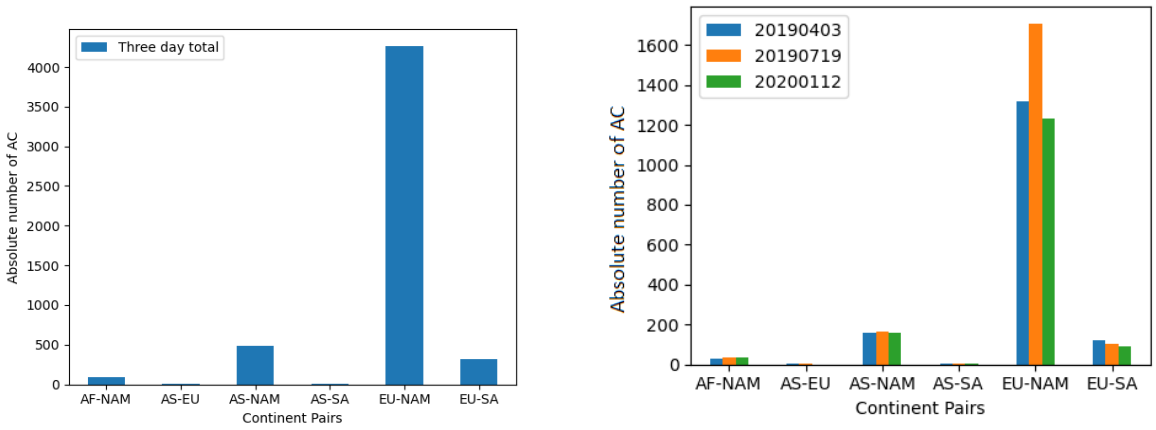

(a) The total number of continent pairs per day after discarding irrelevant pairs.

(b) The percentage of continent pairs per day after discarding irrelevant pairs.

Figure 7-6: The continent pairs after discarding irrelevant pairs.

Flights with one or both airports outside the extraction region are displayed in Figure 7-7 by their continent pairs. This shows a high number of airports outside the extraction region for the AF-NAM, AS-NAM, EU-NAM, and EU-SA continent pairs of which the EU-SA continent pair has a high contribution (over 50%). Around 11% of the aircraft crossing the NAT FIR have one or both airports outside the extraction region. This is a substantial amount and its significance is assessed by looking at the capture ratio Figure 7-8. The capture ratio is defined as the ratio of the trajectory distance outside the extraction region to the total trajectory distance. When taking a closer look at the number, for 87% of the flights 99% or more is captured and for 90% of the flights 95% or more is captured. Therefore, it can be concluded that most flights are sufficiently captured.

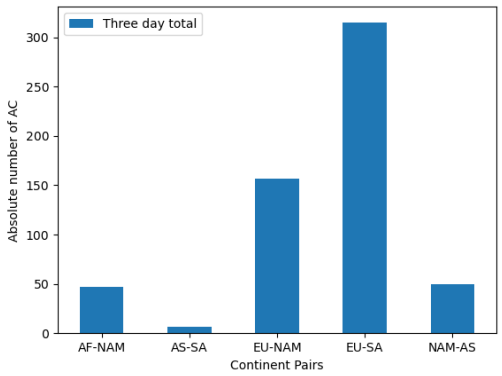

Figure 7-7: The total number of aircraft per continent pair with at least one airports outside the extraction region.

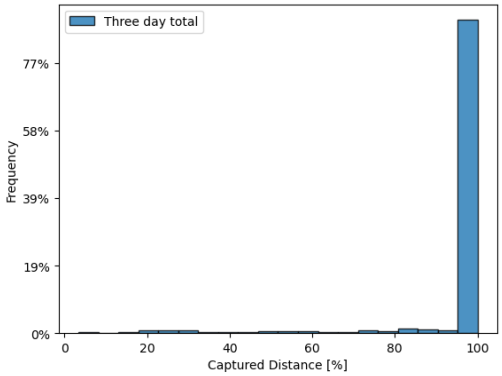

Figure 7-8: The captured distance as percentage of the total distance

Now, the trajectory and flight characteristics can be analyzed. First, the distance of

the trajectory in the NAT FIR as a percentage of the total trajectory is displayed in Figure 7-9. The ratio covers the whole spectrum with the majority between 20% to 60%. A substantial part of the flights has a large part outside the NAT FIR. This should be taken into account when deciding on which part of the flight trajectory to use for trajectory optimization.

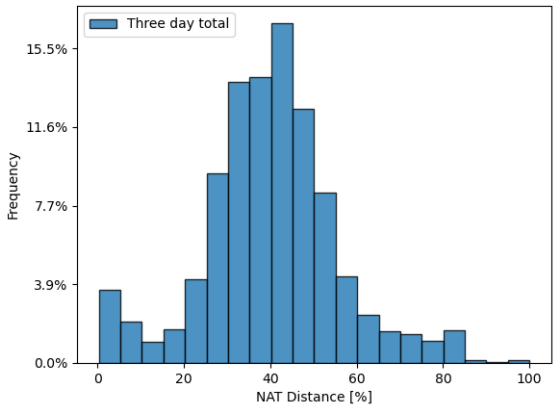

Figure 7-9: The distance in the NAT region as percentage of the total distance.

Another parameter of interest is the distance the aircraft fly. These are displayed in Figure 7-10. Some trips cover a distance of less than 3000 km. These are flights that cover Iceland-Greenland and Canada-Iceland. On the other side of the spectrum, distances of over 13000 km, are predominantly flights between the US-Gulf States and US-Africa. The majority of flights have a distance between 5000 and 10000 km.

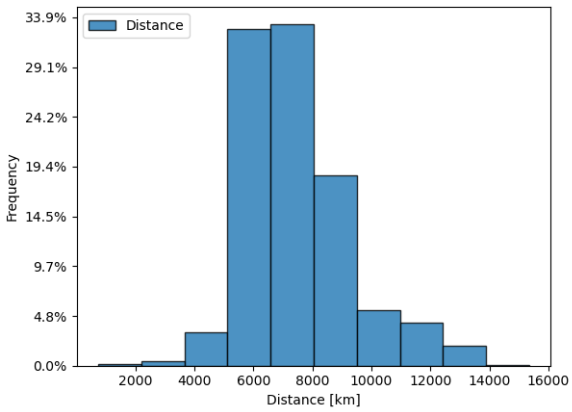

Figure 7-10: The total flight distance of aircraft passing the North Atlantic region.

Furthermore, the aircraft types crossing the North Atlantic region are assessed. For visualization, the aircraft are grouped by their model and different versions are discarded (for example: B747-400 and B747-800 are grouped under B74). Models which are encountered less than six times over the three-day period are discarded. In Figure 7-11,

it can be seen that by far most aircraft crossing the Atlantic are commercial jets of Airbus and Boeing albeit a wide range of models. Most of these aircraft belong to the wide-body aircraft class. Besides the Airbus and Boeing model, there are some models less represented on the right side of the graph. These are mostly private jets, apart from the DH8(B/D) (Turboprop commercial) and the MD11 (Commercial Jet).

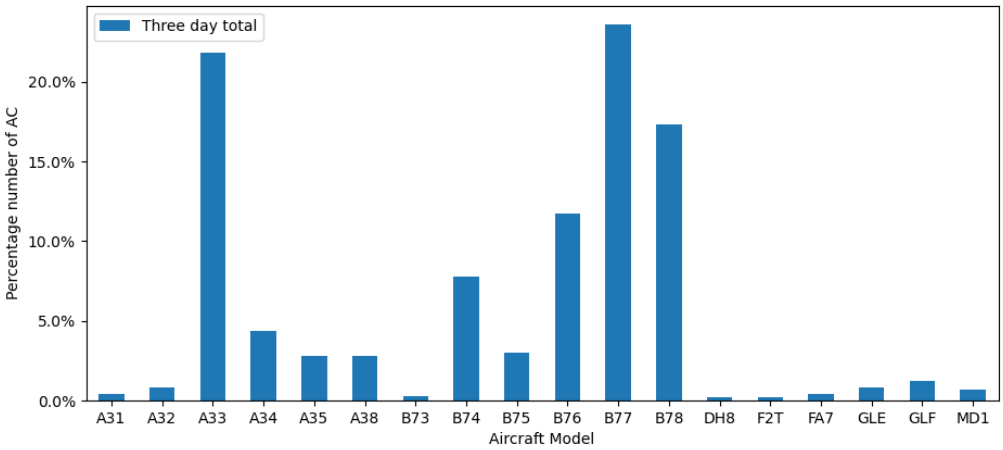

Figure 7-11: The models of the aircraft crossing the North Atlantic region as a percentage of total aircraft.

7-1-4 Additional Data

Besides the flight data, additional data is required. The predicted required data is elaborated upon below and contains geographic and practical data on airports, aircraft, FIR, and North Atlantic Organized Track System (NAT-OTS).

Airport Data

Airport data is used from OurAirports[2]. This data source contains the IATA code, continent, ISO country, elevation, and coordinates, amongst others. This information is used to match airport information about the origin and destination with the flight data in case of missing data. Furthermore, there appears to be an issue in the FlightRadar24 (FR24) data where the destinations stated in Schd_{to} and Real_{to} are incorrect or swapped. Position data is considered to be leading and the correct destination is determined by aligning position data with the airport coordinates presented in the airport data file.

id	ident	type	name	latitude	longitude	elevation_ft	continent	iso_country	iso_region	municipality	scheduled_service	gps_code	iata_code
2513	EHAM	large_airport	Amsterdam Airport Schiphol	52.31	4.76389	-11	EU	NL	NL-NH	Amsterdam	yes	EHAM	AMS

Figure 7-12: Structure of the airport data.

[2] https://ourairports.com/data/, Nov 2020

Aircraft Data

To access aircraft data, the database of OpenSky[3] is used. This database contains ICAO DOC 8643 information on aircraft which are most commonly provided with ATS. It includes information on the aircraft description, designator, number of engines, engine type, and Wake Turbulence Category (WTC), amongst others.

AircraftDescription	Description	Designator	EngineCount	EngineType	ManufacturerCode	ModelFullName	WTC
LandPlane	L2J	J328	2	Jet	328 SUPPORT SERVICES	Dornier 328JET	M

Figure 7-13: Aircraft type data according to DOC8643.

Flight Information Region Data

To determine the boundaries of the FIR, the coordinates have to be obtained. This information has been extracted from[4]. Each flight information region is extracted separately and they are combined to obtain the navigation region. This information is used to determine what part of a flights' trajectory is in the North Atlantic Region.

North Atlantic Track Data

At last, the information of the NAT-OTS location is of interest. Every day Notice to Airman (NOTAM) are transmitted. These can be read and a 365-day database is available at BlackSwan[5]. A local database has been constructed to save a longer time history than 365 days. This local database contains information from Track Message Identification (TMI) 322-2019 up to now. This means that some information on the NAT locations for the first months of the flight data set is missing. The data is stored in the same way as displayed in Figure 2-5.

7-2 Flight Trajectory Construction

With the data analysis performed, the flight trajectories are constructed. The optimization assumptions and boundaries are determined partially based on this analysis. It shows that most flights cover a distance larger than 2000 Nm, which justifies the use of Wind-Optimal Route (WOR) [40]. Furthermore, the literature states that the lower airspace is restricted by operations like Standard Instrument Departures (SID) and Standard Arrival Routes (STAR). This part of the route will not be optimized and the optimization focuses on the part of the trajectory above 10,000 ft.

As mentioned in section 3-2, the vertical and horizontal flight profiles are weakly coupled and are considered individually. Constructing the vertical and horizontal profiles is elaborated upon below.

[3] https://opensky-network.org/datasets/metadata/, Nov 2020
[4] https://www.arcgis.com/home/webmap/viewer, Dec 2020
[5] https://blackswan.ch/northatlantictracks

7-2-1 Vertical Flight Path

To construct the vertical flight profile, aircraft specific information from Base of Aircraft Data (BADA) will be used together with an initial weight estimate as stated in section 5-2-1. As vertical flight path optimization is not a research objective of this thesis, a relatively simplistic approach is taken. This approach is described below. The vertical flight profile starts and ends at 10,000 ft altitude.

First, the climb phase starts by calculating an initial estimate of the optimal cruise altitude for this weight and optimal V_{TAS}. Optimal V_{TAS} is determined by taking the cruise Mach number at maximum altitude for International Standard Atmosphere (ISA). While not within a predefined limit of this estimate, the aircraft climbs according to the in section 3-2-1 stated BADA approach. Meanwhile, the aircraft burns fuel and the weight decrease requires an update for the optimal cruise altitude. As soon as the actual altitude is within a predefined limit of the optimal altitude, the cruise phase starts. The point where descent should start can be calculated by backward calculation from the destination using the BADA descent operations.

The climb and descent operations are already incorporated via a top of descent and top of climb logic in BlueSky. The above approach is taken to determine the optimal cruise altitudes for a randomized initial and decreasing weight.

Depending on the resolution domain of the tactical resolution method, a thrust margin can be incorporated to guarantee sufficient vertical deviation manoeuvre capabilities. This assures that aircraft have sufficient thrust to perform a 1000 ft climb operation to avoid a conflict. The thrust margin is defined as the maximum cruise thrust minus the thrust required to maintain 100 ft/min rate of climb at the selected airspeed and optimal altitude [35] [39].

7-2-2 Horizontal Flight Path

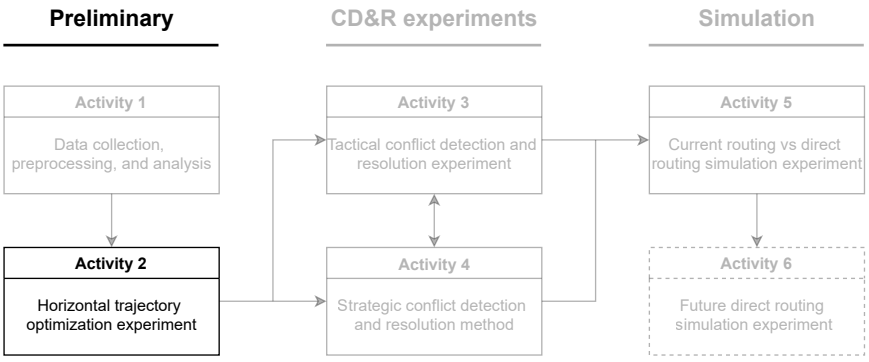

Figure 7-14: Corresponding phase of the thesis flowchart.

To get some preliminary insight into the horizontal trajectory generation process, a preliminary experiment has been set up. This preliminary experiment has been designed for several purposes. First of all, two promising methods are worked out and compared

to choose the best performing one in terms of flight time and computational time. Assessing the flight time is of importance to decide which method results in the highest performance increase, while the computational time is of importance to see whether the method is suited to model all flights crossing the North Atlantic region during a one year period. At last, the number of conflicts is assessed for the best performing method to estimate if a strategic deconfliction method will be required.

From this preliminary experiment, it has been concluded that the ordered upwind algorithm suits the purpose best and will be used for the remainder of this thesis. Computing all flights for the three days yielded an estimated computational time of 36.7 days. A strategic deconfliction method might be necessary due to the characteristics of the wind-optimal trajectories. These findings are used in the methodology for the following research activities. A more detailed discussion on the preliminary experiment can be found in Appendix A.

Based on the preliminary experiment with the mentioned computational time above, some proposals are made to reduce this time. First of all, no optimization is required for flights covering a distance shorter than 2000 NM and these are set to fly their Great Circle Route (GCR) as no significant gains are obtained from flying WOR [40]. Then, flights that depart within the same 3-hour wind data interval with equal origin-destination are grouped to avoid duplicate calculations. These measures would result in an estimated 17.3% reduction, bringing down the computational time to 30.3 days. Using the TU Delft PC's, this would be reduced to around 3.8 days. If this is still considered to be too large, additional measures could be taken. Flights that only have a small percentage in the North Atlantic airspace can be removed. These flights mostly cross the North Atlantic far North connecting Asia/Northern Europe with North America or cross the North Atlantic far south connecting Southern Europe with South America. In general, flights connecting Europe with South America are more south and do not add traffic to the condensed areas. All the above measures combined would lead to a reduction of around 25%, resulting in a computational time of 3.4 days.

If the above-mentioned strategies still not result in a sufficient reduction of computational time, some more aggressive approaches have to be taken. For instance, the number of grid points in the ordered upwind algorithm could be reduced, the wind data grid density could be reduced, the wind data time interval could be increased, trajectory calculations could be used for city pairs within the same region, and the flight data set could be halved by taking every other day. One or a combination of these approaches could be implemented at the cost of decreasing the fidelity of the model.

Furthermore, some adjustments are made compared to the preliminary experiment. The start and end point of the optimization are changed from origin and destination to the first and last location at 10,000 ft. It might be that one or more of these locations are not present in the flight data as they lie outside the extraction region or it is not captured by the ADS-B network. The average distance from departure/arrival to/from FL100 is calculated and used to determine the initial/final location along the GCR (based on origin-destination). The horizontal trajectories will be computed for an the maximum altitude according to BADA. Also, the constant altitude and constant true airspeed during climb and descent assumptions are modified in line with the vertical

flight path construction. Integrating the vertical and horizontal optimization methods will result in a sub-optimal trajectory. However, finding a global optimal trajectory is too computationally expensive (subsection 3-2-2). The optimized routes are validated by comparing the travel time to the actual routes, which should be lower on average.

7-3 Conflict Detection and Resolution

With the optimal trajectories constructed, the safety and the stability of the airspace will be assessed. First, the tactical conflict detection and resolution experiment will be elaborated upon. The performance indicators to measure safety, stability, and efficiency are stated as well. Then, the selected strategic conflict detection and resolution method are explained and how it will be integrated into the thesis if necessary.

7-3-1 Tactical Conflict Detection and Resolution Experiment Design

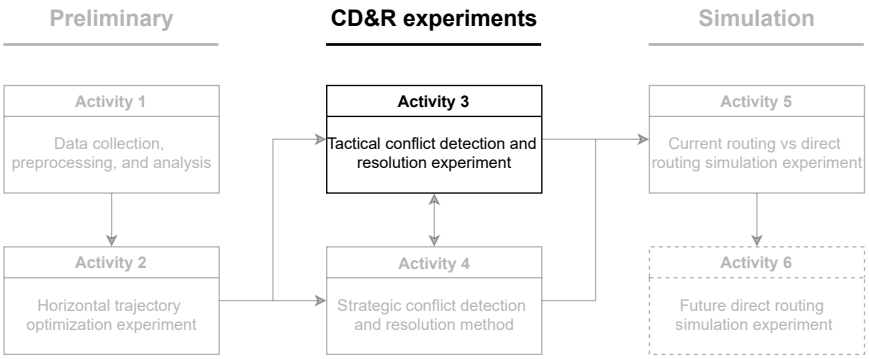

Figure 7-15: Corresponding phase of the thesis flowchart.

As mentioned in subsection 4-1-2, decentralization of ATC by shifting control to the flight deck is advantageous for the overall efficiency, while maintaining safe separation. It can be implemented in remote areas like the North Atlantic region, due to improvements in technology. Several detection and resolution methods have been developed on the tactical level. The method that will be used for this thesis is the Modified Voltage Potential (MVP). This method performs best in terms of route efficiency, time efficiency, fuel efficiency, and other practical aspects [7].

Experiment Goal

Previous research has shown that airspace with a high traffic density remains manageable for a direct routing structure in combination with MVP. Although this has been shown, the safety and stability of the airspace might be influenced by the different routing structure and presumably changing conflict characteristics of flying WOR. An experiment is set up to see how the MVP behaves for different resolution domains under this routing structure.

The main aim of this experiment is to find the most fuel-efficient resolution domain for the wind-optimal trajectories in the North Atlantic region. Besides computing the overall fuel consumption, it has to be shown that safe separation and stability are maintained under the tactical conflict resolution domain. Furthermore, this experiment is conducted to see whether all conflicts are resolved or if a strategic deconfliction method is required.

Traffic Scenarios

The MVP resolution domains that will be researched are the lateral and vertical ones, as speed changes are considered to be fuel inefficient and violate the constant true airspeed constraint for the cruise phase. This results in two simulation scenarios with the MVP resolution method set to either domain. It is of interest how this affects performance for the optimized trajectories, so these trajectories are considered.

To assess the fuel efficiency, the fuel consumption is calculated in BlueSky according to the method elaborated upon in section 5-2. Furthermore, safety and stability are assessed. To measure safety, the number of losses of separation are counted. This is combined with the severity of intrusion to get a more detailed view of the overall safety, as one could argue that a minor intrusion at 5 NM should not count as heavy towards the overall safety as a near miss. To assess the stability of the airspace when a resolution method is used, the primary and secondary conflict count can be determined with the Domino Effect Parameter. To compute this measure, a third scenario without a conflict resolution method has to be simulated. This third scenario allows for verification of the tactical conflict detection and resolution method.

The three scenarios will be simulated for the three previously selected days to get a more extensive overview of how the different resolutions domains perform under different optimized trajectories due to different wind conditions and to different traffic levels. As the resolution domain is researched, the conflict detection parameters are set to 5 NM radius and 1000 ft altitude for the protected zone and a 300 s look-ahead time is used in line with previous research.

Unlike the trajectory optimization region, which covers the whole trajectory within the extraction region, the simulation region is set to roughly the size of the North Atlantic airspace (15°N, 80°W, 90°N, 10°E) in BlueSky. Additional filtering has to be applied to filter out the actual conflicts outside the North Atlantic Region. The reason for this reduced area is that the conflict count outside this region is not representative in absence of remaining traffic. Furthermore, the size of the experiment area is not relevant for the fuel consumption as long as the area is equal for the different scenarios.

Simulation Setup and Procedure

The simulations will be conducted with the use of the BlueSky Air Traffic Management (ATM) simulator. The trajectories will be loaded in a scenario file as waypoints. Two types of waypoints can be used; lateral waypoints (latitude and longitude) and lateral/vertical waypoints (latitude, longitude, altitude, and speed). BlueSky operates

with a soonest climb and latest descent logic based on aircraft specific performance. The optimized routes use the same performance parameters as BlueSky. Therefore, a lateral/vertical waypoint is added at the start of the trajectory, at each step climb during the cruise phase and at the end of descent. Lateral waypoints are used in between these points to indicate heading changes. The implementation in the vertical and lateral plane are shown in Figure 7-16 and Figure 7-17.

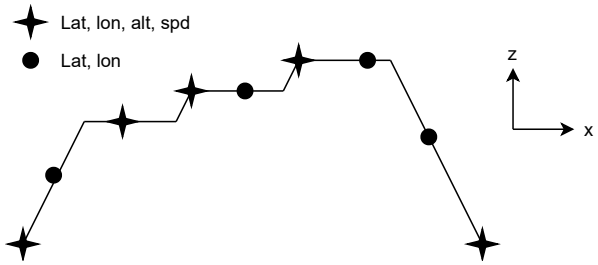

Figure 7-16: Vertical representation of the waypoints for the optimized trajectory in the BlueSky scenario.

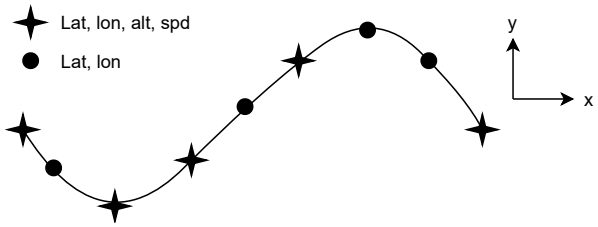

Figure 7-17: Lateral representation of the waypoints for the optimized trajectory in the BlueSky scenario.

To reduce the overall trajectory information passed by the scenario file to the simulation, only points of the optimized trajectory will be used if the aircraft state (altitude, heading, velocity) changes beyond a threshold. This threshold will be based on a trade-off between the simulation time and the trajectory fidelity and applies to all scenarios.

Furthermore, the trajectories have to be written correctly to the scenario files when considering the presence of wind. The BlueSky plugin *WindGFS* is used to load wind fields in the simulation. This plugin extracts reanalysis data from National Oceanic and Atmospheric Administration (NOAA)[6] at a three-hour interval rate. It should be noticed that this source differs from the reanalysis data used by the trajectory optimization algorithm (European Centre for Medium-Range Weather Forecast (ECMWF)). However, it is assumed that the differences are minor and can be neglected. The optimized trajectories take the wind field into account when creating the trajectory by backward propagation but constant true airspeed is assumed for the cruise phase. Therefore, the true airspeed is converted to the calibrated airspeed (kts) assuming ISA and the wind is loaded separately via the plugin.

[6] https://www.ncei.noaa.gov/data/global-forecast-system/access/historical/analysis/, May 2021.

The trajectories of all flights crossing the North Atlantic region during each selected day (24 hr) are included, meaning some exceed the selected day time window either prior or after. One hour before the selected day is included in the simulation to allow for traffic built-up. Then, the data logging happens over the time window of the selected day and the simulation stops at the end of the selected day. The fuel consumption, Loss of Separation (LoS), intrusion severity, and conflicts are logged.

Independent, Control, and Dependent Variables

The independent variables of this experiment are the following:

- Conflict resolution domain (no resolution, lateral, and vertical)

The following control variables are used for this experiment, from which most have been elaborated upon above:

- The traffic for each selected day (trajectory, velocity, and aircraft type)
- The initial mass estimation for each aircraft
- The experiment area
- The simulation duration
- The conflict detection parameters

The dependent variables are the measures that are logged and have already been mentioned in the simulation scenarios paragraph above:

- Total fuel consumption
- Number of LoS
- Intrusion severity
- Domino Effect Parameter

Expectation

The best performing resolution domain will be used for the remainder of this thesis. Although fuel efficiency is considered important for this research, airspace safety and stability are of importance due to the industries' focus on safety. In the unlikely event that both domains perform equally, the vertical domain will be chosen as this is in line with pilot preferences of solving conflicts. It is expected that the vertical resolution domain will perform better due to the shape of the protected zone. Furthermore, the expectation is that all conflicts can be resolved and the simulation does not require a strategic deconflicting method as the traffic densities in the North Atlantic region are relatively low.

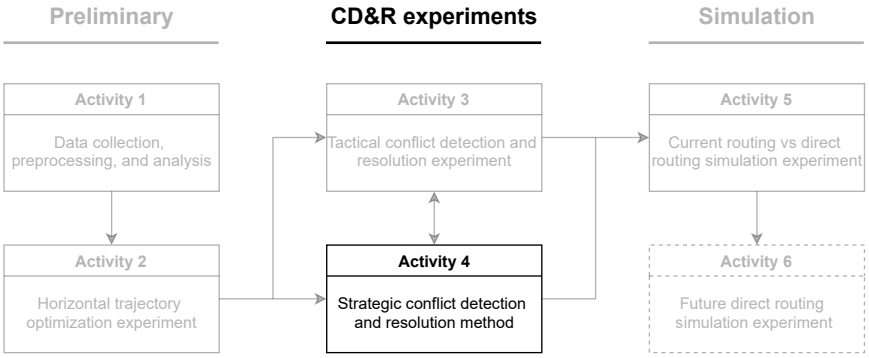

Figure 7-18: Corresponding phase of the thesis flowchart.

7-3-2 Strategic Deconflicting

One of the goals of the tactical resolution experiment is to determine whether the tactical resolution method solves all conflicts and no LoS occur. A strategic resolution method is incorporated into the model if this is not the case. This section elaborates upon the chosen method that will be used if deemed necessary.

Strategic Conflict Detection

Before a strategic resolution method can be applied, conflicts have to be detected upfront. To detect conflicts, the optimized trajectories are investigated before departure. The same protected zone dimensions are used for the tactical method, 5 Nm radius and 1000 ft altitude. A 4D grid approach is taken, based on the protected zone [15] [54]. The spatial dimensions of this grid are 5Nm by 5Nm by 1000 ft. The fourth dimension (time) is chosen such that all conflicts are captured. Assuming a maximum aircraft speed of 500 kts and a maximum wind speed of 100 kts, the maximum total velocity is 600 kts. Therefore, the time step has to be 5NM/(10NM/min) = 30 seconds or smaller. Each trajectory point is stored in a cell laying on the 4D grid. This grid-based interaction detection scheme is stored as a hash table to improve the computational performance. A conflict is identified if a non-empty cell is co-occupied by another aircraft or a surrounding cell (26 cells) contains another aircraft at time t. This complexity can be reduced by setting aircraft altitude to multitudes of 1000 ft leaving only 9 cells to be investigated.

Strategic Conflict Resolution

With the conflicts detected according to the method described in the previous paragraph, the conflicts have to be resolved. The method selected based on the literature research is simulated annealing in combination with a local search algorithm. This method is capable of significantly reducing the number of conflicts within a reasonable time and has been applied to the North Atlantic region in previous research. Furthermore, it is suitable for applying both a time shift and a trajectory modification. This is expected to be a favourable combination for two reasons. First, time shifts add little

to no extra fuel consumption to the system making sure it remains fuel-efficient. Time shifts are assumed to be positive with a maximum of 30 minutes. For a minor shift like this, no change in the wind field is assumed. Secondly, WOR might result in heavily congested areas and the trajectory modification capability allows to direct flights away from these areas. The shape is modified by applying a bijective transformation between an arbitrary curve on a sphere and a curve on the Cartesian plane [17]. A smoothing function is used as in Equation 4-2, where the shape modification is bounded by the function curvature b^f and a maximal deviation value Y.

Both the process of selecting a trajectory and the process of determining whether to use a time shift or a shape modification can be either rule-based or random. It is suggested that a rule is established to find flight pairs with multiple conflicts and deconflict these by applying a time shift first as this is fuel and computationally efficient. Once this has been done, it is tested if the reduction in conflicts is sufficient to be handled by the MVP on the resolution domain selected in research activity 3. If this still yields too many conflicts to be handled, shape modifications can be applied to trajectory pairs that still contain conflicts. The rules should be established in line with the simulated annealing and local search modules of the method.

It is noted that the deconflicting method based on simulated annealing with local gradient search assumes constant altitude which is not the case for this thesis. Modifying the trajectory in shape means flight time increases, impacting the optimal altitude. As altitude increases for decreasing weight, an aircraft will fly at a sub-optimal altitude for the extra added time due to the shape modification. It is assumed that the additional flight time does not influence the initial weight and the aircraft follows the computed vertical profile up to the maximum calculated altitude. The additional flight time due to the shape modification is flown at that altitude up to the start of the descent.

If the strategic deconfliction method does not result in a sufficient decrease of conflicts to be handled by the MVP, the time shift and shape modification constraints can be relaxed. This will come at a cost of decreased fidelity (regarding wind data) and fuel efficiency (large trajectory modifications).

7-4 Simulation Setup

Now the trajectory optimization and conflict detection and resolution methods have been selected by conducting the previous research activities, the simulations are elaborated upon. The first simulation compares the current routing scenario to the direct routing scenario and is described in subsection 7-4-1. When there is time left, the simulation described in subsection 7-4-2 will be conducted.

7-4-1 Current Routing vs. Direct Routing Simulation

This is the research activity where the results of the preliminary activities and the CD&R experiment activities join to create the main simulation and answer the research question.

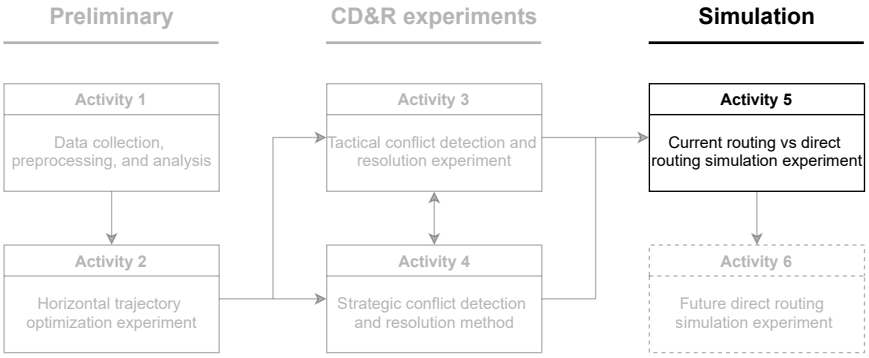

Figure 7-19: Corresponding phase of the thesis flowchart.

Experiment Goal

This research activity is performed to compare flights crossing the North Atlantic region under the current routing structure to the direct routing structure. Part of this research activity is to validate the direct routing scenario by comparing it to the actual flights. The scenarios are compared by the overall fuel consumption, safety, and capacity.

Traffic Scenarios

The two different traffic scenarios are constructed based on the current routes from ADS-B data and the optimized routes. The construction of the optimized routes has been discussed in section 7-2 and, based on the results of research activity 3, in subsection 7-3-2. For this simulation, the year of flight data will be used. The reason for using a year of flight data is that it improves the robustness of the model as the North Atlantic region is subjected to seasonal variations in wind and traffic.

These scenarios will be assessed according to several performance indicators. The fuel consumption for each flight is calculated with the use of BlueSky according to section 5-2 and the overall consumption is compared. The safety is assessed by counting the numbers of losses of separation and the intrusion severity. No base scenario without a tactical resolution method will be constructed and, therefore, no airspace stability will be assessed. At last, the airspace capacity will be assessed by looking at the traffic density of the simulation area according to Equation 5-3. The traffic density is monitored at a fifteen-minute time interval.

Furthermore, the tactical conflict detection parameters are set to a 5 NM radius, 1000 ft altitude, and a 300 s look-ahead time and the resolution domain is set to the result from research activity 3. The simulation area is set to approximately the North Atlantic region (15°N, 80°W, 90°N, 10°E) in BlueSky for the same reason as mentioned in subsection 7-3-1.

Simulation Setup and Procedure

This simulation will make use of the BlueSky ATM simulator as well. Both the actual and the optimized routes will be loaded in separate scenario files. To reduce the computational time and improve the simulation efficiency, the routes are simplified. This

is done by only including points once the aircraft state changes beyond a threshold (as stated in section 7-3-1). Both the optimized and actual routes will have a starting and ending point at an altitude of 10,000 ft to capture the trajectory above this limit. The optimized routes follow the BlueSky climb and descent logic and will be constructed according to the same way as displayed in Figure 7-16 and Figure 7-17. However, the actual routes do not follow a climb and descent procedure that differs from the BlueSky logic and this has to be accounted for when constructing the current routing scenario. The fuzzy logic from section 5-3 is used to determine the points in the climb and descent phase. These points are included to get an accurate representation of the fuel consumption in both phases. For the points that are not part of one of these two phases, the same threshold logic as in section 7-3-1 is used. This yields the representations in Figure 7-20 and Figure 7-21.

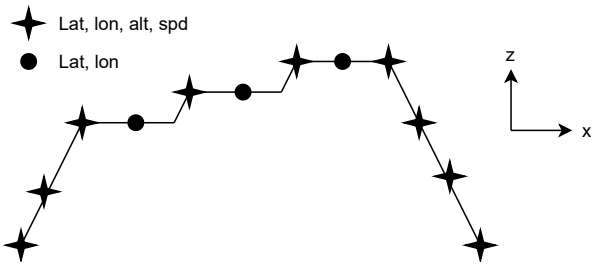

Figure 7-20: Vertical representation of the waypoints for the actual trajectory in the BlueSky scenario.

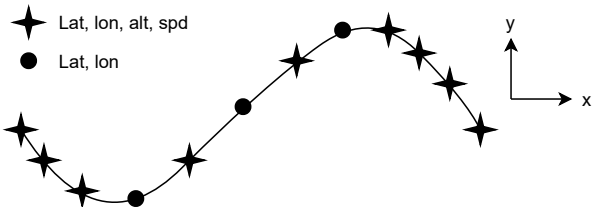

Figure 7-21: Lateral representation of the waypoints for the actual trajectory in the BlueSky scenario.

When incorporating the wind in BlueSky for the optimized trajectories, the same approach as in section 7-3-1 is used. As FlightRadar24 provides the ground speed of the aircraft, the true airspeed is obtained by subtracting the wind speed from the ground speed. This true airspeed is converted to the calibrated airspeed assuming ISA. For both scenarios, the BlueSky *WindGFS* plugin is used to mimic the wind fields in the simulation.

Simulating a year of traffic in BlueSky requires time. Therefore, the simulation is split up in monthly intervals to avoid data loss. Traffic peak hours above the Atlantic are roughly between 01:00 and 19:00 UTC. To start the simulation each month, 1 hour of traffic built-up is allowed, starting at 00:00. The data logging starts at 01:00 on the first day and ends at 23:59 on the last day of the month. All performance indicators are logged.

Independent, Control, and Dependent Variables

The independent variables of this experiment are the following:

- The trajectories of the traffic (actual and optimized)

The following control variables are used for this experiment, from which most have been elaborated upon above:

- The origin, destinations, and aircraft type for each day.
- The initial mass estimation for each aircraft
- The wind field (*WindGFS* plugin)
- The simulation area
- The simulation duration
- The conflict detection parameters
- The conflict resolution domain

The dependent variables are the measures that are logged and have already been mentioned in the traffic scenarios paragraph above:

- Total fuel consumption
- Number of LoS
- Intrusion severity
- Traffic density

Expectation

It is expected that the direct routing scenario performs better in terms of efficiency than the current routing scenario. This means that a reduction of overall fuel consumption is established. No changes in LoS are expected as none are present in the current scenario and it is expected that conflicts will be resolved in the direct scenario. The same holds for the intrusion severity. Aircraft are expected to cross the North Atlantic region faster when flying WOR, resulting in a decreased traffic density.

7-4-2 Future Direct Routing Simulation

North Atlantic travel is expected to increase over the coming years (section 2-1-3) and research has shown that a direct routing structure could decrease the airspace capacity for high levels of traffic due to instability effects. This activity looks into the robustness of the direct routing structure in the North Atlantic region for future forecasted aviation growth.

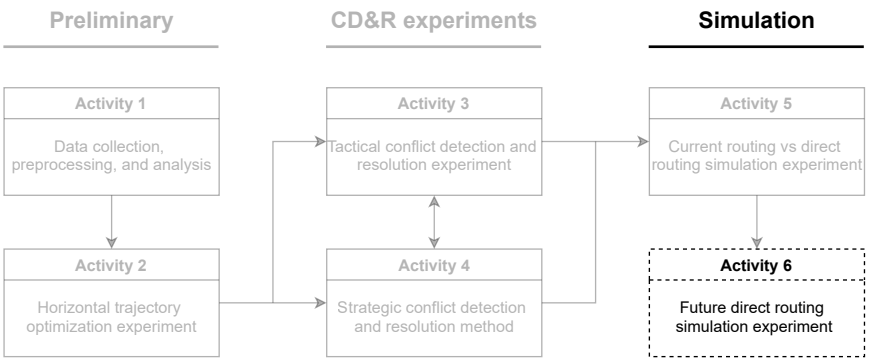

Figure 7-22: Corresponding phase of the thesis flowchart.

Experiment Goal

This research activity aims to show that the direct routing scenario is capable of dealing with the expected growth, rather than showing that the direct routing scenario is a more effective way of dealing with higher traffic levels than the current routing structure. This, as there are various uncertainties in how the current routing structure will develop for increasing traffic. The scenarios are assessed by their safety and capacity.

Traffic Scenarios

To generate the future scenario, a subset of three days is created by selecting the three days with the highest number of aircraft crossing the North Atlantic region. These days are considered to be in the peak week traffic of either 2019 or 2020. According to Figure 2-6, the traffic level on each selected day is scaled percentage-wise to the 2038 high traffic level forecast. The increase in traffic is realized by adding dummy flights to the flight data sets of the selected days. As there are uncertainties to how the network will develop, the origin-destination pairs are picked at random from a set of existing pairs. Eastbound and westbound flights are set to depart at random times within the NAT-OTS peak times as departures are considered to be constraint by customer demands. No flight can depart from the same airport at the same time as another flight. The trajectory is similar to the trajectory of an origin-destination pair of that particular day if their departures are within a three-hour window (wind field update interval). Otherwise, the trajectory has to be computed.

This future scenario is compared to the results of the direct routing scenario for the selected days. They are compared by their safety and capacity. The safety is quantified by the number of losses of separation and the intrusion severity, the capacity by the traffic density in the simulation area as explained in research activity 5.

Furthermore, the tactical conflict detection and resolution method are set to the results of research activity 3. Whether a strategic deconfliction method is used, is based on the results of research activity 3, hence, the implementation of such a method in the optimized routes of activity 5. The simulation area is set to approximately the North Atlantic region (15°N, 80°W, 90°N, 10°E) in BlueSky for the same reason as mentioned in subsection 7-3-1.

Simulation Setup and Procedure

All the trajectories in the future scenario are wind optimized trajectories that follow the BlueSky climb and descent logic. Therefore, the trajectories written to the scenario file are constructed the same way as the optimized routes in Figure 7-16 and Figure 7-17 and the same threshold logic applies. Also, the future scenario uses the wind plugin to mimic the same conditions as in the simulation of activity 5.

To compare the same performance metrics, it has to be decided if the selected days are the first day of the month. If so, a traffic built-up of an hour from 00:00 UTC is used and the data is logged over the remainder of the day. If this is not the case, the traffic can be built up from 23:00-23:59 UTC the day before and the data is logged over the whole day to create equal circumstances for a fair comparison with the direct routing scenario. All performance indicators mentioned above are logged.

Independent, Control, and Dependent Variables

The independent variables of this experiment are the following:

- The traffic level in the North Atlantic region (current and forecasted)

The following control variables are used for this experiment, from which most have been elaborated upon above:

- The wind optimized trajectories of the current traffic
- The origins, destinations, and aircraft types for each day
- The initial mass estimation for the current flights
- The wind field (*WindGFS* plugin)
- The simulation area
- The simulation duration
- The conflict detection parameters
- The conflict resolution domain

The dependent variables are the measures that are logged and have already been mentioned in the traffic scenarios paragraph above:

- Number of LoS
- Intrusion severity
- Traffic density

Expectation

Overall, the future network is prone to several uncertainties including but not limited to demographics, governance, innovations, and customer demand. Only limited conclusions for the future direct routing structure can be drawn from this research activity, taking into account that the future scenario is merely an extrapolation of the current circumstances.

Chapter 8

Conclusion

Air traffic in the North Atlantic region is restricted by a predefined Organized Track System (OTS). In absence of Air Traffic Control (ATC) in remote areas, means of safe separation have been established in the past. The OTS facilitates east- and westbound tracks based on weather and flight information that guarantee safe separation. These restrictions result in an inefficient system as aircraft fly sub-optimal routes. The ever-growing flight demand in the North Atlantic corridor, together with a growing commitment to reduce emissions, urges the system to innovate. Technological advancements in surveillance, communication, and navigation systems such as Automatic Dependent Surveillance-Broadcast (ADS-B) allow for this restructuring. Research shows that the free flight principle is capable of lifting the posed limitations on the current airspace structure. Challenging the current, centralized Air Traffic Management (ATM) structure with a decentralized, direct routing approach is the subject of this thesis.

The research into this problem is divided into three phases; analyzing the obtained data and investigating the best horizontal trajectory optimization approach, researching Conflict Detection and Resolution (CD&R) methods, and simulating several scenarios. The data analysis shows that the aircraft data obtained from FlightRadar24 captures most of the flights that cover the North Atlantic region. For 90% of all flights, 95% of the trajectory is captured. Besides some private jets, most of the flights belong to the commercial class. The majority of the flights cover a distance over 2000 NM, being likely to benefit from flying Wind-Optimal Route (WOR).

The last outcome of the data analysis sparked the preliminary experiment in the best performing horizontal trajectory optimization method in presence of winds. Concluding that the ordered upwind algorithm is the best performing one considering both flight and computational time. Further simplifications such as grouping flights within 3-hour intervals and computing the Great Circle Route (GCR) for flights with distances lower than 2000 NM give the intended overall computational time. The horizontal trajectory is created for constant maximum altitude at Maximum Take-Off Weight (MTOW) according to the Base of Aircraft Data (BADA). The vertical flight profile is created by

assuming constant true airspeed during cruise and climbs & descents following BADA protocol. The overall structure of the WOR results in trajectories clusters, indicating that a strategic deconflicting method might be required.

Besides the preliminary phase, this report establishes a framework of activities to be conducted during the main phase. First, the conflict detection and resolution experiment phase is conducted. It is investigated which tactical resolution domain of the Modified Voltage Potential (MVP) performs best under the WOR routing structure. Both the vertical and horizontal resolution domain are compared and assessed by efficiency, safety, and stability. Once this experiment is conducted, a strategic deconflicting method based on simulated annealing with local gradient search is implemented if necessary. Once these two activities are completed, the simulation phase is conducted. The created direct routing scenario is simulated and compared to the current ATM structure scenario. At last, the future direct routing scenario is created and simulated. All simulations are performed in the ATM simulator BlueSky.

Due to time constraints, it is only possible to create a model with limited fidelity and sub-optimal airspace optimization. Further improvements to the model fidelity can be made by including Special Use Airspace (SUA) and all traffic (private/military) crossing the North Atlantic region. The trajectories can be further optimized by computing globally optimal 4D trajectories and reducing the wind interval rate.

Appendix A

Preliminary Experiment

During the preliminary phase of this thesis, an initial experiment has been conducted that is elaborated upon in this appendix. First, the experimental setup is outlined, then the results are stated and at last, conclusions are drawn.

A-1 Experiment Set-Up

To select a horizontal trajectory optimization strategy in presence of wind, two methods that have been promising in literature are implemented and compared. The initial goal is to select the best-performing method. They will be assessed according to two criteria that are deemed most relevant. First, the route efficiency will be determined by comparing the average flight time in seconds. The flight time is of importance to determine the most fuel-efficient method. Then, the computational efficiency will be assessed by comparing the average time to compute a single trajectory. This is important to make sure that all flights crossing the North Atlantic region during one year can be modeled within a reasonable time. The additional preliminary experiment goals are elaborated upon in the advanced analysis paragraph.

The selected methods are wind optimal extremals based on Zermelo's problem and the ordered upwind algorithm, on which more below. These two methods are compared without comparing them to the actual routes as literature supports that both methods result in a reduction of flight time/fuel consumption (subsection 3-2-2). As only horizontal strategies are considered and these are weakly coupled with the vertical strategy, a constant optimal cruise altitude is considered for the comparison next to assuming constant and equal cruise velocity. Flights from LHR to JFK and JFK to LHR (aircraft type B744) on the dates mentioned in 7-1-2 are used for the comparison.

Reanalysis data is obtained from the European Centre for Medium-Range Weather Forecast (ECMWF), consisting of the eastward (u) and the northward (v) wind components. Data covering the extraction region including bounds where possible (165.25W, 90N, 85.25E, 14.75S) is obtained. This extra observation is included to guarantee the interpolation of the wind data near the extraction region boundary. The data has a

horizontal resolution of 0.25x0.25 degrees and covers pressure levels corresponding to 9,882-44,647 ft at ISA. Wind data is updated at a 3-hour rate as wind changes at this rate are sufficiently minor, data storage is limited, and this is in line with the BlueSky wind extraction plugin.

Wind-Optimal Extremals

First, wind optimal extremals based on Zermelo's problem are used to construct horizontal trajectories. As mentioned in section 3-2-2, the main disadvantage of such methods is to find a good initial condition. Therefore, the algorithm is implemented on flights from LHR to JFK to assess its behavior with initial values spanning a 45-degree range (125-170 degrees) with an interval of 0.1 degrees. These trajectories are displayed in Figure A-1. Abrupt trajectory deviations are observed around 55-70°N, 30-40°W and around 30-40°N, 40-80°W. These deviations are caused by singularities in the trigonometric equations.

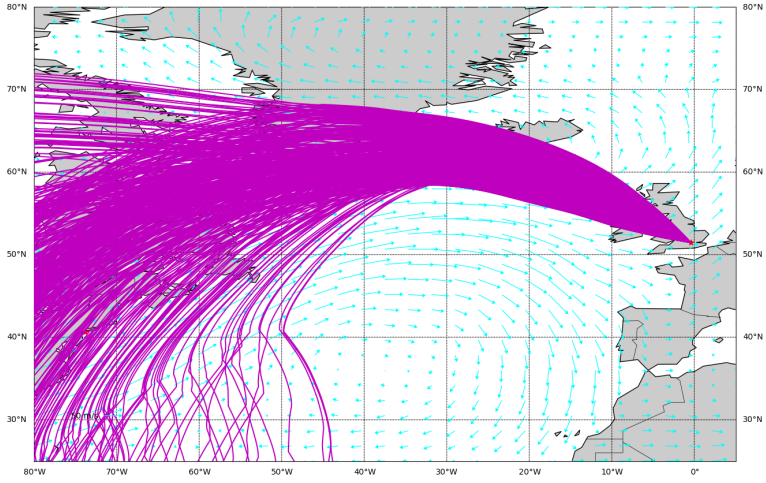

Figure A-1: Trajectories generated by wind-optimal extremals based on Zermelo's problem spanning a 45 degree initial heading range with a 0.1 degree interval.

Setting an upper limit for these changes in heading angle ($\dot{\psi}$) can solve this issue. However, choosing the exact limit is challenging as a high value does not solve for the large deviations and a low value does not allow for enough deviation resulting in unreachable areas (displayed in Figure A-2 on a Lambert conic conformal projection). The reachable area is specified as any location surrounded by two sufficiently close extremals. In the situation above, the southerly extremal is considered to be too far away. Other factors influencing the size of the unreachable area are the heading range interval and the orientation of the wind field.

To assess the performance and efficiency of the algorithm the following initial conditions are chosen. A heading range of 40 degrees (+-20 degrees) around the Great Circle Route (GCR) heading angle, a heading angle interval of 0.2 degrees, an upper limit of 3.5 degrees, and an integration time step of 10 seconds are set to make sure that the destination location lies within the reachable area.

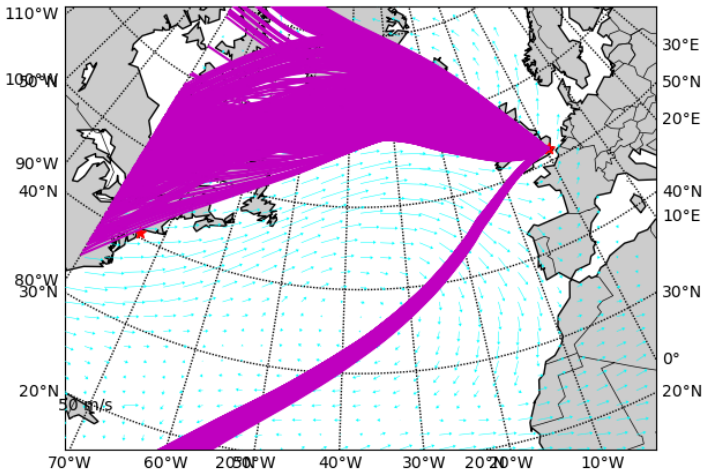

Figure A-2: Trajectories spanning a 90 degree initial heading range with a 0.1 degree interval and a heading rate upper limit of 0.1 degree leaving an unreachable area.

Ordered Upwind

Now, the setup for wind optimal trajectories based on the ordered upwind algorithm is elaborated upon. As mentioned in section 3-2-2, trajectories are established by using an irregular 2D grid. The boundaries of this grid are defined by the location of the origin and destination with some margin. The latitude bounds are set as in Equation A-1 with a high upper bound as flights crossing the North Atlantic often cruise through higher latitudes due to the spherical Earth. The longitudes bounds are stated in Equation A-2 and have a larger margin at the side of the origin. The propagation front expands from there and will form a sink, therefore, more points are required in this region to increase the accuracy. As the upwind algorithm terminates when the destination is reached, a small margin is necessary to make sure the destination falls within the boundaries.

$$[\max(\min(lats), \min(lat_{orig}, lat_{dest}) - 10), \min(88, \max(lat_{orig}, lat_{dest}) + 35)] \quad \text{(A-1)}$$

$$\begin{aligned} &[lon_{orig} - 10, lon_{dest} + 2], \quad \text{if } lon_{orig} < lon_{dest} \\ &[lon_{dest} - 2, lon_{orig} + 10], \quad \text{if } lon_{orig} > lon_{dest} \end{aligned} \quad \text{(A-2)}$$

The grid points are created with the use of a Poisson disc sampling algorithm[1] and the aforementioned bounds. The grid is created on the Lambert Conic Conformal projection plane with minimum distance r set to 30000 and number of reference points around each point k set to 30 to guarantee an equal distribution of points over the grid. An iterative approach is taken to make sure that the number of points is below 175 for

[1] https://github.com/scipython/scipython-maths/blob/master/poisson_disc_sampled_noise/poisson.py, December 2018.

performance purposes. As there is some randomness to the grid creation, logic is applied to make sure the origin and destination are always within the limits of the created grid points. Due to this randomness in grid creation, an average of five computations is taken to assess the performance and efficiency.

Furthermore, the accepted front is updated with the use of a concave hull algorithm[2]. To construct the actual trajectories via backward propagation, a time step of 60 seconds is used as this is closest to the update time used by FlightRadar24 (FR24) during cruise, but remains susceptible to change.

Additional Analysis

After the best-performing method has been selected, additional analysis will be performed. The first goal of this additional analysis is to determine the average computational time for multiple flights with different flight distances. This is done by computing all trajectories for the three selected days. For each separate day, all flights are loaded in and parallel computing tools are used to further increase the performance.

The second goal is to estimate if there might be the necessity of incorporating a strategic deconflicting method. Wind optimal trajectory generation processes can result in clustered trajectories due to their characteristics. This could lead to conflicts and such a method might be necessary to avoid conflicts. It is of interest to know if and how this clustering of flights influences the emergence of conflicts. Therefore, the number of conflicts and their location are determined. A conflict is detected when an intruder enters the protected zone of the ownship according to the definition in subsection 4-1-1 (5 NM radius and 1000 ft vertical separation). Trajectories are sampled at a certain time interval and no interpolation method is used. Therefore, this might result in not every conflict being captured, especially for large-angle conflicts. Decreasing the sample time step might result in a higher resolution and more conflicts. However, for this step it is not necessary to get all possible conflicts, an initial estimate of the number of possible conflicts and the location of the conflicts is sufficient.

The last goal is to visually assess how the trajectory changes over varying altitudes. As mentioned in the literature study, computing optimal 4D trajectories are computationally expensive. If the horizontal trajectory does not deviate significantly for varying altitudes, the horizontal trajectory is set to a single level. For each of the LHR to JFK and JFK to LHR flights, trajectories at three different altitudes are computed. These are based on the limits of the economically viable region (FL300 and FL400) and the aircraft's maximum cruise altitude according to BADA (aircraft dependent). The same calibrated airspeed is used for all flight levels.

A-2 Results

To compare the results of both methods, the route efficiency and computational efficiency are compared. These are presented in Table A-1 for wind optimal extremals and

[2] https://gist.github.com/AndreLester/589ea1eddd3a28d00f3d7e47bd9f28fb.js, August 2018

in Table A-2 for ordered upwind. The first column presents the day of the flight and the second column the origin-destination pair and flight number. The computational efficiency in the case of wind optimal extremals is the time it takes to find an initial heading that generates a trajectory that reaches the destination within ΔNM while the value within brackets is the time it takes to compute the trajectory with the initial heading known. The average routing and computational efficiency for both methods are displayed in Table A-3.

Table A-1: Flight performance and efficiency of Zermelo's problem based extremals (B744 aircraft).

Day	Trip	Route Efficiency [s]	Computational Efficiency [s]
3 Apr 2019	LHR-JFK BA177	28005	2665.8 (37.3)
3 Apr 2019	JFK-LHR BA178	21764	161.7 (24.7)
19 Jul 2019	LHR-JFK BA175	24024	3363.8 (16.5)
19 Jul 2019	JFK-LHR BA178	20636	1025.4 (19.4)
12 Jan 2020	LHR-JFK BA175	26945	132.7 (24.4)
12 Jan 2020	JFK-LHR BA178	19575	372.0 (13.5)

Table A-2: Flight performance and efficiency of ordered upwind algorithm (B744 aircraft).

Day	Trip	Route Efficiency [s]	Computational Efficiency [s]
3 Apr 2019	LHR-JFK BA177	23923	9.8
3 Apr 2019	JFK-LHR BA178	20853	9.4
19 Jul 2019	LHR-JFK BA175	22973	10.3
19 Jul 2019	JFK-LHR BA178	21029	9.8
12 Jan 2020	LHR-JFK BA175	24740	9.9
12 Jan 2020	JFK-LHR BA178	19810	9.7

Table A-3: Performance and efficiency comparison between wind-optimal extremals and ordered upwind algorithm for horizontal trajectory generation at constant altitude and speed.

Method	Route Efficiency [s]	Computational Efficiency [s]
Extremals	23492	1287 (22.6)
Ordered Upwind	22221	9.8

Furthermore, the horizontal trajectory computed by both methods and the actual route can be compared visually. Both a case with an extreme deviation and a case with a highly similar result is displayed. The GCR is displayed by the lime green line for visual comparison reasons. Beware that the horizontal trajectory assumes constant true airspeed and altitude, while the actual trajectory does not. The trajectories computed by wind optimal extremals for flights JFK-LHR and LHR-JFK are displayed in Figure A-3 and Figure A-4. The trajectories computed by ordered upwind are displayed in Figure A-5 and Figure A-6.

It can be observed that the difference in trajectories generated by wind optimal extremals and the actual routes is relatively minor for both directions. Still, it can be

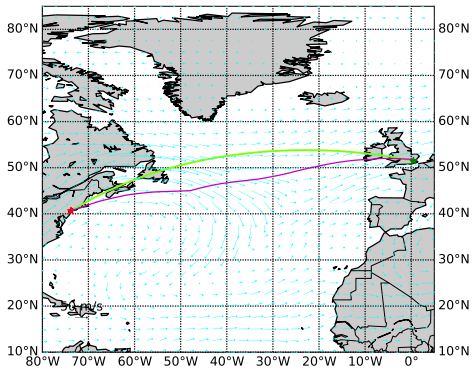

(a) Wind-optimal trajectory (magenta) andGCR (lime).

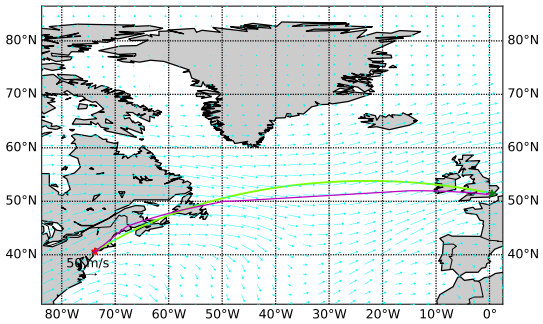

(b) Actual trajectory (magenta) and GCR (lime).

Figure A-3: Wind-optimal extremal and actual trajectory for a flight from JFK (red star) to LHR (green star) on 12 Jan 2020.

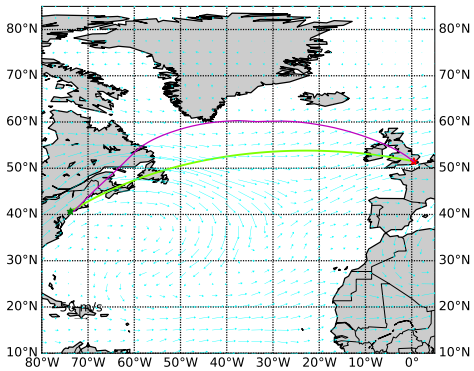

(a) Wind-optimal trajectory (magenta) and GCR (lime).

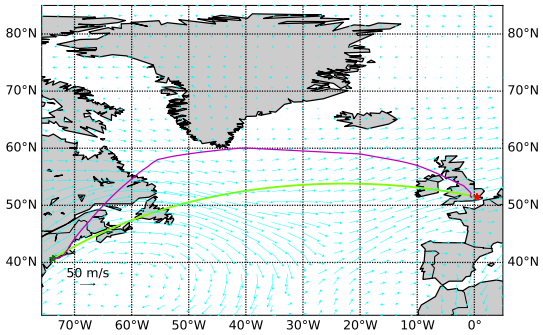

(b) Actual trajectory (magenta) and GCR (lime).

Figure A-4: Wind-optimal extremal and actual trajectory for a flight from LHR (red star) to JFK (green star) on 12 Jan 2020.

seen that the trajectory of the actual flight has less curvature and consists of some straight segments.

When looking at the trajectories generated by the ordered upwind algorithm versus the actual trajectories, the differences become more apparent. Still, the flight JFK-LHR is similar apart from some straight segments. However, the flight LHR-JFK results in a substantial difference. On this particular day, six North Atlantic Tracks were active, located between 57°N and 63°N. Although this flight probably has been assigned to one of the lower three tracks, it can be seen that the route is not ordered upwind wind optimal and likely to have contributed to an increased flight time and fuel usage.

The trajectories of the other flights that have been evaluated are displayed at the end of this appendix in section A-4.

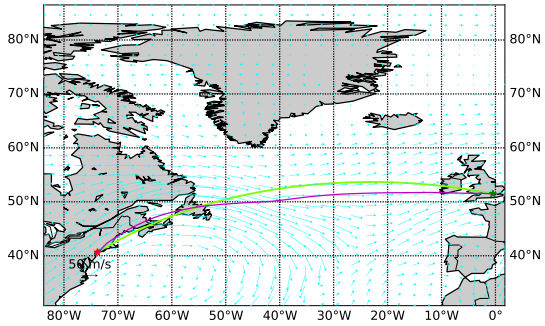

(a) Wind-optimal trajectory (magenta) and GCR (lime).

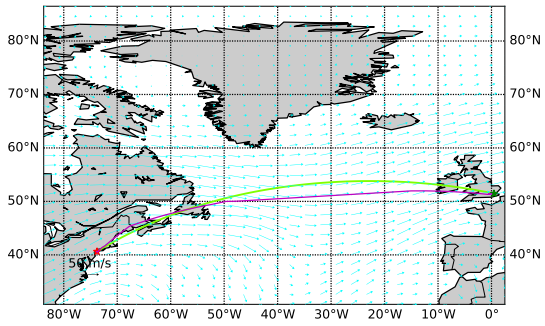

(b) Actual trajectory (magenta) and GCR (lime).

Figure A-5: Ordered upwind wind-optimal and actual trajectory for a flight from JFK (red star) to LHR (green star) on 12 Jan 2020.

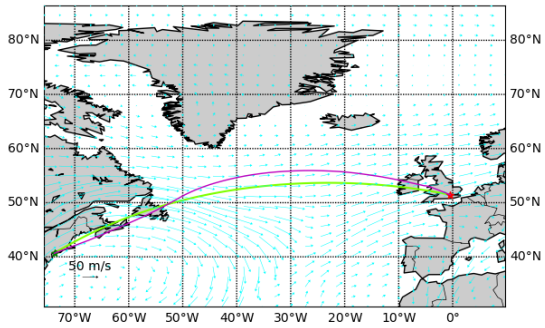

(a) Wind-optimal trajectory (magenta) and GCR (lime).

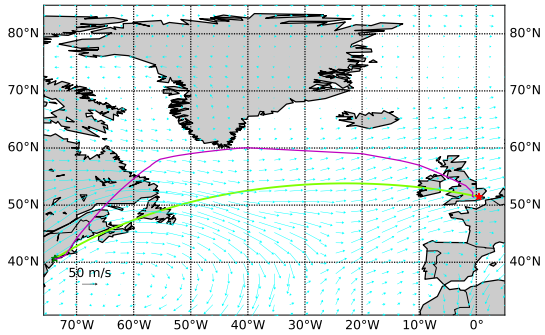

(b) Actual trajectory (magenta) and the GCR (lime).

Figure A-6: Ordered upwind wind-optimal and actual trajectory for a flight from LHR (red star) to JFK (green star) on 12 Jan 2020.

A-2-1 Additional Analysis

Based on the previous results, the ordered upwind method has been selected. Now, all trajectories for the three selected days are computed and analyzed. First, the computational efficiency for each day is stated in Table A-4 together with the efficiency per trajectory. These trajectories are plotted for two different days in Figure A-7 and Figure A-8 as these two days yield significantly different results while the flights of Jan 1^{st} 2020 behave somewhat similar to the flights on Apr 3^{rd}. A darker color of magenta indicates that more routes cross there. It can be observed that the flights predominantly have the same origin and destination locations and that some major hubs accommodate a large part of all flights. Furthermore, the difference in wind fields results in different optimal trajectories. The west- and eastbound flights on April 3^{th} appear to follow the same route more or less, while there is a clear difference between

both directions on July 19^{th}.

Table A-4: Additional analysis for all flights for one of the selected days.

Day [s]	Efficiency [s]	Efficiency per trajectory [s]	Conflicts [-]	Conflict pairs [-]
3 Apr 2019	8167	5.1	1501	358
19 Jul 2019	10123	5.1	2111	440
12 Jan 2020	7719	5.1	1340	330

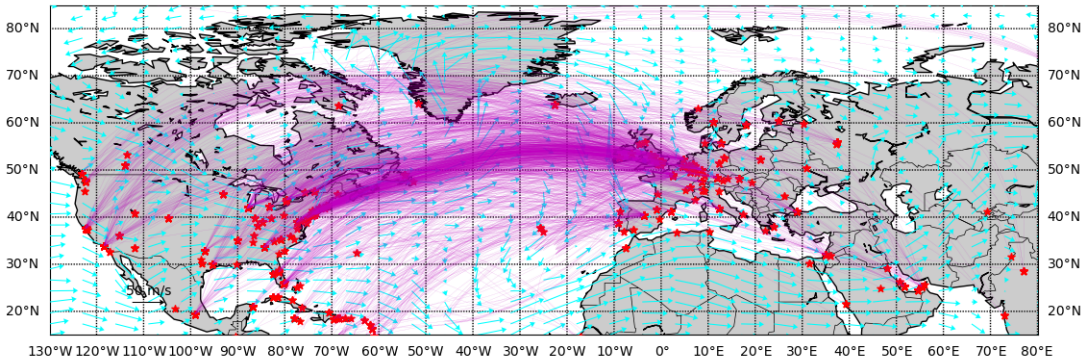

Figure A-7: Wind-optimal trajectories (magenta) for all flights crossing the North Atlantic region on 3 Apr 2019. Origins and destinations are indicated by a red star.

Furthermore, the conflicts have been detected based on the current trajectory generation time step and are also stated in Table A-4. The conflicts for April 3^{th} and July 19^{th} are indicated by lime dots in Figure A-9a and Figure A-9b, respectively. As conflicts are investigated point-wise, multiple conflicts in a row are likely to indicate two aircraft conflicting over a longer part of their trajectories. As conflicts usually get resolved, conflicts are grouped by pairs and stated in Table A-4 to get an overview of the total number of conflicts. Most conflicts appear around the west- and eastbound trajectory clusters.

At last, the trajectories for varying altitudes are visually assessed. The flight levels 300, 354, and 400 are displayed for the three different days in Figure A-18 up to Figure A-23. This figure display minor changes in horizontal optimal trajectories at different altitudes.

A-3 Conclusion

Altogether, it can be concluded that the ordered upwind algorithm on average performs better in terms of routing efficiency and computational efficiency for the selected flights than the wind-optimal extremals algorithm. Furthermore, the ordered upwind algorithm is a more robust method as it is less sensitive to changes in initial condi-

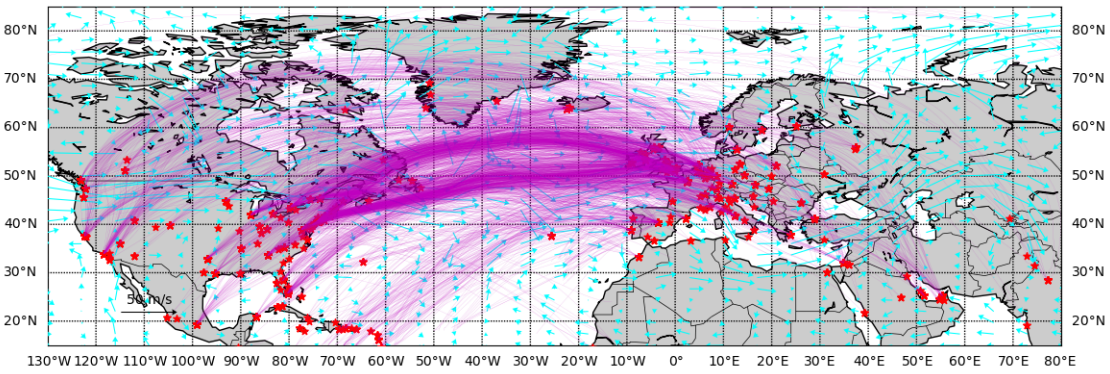

Figure A-8: Wind-optimal trajectories (magenta) for all flights crossing the North Atlantic region on 19 Jul 2019. Origins and destinations are indicated by a red star.

tions. Therefore, this method is more suited for this research and will be used for the remainder of this thesis.

When considering the overall computational time for the three selected days, an overall average of 5.1 seconds computational time per trajectory is obtained. Taking the three days as a valid representation of the year (a busy day for two normal days) would imply an overall computational time of 36.7 days.

Considering the number of conflicts and their locations in the current situation, it can be concluded that a strategic deconfliction method in line with existing literature might be necessary. Even if tactical resolution methods are sufficient for current traffic levels, such a method might be necessary when considering an increase in future traffic levels.

From the analysis for the flights at different altitudes, it can be concluded that the variations are minor. Therefore, the optimal trajectory in the horizontal plane is assumed to be equal of varying vertical altitude.

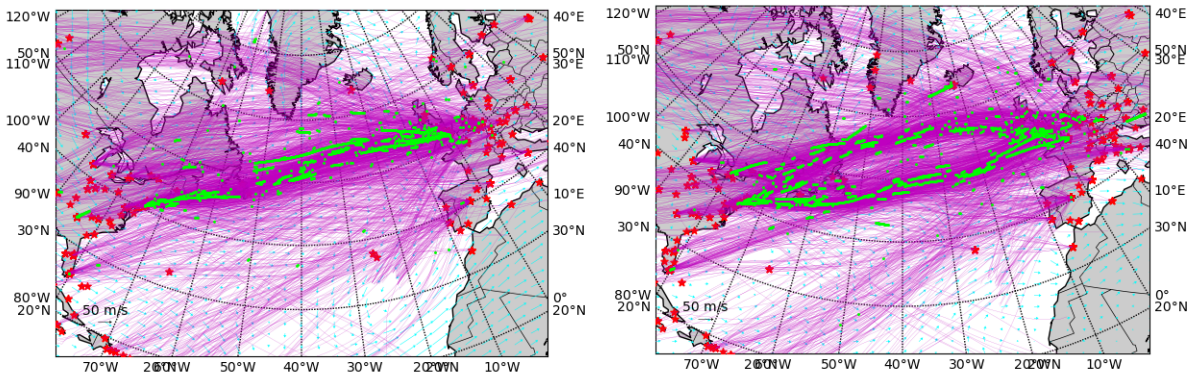

(a) Conflicts emerging on 3 Apr 2019.

(b) Conflicts emerging on 19 Jul 2019.

Figure A-9: Conflicts (lime) for wind-optimal trajectories on a Lambert conic conformal projection.

A-4 Additional Figures

This section contains additional figures for the preliminary experiment.

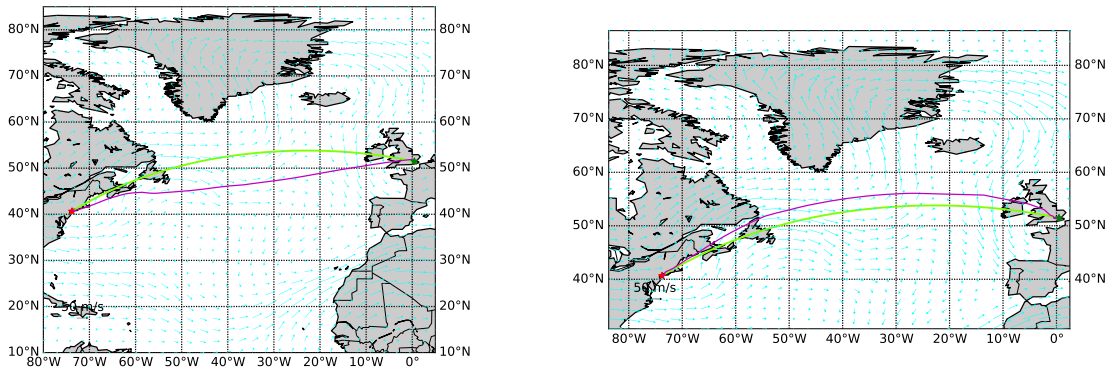

(a) Wind-optimal trajectory (magenta) and GCR (lime).

(b) Actual trajectory (magenta) and GCR (lime).

Figure A-10: Wind-optimal extremals and actual trajectory for a flight from JFK (red star) to LHR (green star) on 3 Apr 2019.

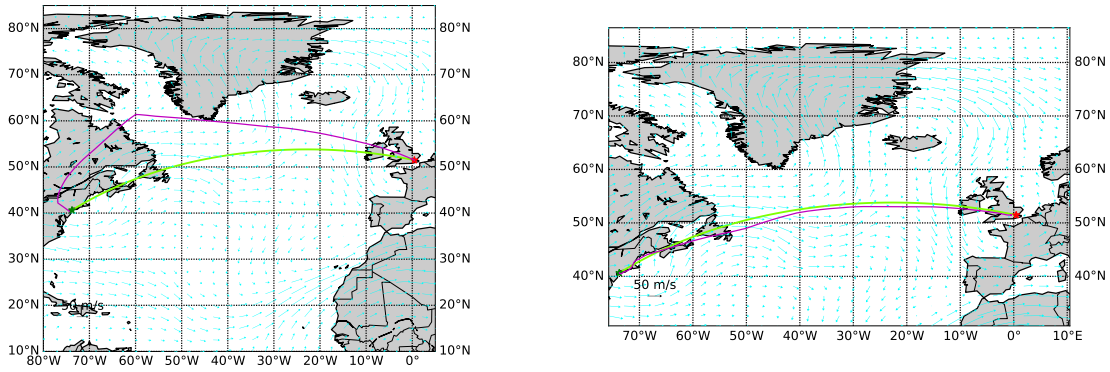

(a) Wind-optimal trajectory (magenta) and GCR (lime). **(b)** Actual trajectory (magenta) and GCR (lime).

Figure A-11: Wind-optimal extremals and actual trajectory for a flight from LHR (red star) to JFK (green star) on 3 Apr 2019.

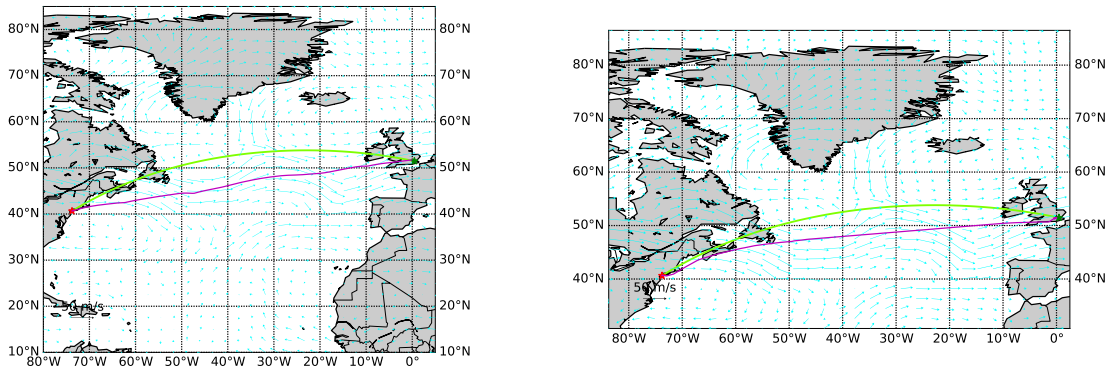

(a) Wind-optimal trajectory (magenta) and GCR (lime). **(b)** Actual trajectory (magenta) and GCR (lime).

Figure A-12: Wind-optimal extremal and actual trajectory for a flight from JFK (red star) to LHR (green star) on 19 Jul 2019.

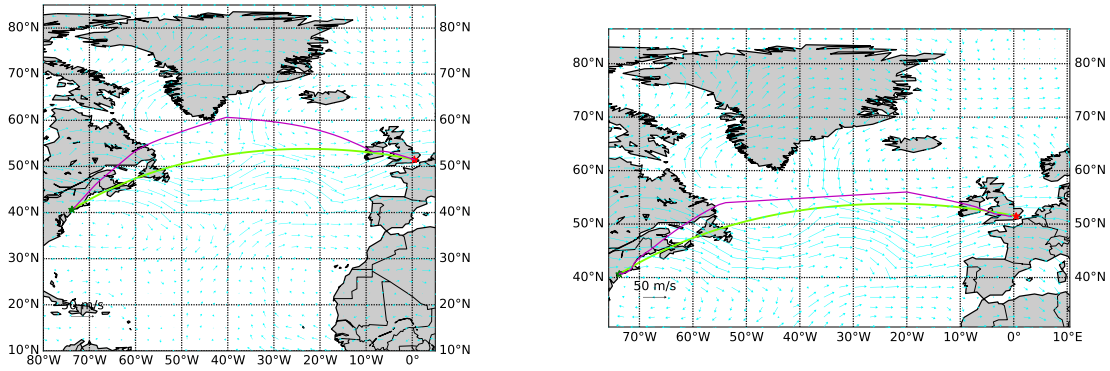

(a) Wind-optimal trajectory (magenta) and GCR (lime). **(b)** Actual trajectory (magenta) and GCR (lime).

Figure A-13: Wind-optimal extremal and actual trajectory for a flight from LHR (red star) to JFK (green star) on 19 Jul 2019.

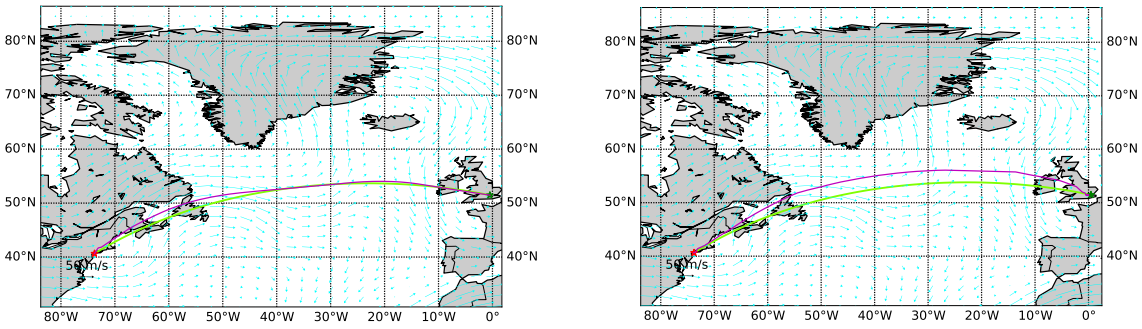

(a) Wind-optimal trajectory (magenta) and GCR (lime). **(b)** Actual trajectory (magenta) and GCR (lime).

Figure A-14: Ordered upwind wind-optimal and actual trajectory for a flight from JFK (red star) to LHR (green star) on 3 Apr 2019.

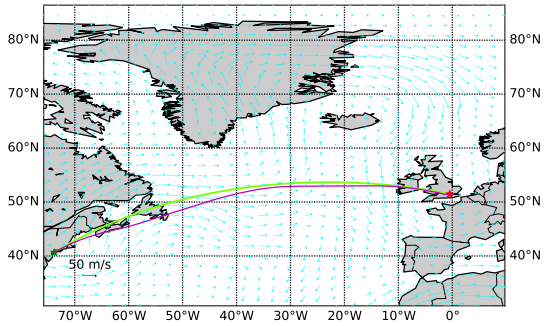

(a) Wind-optimal trajectory (magenta) and GCR (lime).

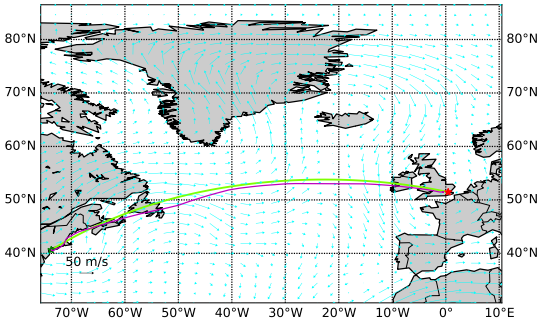

(b) Actual trajectory (magenta) and GCR (lime).

Figure A-15: Ordered upwind wind-optimal and actual trajectory for a flight from LHR (red star) to JFK (green star) on 3 Apr 2019.

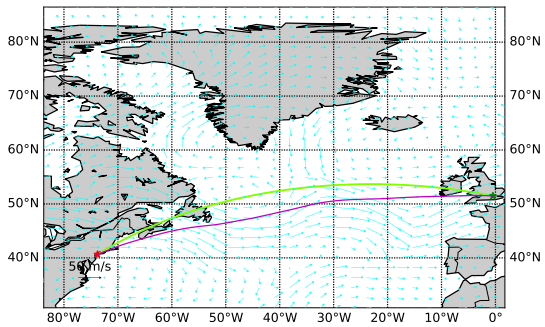

(a) Wind-optimal trajectory (magenta) and GCR (lime).

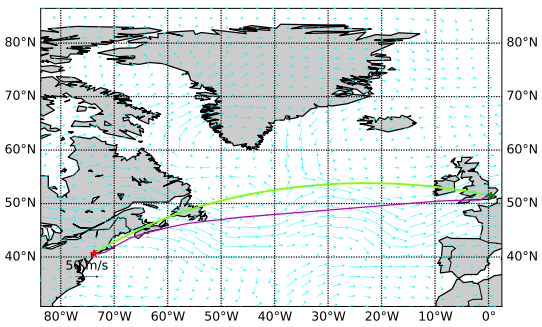

(b) Actual trajectory (magenta) and GCR (lime).

Figure A-16: Ordered upwind wind-optimal and actual trajectory for a flight from JFK (red star) to LHR (green star) on 19 Jul 2019.

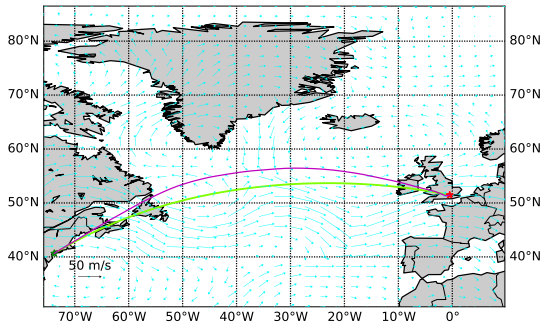

(a) Wind-optimal trajectory (magenta) and GCR (lime).

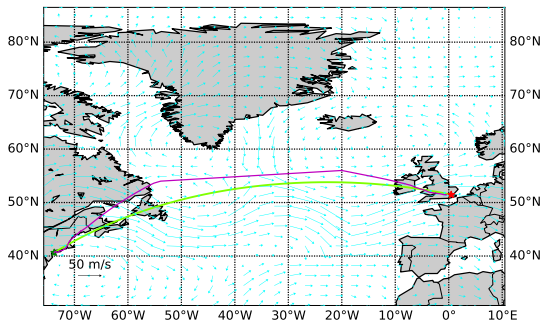

(b) Actual trajectory (magenta) and GCR (lime).

Figure A-17: Ordered upwind wind-optimal and actual trajectory for a flight from LHR (red star) to JFK (green star) on 19 Jul 2019.

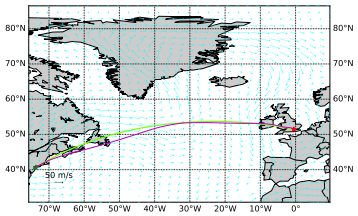

(a) Wind-optimal trajectory (magenta) and GCR (lime) at FI300.

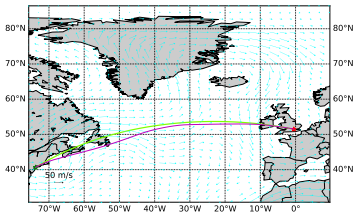

(b) Wind-optimal trajectory (magenta) and GCR (lime) at FL354.

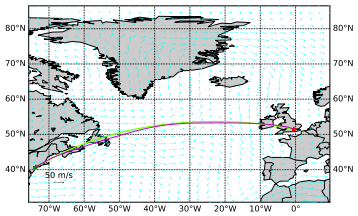

(c) Wind-optimal trajectory (magenta) and GCR (lime) at FL400.

Figure A-18: Ordered upwind wind-optimal trajectories for different altitudes for a flight from LHR (red star) to JFK (green star) on 3 April 2019.

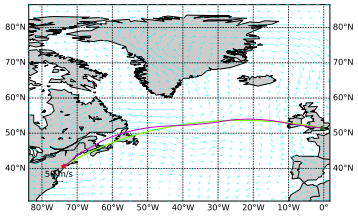

(a) Wind-optimal trajectory (magenta) and GCR (lime) at FL300.

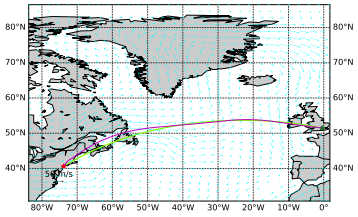

(b) Wind-optimal trajectory (magenta) and GCR (lime) at FL354.

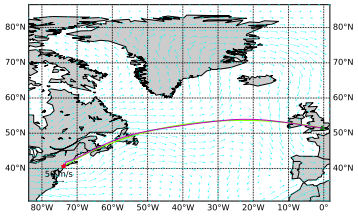

(c) Wind-optimal trajectory (magenta) and GCR (lime) at FL400.

Figure A-19: Ordered upwind wind-optimal trajectories for different altitudes for a flight from JFK (red star) to LHR (green star) on 3 April 2019.

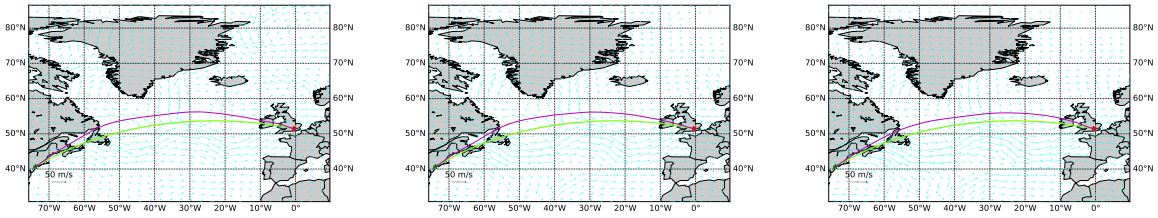

(a) Wind-optimal trajectory (magenta) and GCR (lime) at FL300.

(b) Wind-optimal trajectory (magenta) and GCR (lime) at FL354.

(c) Wind-optimal trajectory (magenta) and GCR (lime) at FL400.

Figure A-20: Ordered upwind wind-optimal trajectories for different altitudes for a flight from LHR (red star) to JFK (green star) on 19 Jul 2019.

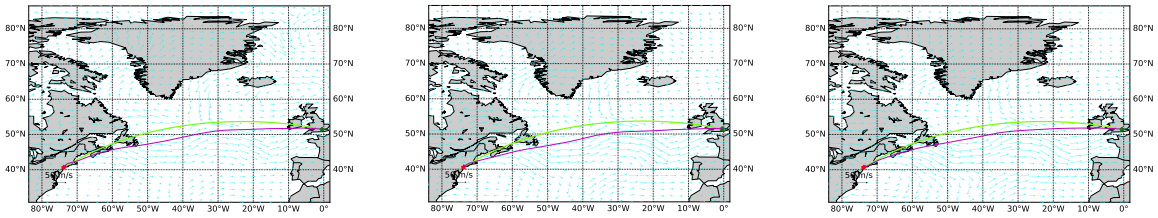

(a) Wind-optimal trajectory (magenta) and GCR (lime) at FL300.

(b) Wind-optimal trajectory (magenta) and GCR (lime) at FL354.

(c) Wind-optimal trajectory (magenta) and GCR (lime) at FL400.

Figure A-21: Ordered upwind wind-optimal trajectories for different altitudes for a flight from JFK (red star) to LHR (green star) on 19 Jul 2019.

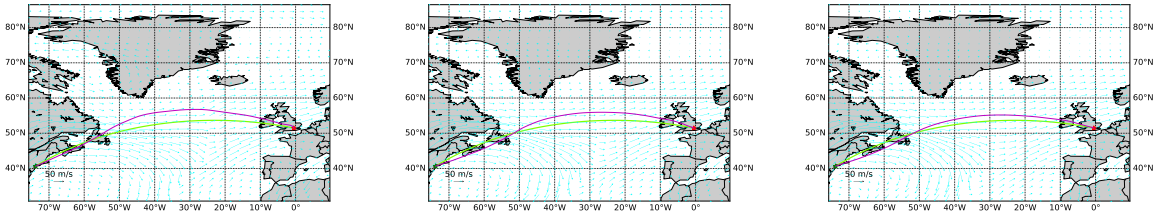

(a) Wind-optimal trajectory (magenta) and GCR (lime) at FL300.

(b) Wind-optimal trajectory (magenta) and GCR (lime) at FL354.

(c) Wind-optimal trajectory (magenta) and GCR (lime) at FL400.

Figure A-22: Ordered upwind wind-optimal trajectories for different altitudes for a flight from LHR (red star) to JFK (green star) on 12 Jan 2020.

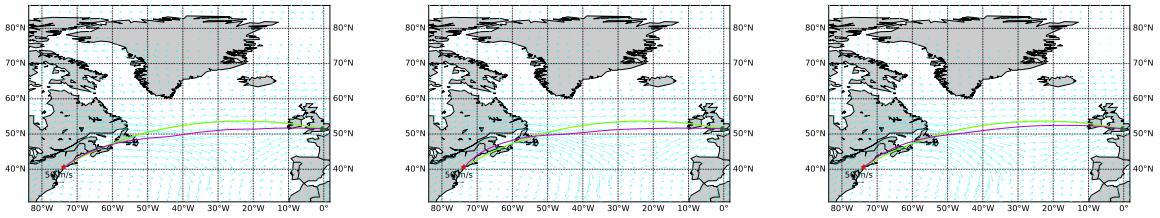

(a) Wind-optimal trajectory (magenta) and GCR (lime) at FL300.

(b) Wind-optimal trajectory (magenta) and GCR (lime) at FL354.

(c) Wind-optimal trajectory (magenta) and GCR (lime) at FL400.

Figure A-23: Ordered upwind wind-optimal trajectories for different altitudes for a flight from JFK (red star) to LHR (green star) on 12 Jan 2020.

Appendix B

Code Structure

Table B-1: Overview of the modules in the code structure.

File	Input	Output	Description
BS_log_analyzer	Txt file of conflict logs	Conflict metrics	Tool to analyze several conflict metrics such as altitude and angle.
ConcaveHull[1]	Array of points	Array of points	This class takes an array of points and returns the concave hull based on a set tolerance level.
Create_dummies	Actual flight data	Dummy flights	Creates dummy flights to increase the traffic level.
ECWMF_ extraction	ECMWF-API	NetCDF wind data	Fetches date ordered reanalysis data for several pressure levels via the webAPI.
FIRArea	Txt file with area coordinates	Polygon	Creates a polygon of the required navigational area(s) based on the corresponding FIRs.
Flightphase[2]	None	Membership functions	Create membership functions to use for the flight phase identification.
Flightphase-identification[2]	Csv with flight position data	Csv position data with phase labels	Uses the Flightphase membership functions to determine the flight phase labels for the actual flights.
FlightstoBSscenario	Csv flight data	Scenario file	Writes the flight information and trajectories to a scenario file.
FR24_data_analysis	FR24 data	Modified flight data	Preprocessing and analysis of the flight data.

[1]Copyright (C) 2018 Andre Lester Kruger https://gist.github.com/AndreLester/589ea1eddd3a28d00f3d7e47bd9f28fb.js

OU_multiprocessing	Csv flight data	Csv optimized trajectories	File to support multiprocessing for TO_optimization_OU.
TO_grid	Area data	Grid coordinates	Create the *far* grid points based on the origin, destination, and optimization area.
TO_optimization_OU	Csv flight data	Csv optimized trajectories	Computes the wind optimal horizontal trajectories and stores them in a csv file.
TO_vertical	Csv flight data	Csv optimized trajectories	Computes the optimal horizontal trajectories based on the initial weight at the starting point and the destination.
Weight	BADA files	Initial weight estimate for the aircraft	Draws a random initial weight from a Gaussian distribution based on BADA aircraft specific weight

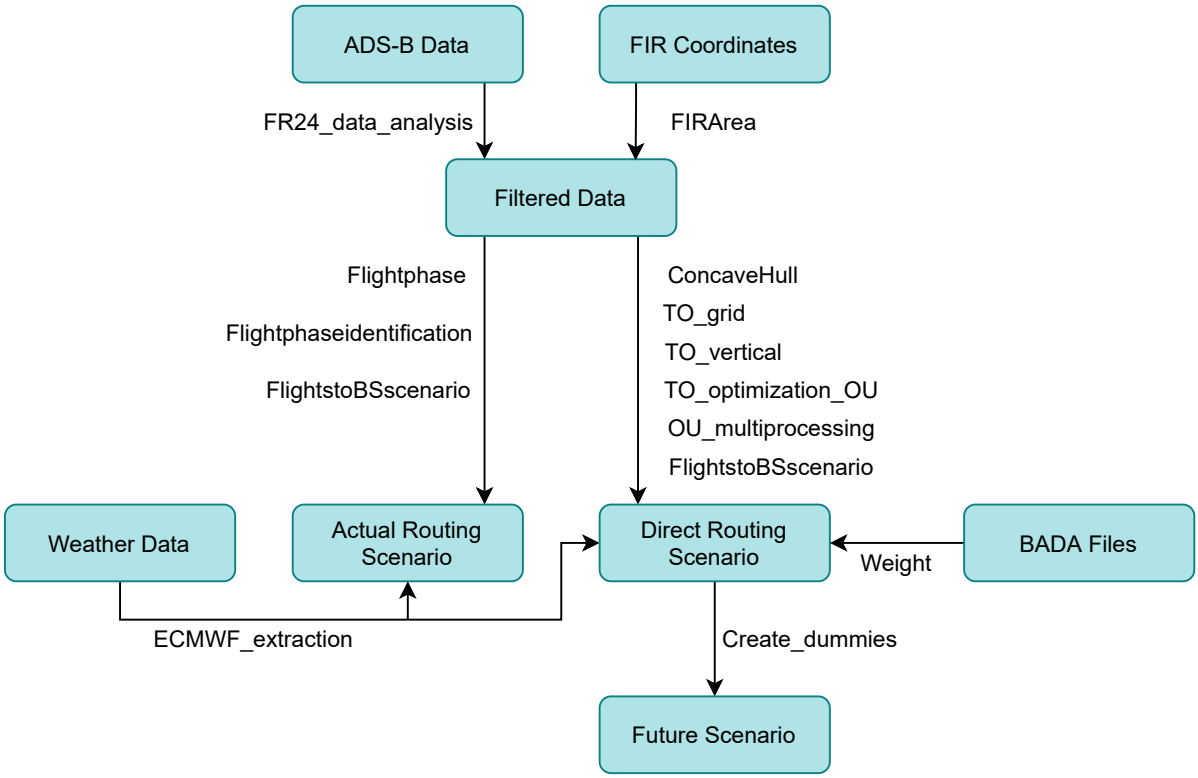

Figure B-1: Preliminary flowchart of the modules in the code structure.

[2]Based on [57] https://github.com/junzis/flight-data-processor.git, May 2021

Appendix C

Gantt Chart

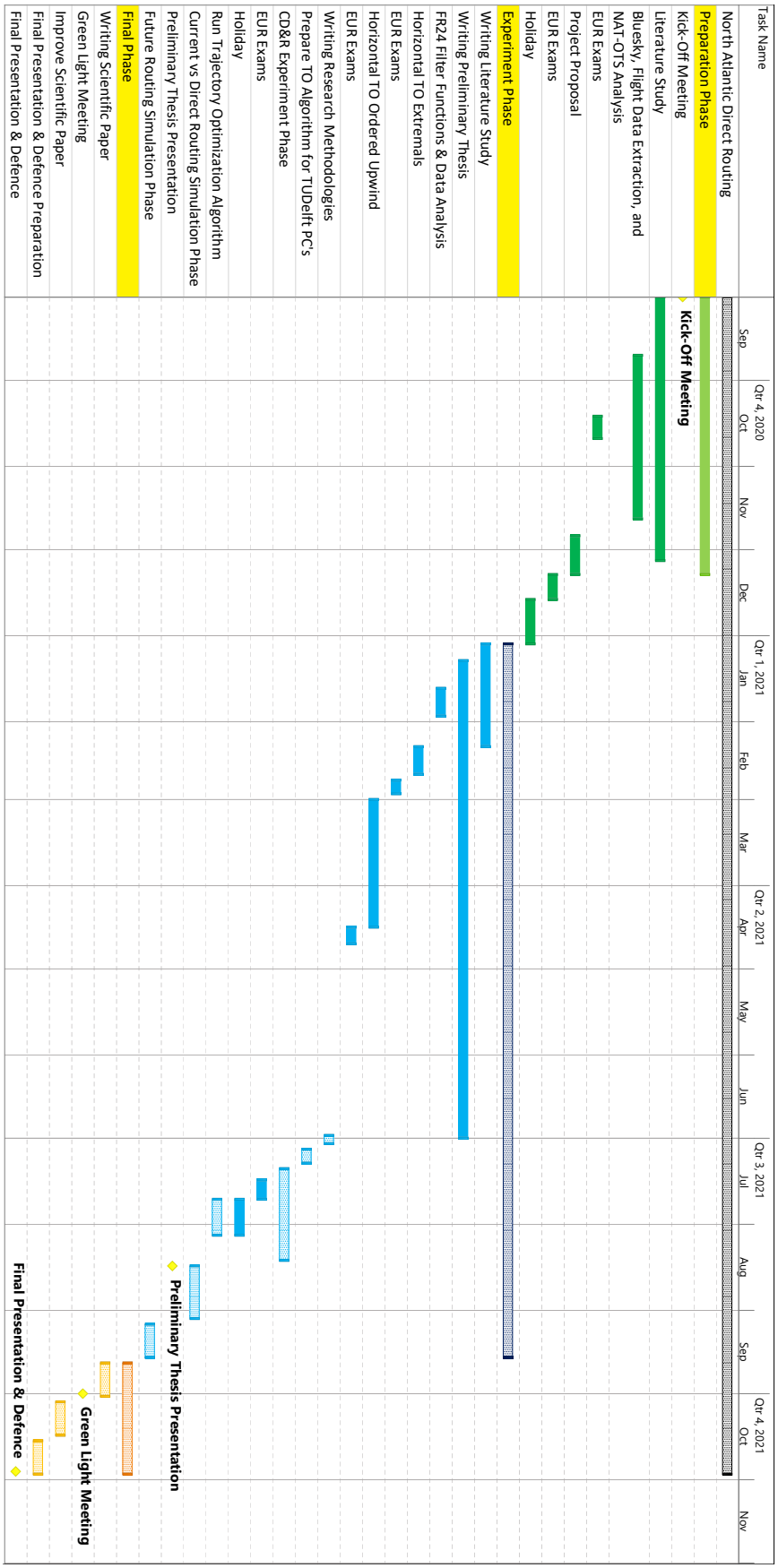

Figure C-1: Gantt Chart

Appendix D

Activity Log

Date	Tasks performed	Tasks to continue with	Other
03/09/20	I have been researching the airspace (FIR) and I have been running some simple tests on random flights to see if the GCR is a lot different from the actual route.	- The FIR in the likely to be used regions have to be specified. - The NATS have to be researched and a framework on how they are established and where they lay should be established. Check out Gander and TFMS centre. - Look for review papers	
04/09/20	Sorted out the FIR and basics of the North Atlantic Track System. Found out how the OTS are communicated. Furthermore, a institute for aviation weather has been identified (NOAA).	-Research how the NAT-OTS are determined and computed. Therefore, the Gander (Automated Traffic System), Shanwick and TFMS centre websites can be visited. -Look for review papers. -READ STRATEGIC PLANNING OF EFFICIENT OCEANIC FLIGHTS	Bad day due to very poor network connection.

07/09/20	Read three papers about planning of oceanic routes, wind-optimal routes and trajectory optimization by taking the climate effect into account from a broader perspective (GWP).	-Research how the NAT-OTS are determined right now. Conduct further research on WOR, don't forget to look into different optimization strategies (contrails, time, airspace capacity). -Look for review papers.	
08/09/20	Three papers have been studied Today. Two about strategic trajectory planning with wind. Of which one about optimizing trajectories in wind by separation of vertical (fuel burn) and horizontal optimization (wind) and one about taking areas of turbulence into account (which could be a nice real-life feature). One paper about conflict resolution for wind-optimal aircraft trajectories has been studied. Mostly, uncertainties in winds where modelled and how strategic flight planning is affected by that.	-Continue looking for review papers. -Read the meeting1 and structure notes to look into new fields of research. -Don't forget to look into different optimization strategies (contrails, time, airspace capacity) -Look up Collocation algorithm.	
09/09/20	Read an article about UAV trajectory optimization in presence of wind and sun, an article about in-flight synthesis of optimal trajectory option sets, and another article about trajectory optimization based on a genetic algorithm. Found a review paper regarding optimal flight trajectories (2016) and CD&R (2020).	-Use some part of the day to restructure the latex mess and to start writing more concise already. -Continue with review papers.	

10/09/20	I have restructured the overleaf file, which is a much clearer read. Started on the PPP for meeting 2. And started reading the review paper of CD&R	- Continue reading the review papers. -Continue with the PowerPoint for the presentation next week.	
11/09/20	-Finished CD&R review paper and started trajectory review paper	-Continue with trajectory review paper. -Read free flight paper Hoekstra. -Look more specifically at structure to determine which steps to take before Thursday. -Continue with the PPP	
14/09/20	Finished the review paper on multi-objective trajectory optimization. I have read a paper about free flight from eby	-continue with the direct routing papers. -Look more specifically at structure to determine which steps to take before Thursday. -Continue with the PPP	Bad day due to warm weather
15/09/20	Read three papers on free flight and direct routing.	Prepare for the second meeting	Bad day due to warm weather.
16/09/20	Prepared the meeting for tomorrow.	-Evaluate the second meeting and determine strategy for the two weeks to come.	
17/09/20	Had the second meeting, which was good. Discussed some critical issues. Contacted the SPA because of the declined kick-off form. Started to look into ADS-B data mining.	-Set-up GitHub -Continue ADS-B data mining -Look into BlueSky -Look into BADA -Read 2005 NASA Analytical Relationship between Conflicts Counts and Airtraffic Density	
18/09/20	A Github repository has been created to store python files. Requested FR24 API and ECMWF from Junzi Sun. Started to work on this API	-Continue ADS-B data mining -Look into BlueSky -Look into BADA	

21/09/20	Read a paper and installed BlueSky	-Look at BS functionalities -Look into BADA. -Look into ADS-B mining.	Took really long time as BS sky indicated that py2.7 was required
22/09/20	Played around with BlueSky all day	Look into BADA. -Look into ADS-B mining.	
23/09/20	Another day of exploring BlueSky, starting to get the hang of it	Try to extract ADS-B data, if too complicated, start writing program to create NATS simulation	
24/09/20	Working on the webscraper	Continue working on the webscraper	
25/09/20	Working on the webscraper	Look into BADA, finish webscraper and start writing program to create NATS simulation	
28/09/20	-	-	Worked on SysID assignment
29/09/20	Working on the webscraper, which finally works	Convert scraped data to BlueSky input	
30/09/20	Took a whole day to try and integrate the pymongo with BlueSky, decided to write it to scenario file instead	Start writing program for NATs simulation	
01/10/20	Worked out the theoretical capacity (not a success). Had my third meeting from which I gathered some interesting information	Look at the meeting 3 word doc and decide upon how to continue	Promising email contact with FR24 via Junzi Sun.

02/10/20	-	-	Had to work on some econometrics assignment
05/10/20	Worked on figuring out how mongoDB stores data (online or only on PC) and worked on a way to scrape the NAT data.	Did not succeed, thus did it manually	Continue with the mongoDB script
06/10/20	Worked on integrating the FR24 data with the BlueSky.	-Filter the flights from actual flight which cross the North-Atlantic (OTS). -Make OpenSky webscraper and integrate the data with the BlueSky. -Read the paper Girardet mentioned. -Email Jacco and Joost for meeting.	
07/10/20	Worked on the filter -NAT-flights function to filter out AC' that do not cross the NAT region	-Make OpenSky webscraper and integrate the data with the BlueSky. -Read the paper Girardet mentioned. -Email Jacco and Joost for meeting.	
08/10/20	Extracted and filtered data form OpenSky for comparison with FR24. Discussed that TU is likely to sign the FR24 limited data licence agreement	Get data of FR24 and OpenSky to work in BlueSky, probably something with stack command input density. -Make filter that separates flights which made it to the destination. -Read the paper Girardet mentioned.	
09/10/20	-	-	Worked on econometric assignments, exams coming up.

12/10/20	Finished origin-destination filter. Collected NAT data of 2020. Working on filter for flights that have followed the NATS.	-continue with the filter for NAT. -Get BS to work. -Read paper Girardet.	
13/10/20	Worked on NAT filter all day	-continue with the filter for NAT. -Get BS to work. -Read paper Girardet.	Lots of geopandas issues, took a long time
14/10/20	-	-	EUR exam preparation
15/10/20	-	-	EUR exam preparation
16/10/20	-	-	EUR exam preparation
19/10/20	-	-	EUR exams
20/10/20	-	-	EUR exams
21/10/20	-	-	EUR exams
22/10/20	Finalized the filtering by NAT locations	-	PC crash, took all damn day
23/10/20	Looking into "drunk pilot problem" BS	-continue with drunk pilot problem	
26/10/20	Looked at drunk pilot problem, which is caused by the way the cmds are orderd over time (should be given a-priori). Looked at performance measurements	Continue with the performance measurements	-

27/10/20	Read paper on trajectory optimization of Girardet. Restructed the cmds oder input. Took a look at the NAT inclusion of the named waypoint.	Continue with named waypoint. Read other paper of Girardet.	
28/10/20	Split the NAT function to get one which includes the named waypoints for visualization purposes.	-Read other paper of Girardet. -Create webscraper NOTAMs. -Fix dirty strings from NAT	Computer crashed for several hours.
29/10/20	Read the paper from Girardet, look at scholar citations, seems to be a lot there.	Look at previous days.	-PC issues all day
30/10/20	-	-	-PC issues all day
02/11/20	Pinpoint where I am currently at and determine how to proceed. Finished dirty string fixer from NAT	-Call legal services for contract. -Continue with the pinpoint structure (Direct Routing papers first). -Continue structuring overleaf.	
03/11/20	Documentation of Direct Routing and CD&R and continue with reading papers	- Continue with Direct Routing and CD&R	
04/11/20	Documentation of Direct Routing and CD&R and read papers	- Continue with Direct Routing and CD&R -Look into scholar citations of properties of air traffic conflicts...	
05/11/20	Read papers about direct routing	-continue with the particle filtering paper from ETHZ	
06/11/20	Read the paper from ETHZ about particle filtering	-Continue with CD&R method papers	inefficient day
09/11/20	Added extra component to runscript() to delay start of execution. Modified area.py to output desired info		
10/11/20	-Added additional outputs to the area.py file. -Created functions to analyze the conflict logger for the area.py file	-Continue with CD&R method papers	

11/11/20	Read paper on online multi-ac detection. -Continued with NOTAM scraper	-Continue with CD&R method papers. -Start writing. -Perform analysis on track data. - Prepare presentation	
12/11/20	Read paper on 4-D trajectory generation and finished the NOTAM scraper (only requires runscript() function to fetch and write periodically)	-Continue with CD&R method papers. -Start writing. -Perform analysis on track data. - Prepare presentation	
13/11/20	-Modified the area.py file to extract altitude and model information. -Started with getaltitude in BSloganalyzer.py	Continue with the getaltitude	Followed first ATM lecture
16/11/20	Finished getaltitude and visualizealtitude commands. Gathered information on the FIR coordinates. Started with the angle and altitude simulations	-Add 2019 NAT data to file -Finish FIR extraction and coordinate transformation script	
17/11/20	Meeting 4, see documents for further elaboration		
18/11/20	Continued on the fir extractions.		
19/11/20	Continued on the fir extractions. Updated analyser. Got in touch with Joanna of FR24 about data request.	Get resulting NATS from blackswan.ch!	
20/11/20	Getting familiar with FR24 flight options. -Added all NATs to file		ATM lecture
23/11/20	Continued reading the CD&R papers. -Received a test data set from FR24 and started to work on this to determine applicable filter for FR24.		
24/11/20	Looked through the tactical CD&R. -Started to look on strategic CD&R methods suitable for oceanic environments. -Looked into the ECMWF CDS API.	Continue with strategic CD&R and TO methods	

25/11/20	Looked into the oceanic strategic papers and found some new leads to research on trajectory optimization.	-Look into a data mining approach for strategic planning. Look at clusters of conflicts and try to identify characteristics.	
26/11/20	-	-	
27/11/20	-	-	
30/11/20	-	-	
01/12/20	Further looked into trajectory optimization and the connection with strategic deconflicting	Continue with TO research and work on a data mining approach for strategic planning. Look at clusters of conflicts and try to identify characteristics.	
02/12/20	Looked into ordered upwind model		
03/12/20	Established an overview of the possible TOP algorithms		
04/12/20	-	-	
07/12/20	Looked into the weather and climate impact papers and gathered some potentially interesting papers. Looked into how to modify weather data.	Prepare meeting 5	
08/12/20	Prepared meeting 5 and thought about how to continue after this. Meeting 5 basically confirmed what I already knew.	Continue reading papers	
09/12/20		Analyse obtained FR24 data	
10/12/20	-	-	EUR exams
11/12/20	-	-	EUR exams
14/12/20	-	-	EUR exams
15/12/20	-	-	EUR exams
16/12/20	-	-	EUR exams
17/12/20	-	-	EUR exams
18/12/20	-	-	EUR exams

21/12/20	-	-	Holiday
22/12/20	-	-	Holiday
23/12/20	Downloading and checking FR24 data	Continue with this	
24/12/20	Downloading and checking FR24 data	Continue with this	
25/12/20	-	-	Christmas
28/12/20	-	-	Holiday
29/12/20	-	-	Holiday
30/12/20	-	-	Holiday
31/12/20	-	-	Holiday
01/01/21	-	-	New Years Day
04/01/21	Started writing the preliminary report with the content up so far. Working on backup of FR24 files.	Continue both	
05/01/21	Finished the backup of the FR24 files and continued writing the preliminary report Airspace	Continue writing preliminary report	
06/01/21	Continued writing preliminary report Airspace	continue with preliminary report	
07/01/21	Continued writing preliminary report Weather and Emissions	continue with preliminary report	
08/01/21	Continued writing preliminary report CD&R	continue with preliminary report	ATM lecture
11/01/21	Continued writing preliminary report CD&R	continue with preliminary report	
12/01/21	Continued writing preliminary report CD&R	continue with preliminary report	
13/01/21	Continued writing preliminary report Flight Data	continue with preliminary report	
14/01/21	Continued writing preliminary report Flight Data	continue with preliminary report	
15/01/21	Continued writing preliminary report Performance Assessment	continue with preliminary report	

18/01/21	Continued writing preliminary report Performance Assessment	continue with preliminary report	Solving computer issues most time of the day
19/01/21	-	-	Computer issues all day
20/01/21	Analyzing flight data (FR24 data analysis)	Continue with this analysis	
21/01/21	Analyzing flight data (FR24 data analysis)	Continue with this analysis	
22/01/21	Analyzing flight data (FR24 data analysis)	Continue with this analysis	
25/01/21	Analyzing flight data (FR24 data analysis)	Continue with this analysis	
26/01/21	Analyzing flight data (FR24 data analysis)	Continue with this analysis	
27/01/21	Analyzing flight data (FR24 data analysis)	Continue with this analysis	
28/01/21	Analyzing flight data (FR24 data analysis)	Continue with this analysis	
29/01/21	Analyzing flight data (FR24 data analysis)	Continue with this analysis	
01/02/21	Preparation of meeting 6 and started with writing down TO section preliminary report	Continue with the writing down TO section	
02/02/21	Looked at ECMWF API for weather data extraction and played around with it and created some plotting functions.	Continue with the writing down TO section	
03/02/21	Continued writing preliminary report TO and looked into vertical profile optimization	Continue writing down TO section	
04/02/21	Continued writing preliminary report TO and looked into horizontal profile optimization	Continue writing down TO section	
05/02/21	Continued writing preliminary report TO and looked into horizontal profile optimization	Continue writing down TO section	

08/02/21	Continued writing preliminary report TO and looked into horizontal profile optimization	Continue writing down TO section	
09/02/21	Looked into ECMWF data manipulation	Work out TO algorithms	
10/02/21	Working out TO Zermelo	Continue working out TO Zermelo	
11/02/21	Working out TO Zermelo	Continue working out TO Zermelo	
12/02/21	Working out TO Zermelo	Continue working out TO Zermelo	
15/02/21	Working out TO Zermelo	Continue working out TO Zermelo	
16/02/21	Working out TO Zermelo	Continue working out TO Zermelo	
17/02/21	Working out TO Zermelo	Continue working out TO Zermelo	
18/02/21	Working out TO Zermelo	Continue working out TO Zermelo	
19/02/21	Working out TO Zermelo	Continue working out TO Zermelo	
22/02/21	-	-	EUR exams
23/02/21	-	-	EUR exams
24/02/21	-	-	EUR exams
25/02/21	-	-	EUR exams
26/02/21	-	-	EUR exams
01/03/21	Working out TO OU	Continue working out TO OU	
02/03/21	-	-	TO70 workshop and Aviation Symposium VSV
03/03/21	Working out TO OU	Continue working out TO OU	
04/03/21	Working out TO OU	Continue working out TO OU	
05/03/21			-
08/03/21	Working out TO OU	Continue working out TO OU	

09/03/21	Create function to construct suitable grid	Continue working on grid	
10/03/21	Create function to construct suitable grid	Continue working out TO OU	
11/03/21	Working out TO OU	Continue working out TO OU	
12/03/21	Working out TO OU	Continue working out TO OU	
15/03/21	Working out TO OU	Continue working out TO OU	
16/03/21	Working out TO OU	Continue working out TO OU	
17/03/21	Working out TO OU	Continue working out TO OU	
18/03/21	Working out TO OU	Continue working out TO OU	
19/03/21	Working out TO OU	Continue working out TO OU	
22/03/21	Working out TO OU	Continue working out TO OU	
23/03/21	Working out TO OU	Continue working out TO OU	
24/03/21	Working out TO OU	Continue working out TO OU	
25/03/21	Working out TO OU	Continue working out TO OU	
26/03/21	-	-	Day off
29/03/21	Improving TO Performance	Continue improving performance	
30/03/21	Improving TO Performance	Continue improving performance	
31/03/21	Improving TO Performance	Continue improving performance	
01/04/21	Improving TO Performance	Continue improving performance	
02/04/21	-	-	Good Friday
05/04/21	-	-	Easter
06/04/21	Improving TO Performance	Continue improving performance	
07/04/21	Improving TO Performance	Continue improving performance	
08/04/21	Improving TO Performance	Continue improving performance	
09/04/21	Fixing bug concave hull	Continue improving pefor-mance	
12/04/21	Fixing bug in FR24 data filter	Continue with this	
13/04/21	Fixing bug in FR24 data filter	Create trajectories	
14/04/21	Fixing bug in TO OU algorithm	Create trajectories	
15/04/21	Finalised and tuned model	run it	
16/04/21	-	-	EUR exams

19/04/21	-	-	EUR exams
20/04/21	-	-	EUR exams
21/04/21	-	-	EUR exams
22/04/21	Implementing multiprocessing for OU algorithm	Continue with implementing MP	
23/04/21	Implementing multiprocessing for OU algorithm	Continue with implementing MP	
26/04/21	Working on visualization of trajectories	Write trajectories to BlueSky scenario for conflict detection	
27/04/21	-	-	Kingsday
28/04/21	-	-	-
29/04/21	Finished visualization of trajectories and continued with BlueSky scenario	Continue with BlueSky Scenario	
30/04/21	Run scenario in BlueSky	Continue with conflict detection function	
03/05/21	Working on conflict detection function	Continue with conflict detection function	Inhousedag
04/05/21	Finished conflict detection function	Write Methodology on TO in preliminary	
05/05/21	Found bug in ordered upwind trajectory optimization and fixed it	Writing preliminary	
06/05/21	Writing preliminary	Continue writing preliminary	Inhousedag
07/05/21	Writing preliminary	Continue writing preliminary	
10/05/21	Writing preliminary	Continue writing preliminary	
11/05/21	Writing preliminary	Continue writing preliminary	
12/05/21	Writing preliminary	Continue writing preliminary	
13/05/21	-	-	Ascension
14/05/21	Writing preliminary	Continue writing preliminary	
17/05/21	Writing preliminary	Continue writing preliminary	
18/05/21	Writing preliminary	Continue writing preliminary	
19/05/21	Writing preliminary	Continue writing preliminary	
20/05/21	Writing preliminary	Continue writing preliminary	
21/05/21	-	-	-
24/05/21	Writing preliminary	Continue writing preliminary	
25/05/21	Writing preliminary	Continue writing preliminary	
26/05/21	Improving TO Performance	Continue improving performance	

27/05/21	Improving TO Performance	Continue improving performance	
28/05/21	Improving TO Performance	Continue improving performance	
31/05/21	Writing preliminary	Continue writing preliminary	
01/06/21	Fixing the issue with BlueSky WindGFS plugin	Continue writing preliminary	
02/06/21	-	-	EUR deadline
03/06/21	-	-	EUR deadline
04/06/21	Writing preliminary	Continue writing preliminary	
07/06/21	Writing preliminary	Continue writing preliminary	
08/06/21	-	-	EUR deadline
09/06/21	Writing preliminary	Continue writing preliminary	
10/06/21	Writing preliminary	Continue writing preliminary	
11/06/21	Writing preliminary	Continue writing preliminary	
14/06/21	-	-	EUR deadline
15/06/21	Writing preliminary	Continue writing preliminary	
16/06/21	Writing preliminary	Continue writing preliminary	
17/06/21	Writing preliminary	Continue writing preliminary	
18/06/21	-	-	EUR deadline
21/06/21	Writing preliminary	Continue writing preliminary	
22/06/21	Looking into BlueSky climb and descent operations	Continue writing preliminary	
23/06/21	Looking into BlueSky climb and descent operations and writing preliminary	Continue writing preliminary	
24/06/21	Writing preliminary	Continue writing preliminary	
25/06/21	Writing preliminary	Continue writing preliminary	
28/06/21	Writing preliminary	Continue writing preliminary	
29/06/21	Writing preliminary	Continue writing preliminary	
30/06/21	Writing preliminary	Continue writing preliminary	

Appendix E

Paper Overview by Topic

(NAT) Airspace		
Regional Supplementary Procedures	ICAO	2008
Aircraft Navigation	Hagström, M. et al.	2010
The Influence of Traffic Structure on Airspace Capacity	Sunil, E. et al.	2016
Procedures for Air Navigation Services Air Traffic Management	ICAO	2016
NAT Systems Planning Group - Appendix M NAT Traffic Forecast	ICAO	2019
North Atlantic Operations and Airspace Manual	ICAO	2020
Weather Models/Climate Impact		
An Event-Based Jet-Stream Climatology and Typology	Koch, P. et al.	2005
An advanced particle filtering algorithm for improving conflict detection in Air Traffic Control	Lymperopoulos, I. et al.	2010
Characterizing North Atlantic Weather Patterns for Climate-Optimal Aircraft Routing	Irvine, E. A. et al.	2013
On Board a Sustainable Future: 2016 Environmental Report	ICAO	2016
The Global Scale, Distribution and Growth of Aviation: Implications for Climate Change	Gössling, S. et al.	2020
Direct Routing/Free Flight		
A Self-Organizational Approach for Resolving Air Traffic Conflicts	Eby, M.S.	1994
Conflict-free Direct Routings in European Airspace	Davids, H.	1997
The Effect of Direct Routing on ATC Capacity	S A N Magill	1998
Conceptual Design of Free Flight with Airborne Separation Assurance	Hoekstra et al.	1998
Performance Evaluation of Airborne Separation Assurance in Free Flight	Bilimoria, K. et al.	2000
Properties of Air Traffic Conflicts for Free and Structured Routing	Lee, H.Q. et al.	2001
Designing for Safety: The Free Flight Air Traffic Management Concept	Hoekstra et al.	2002
Analytical Relationships Between Conflict Counts and Air-Traffic Density	Jardin, M.R.	2005
Trajectory Optimization		
Über die Navigation in der Luft als Problem der Variationsrechnung	Zermelo, E.	1930
Concepts for Generating Optimum Vertical Flight Profiles	Sorensen, J.	1979
Airplane Design: Preliminary Sizing of Airplanes	Roskam, J.	1985
Map Projections - A Working Manual	Snyder, J.P.	1987
Optimum Cruise Profiles in the Presence of Winds	Liden, S.	1992
Neighboring Optimal Aircraft Guidance in Winds	Jardin, R et al.	2001
Fundamentals of Airplane Flight Mechanics	Hull, D. G. et al.	2007
Dijkstra-Like Ordered Upwind Methods for Solving Static Hamilton-Jacobi Equations	Alton, K.	2010
Research on a New Aircraft Point-Mass Model	Imado, F. et al.	2011
Cross-Polar Aircraft Trajectory Optimization and the Potantial Climate Impact	Sridhar, B et al.	2011
A Practical Approach for Optimizing Aircraft Trajectories in Winds	Ng, K. Hok et al.	2012
Optimization of Aircraft Trajectories in North Atlantic Oceanic Airspace	Rodionova, O et al.	2012
Generating Optimal Aircraft Trajectories with respect to Weather Conditions	Girardet, B. et al.	2013
Wind-Optimal Path Planning: Application to Aircraft Trajectories	Girardet, B. et al.	2014
North Atlantic Aircraft Trajectory Optimization	Rodionova, O et al.	2014
Combined Winds and Turbulence Prediction System for Automated Air-Traffic Management Applications	Kim, J. H. et al.	2015
Computing Wind-Optimal Routes for Flight Performance Benchmarking	Cheng, F. et al.	2016
Multi-Objective Optimisation of Aircraft Flight Trajectories in the ATM and Avionics Context	Gardi, A. et al.	2016
The Gnomonic Projection for B-Spline Parameterized 4-D Trajectory Optimization Problems	Muller, R. et al.	2020
Reducing Transatlantic Flight Emissions by Fuel-Optimised Routing	Well, C. A. et al.	2021

Figure E-1: Overview of papers grouped by subject (1/2).

Conflict Detection & Resolution		
Evaluation of a Cooperative Air Traffic Management Model Using Principled Negotiation Between Intelligent Agents	Jacolin, L. et al.	1998
Motion Planning in Dynamic Environments Using Velocity Obstacles	Fiorini, P.	1998
System Performance Characteristics of Centralized and Decentralized Air Traffic Separation Strategies	Krozel, J. et al.	2001
Designing for Safety: The Free Flight Air Traffic Management Concept	Hoekstra et al.	2002
Comparison of Pilots' and Controllers' Conflict Resolution Maneuver Preferences	Rantanen, E. M. et al.	2006
Genetic Algorithms Applied to Air Traffic Management	Durand, N. et al.	2006
The Use of Intent Information in an Airborne Self-Separation Assistance Display Design	van Dam, S. et al.	2009
A Ground Holding Model for Aircraft Deconfliction	Durand, N. et al.	2010
Trajectory Deconfliction with Constraint Programming	Barnier, N.	2012
Optimization of Aircraft Trajectories in North Atlantic Oceanic Airspace	Rodionova, O et al.	2012
A Hybrid Metaheuristic Optimization Algorithm for Strategic Planning of 4D Trajectories at the Continental Scale	Chaimatanan, S. et al.	2014
Strategic Planning of Efficient Oceanic Flights	Sridhar, B et al.	2015
Deconflicting Wind-Optimal Aircraft Trajectories in North Atlantic Oceanic Airspace	Rodionova, O. et al.	2016
Conflict Resolution for Wind-Optimal Aircraft Trajectories in North Atlantic Oceanic Airspace with Wind Uncertainties	Rodionova, O. et al.	2016
A New Trans-Atlantic Route Structure for Strategic Flight Planning over the NAT Airspace	Dhief, I. et al.	2017
Review of Conflict Resolution Methods for Manned and Unmanned Aviation	Ribeiro, M. et al.	2020
Performance Modelling		
Base of Aircraft Data (BADA) Aircraft Performance Modelling Report	Eurocontrol	2009
Automatic Dependent Surveillance-Broadcast (ADS-B) Out Performance Requirements to Support Air Traffic Control (ATC) Service; Final Rule	FAA	2010
Laying Down Requirements for the Performance and Interoperability of Surveillance for the Single European Sky	European Commision	2011
User Manual for the Base of Aircraft Data (BADA) Revision 3.12	Eurocontrol	2014
BlueSky ATC Simulator Project: An Open Data and Open Source Approach	Hoekstra, J. M. et al.	2016
Aircraft Performance for Open Air Traffic Simulations	Metz, I. et al.	2016
Flight Extraction and Phase Identification for Large Automatic Dependant Surveillance-Broadcast Datasets	Sun, J. et al.	2017
OpenAP: An Open-Source Aircraft Performance Model for Air Transportation Studies and Simulations	Sun, J. et al.	2020

Figure E-2: Overview of papers grouped by subject (2/2).

Bibliography

[1] J. Krozel, M. Peters, K. D. Bilimoria, C. Lee, and J. S. Mitchell, "System performance characteristics of centralized and decentralized air traffic separation strategies," *Air Traffic Control Quarterly*, vol. 9, no. 4, pp. 311–332, 2001.

[2] ICAO, *Regional Supplementary Procedures*. International Civil Aviation Organisation, 999 University Street, Montréal, Quebec, Canada, 5 ed., 2008.

[3] ICAO, *North Atlantic Operations and Airspace Manual*. International Civil Aviation Organisation, 92522 Neuilly-sur-Seine CEDEX, France, 1 ed., Jan 2020.

[4] I. T. Mulder and D. I. C. Borst, "Air traffic control & air traffic management," in *Avionics and Operations*, 2018.

[5] N. SPG, *NAT Systems Planning Group - Appendix M NAT Traffic Forecast*. ICAO, EUR/NAT Office, 55 ed., 2019.

[6] B. Girardet, L. Lapasset, D. Delahaye, and C. Rabut, "Wind-optimal path planning: Application to aircraft trajectories," in *2014 13th International Conference on Control Automation Robotics & Vision (ICARCV)*, pp. 1403–1408, IEEE, 2014.

[7] J. M. Hoekstra, R. N. van Gent, and R. C. Ruigrok, "Designing for safety: The 'free flight' air traffic management concept," *Reliability Engineering & System Safety*, vol. 75, no. 2, pp. 215–232, 2002.

[8] M. Ribeiro, J. Ellerbroek, and J. Hoekstra, "Review of conflict resolution methods for manned and unmanned aviation," *Aerospace*, vol. 7, no. 6, p. 79, 2020.

[9] J. Roskam, *Airplane Design: Preliminary sizing of airplanes*. DARcorporation, 1985.

[10] E. E. Centre, *User Manual for the Base of Aircraft Data (BADA) Revision 3.12*. Eurocontrol, Centre de Bois des Bordes, B.P. 15, F-91222 Bretigny-sur-Orge CEDEX France, 3.12 ed., 2014.

[11] E. M. Rantanen, J. Yang, and S. Yin, "Comparison of pilots' and controllers' conflict resolution maneuver preferences," in *Proceedings of the Human Factors and Ergonomics Society Annual Meeting*, vol. 50, pp. 16–19, Sage Publications Sage CA: Los Angeles, CA, 2006.

[12] E. Sunil, J. Hoekstra, J. Ellerbroek, F. Bussink, A. Vidosavljevic, D. Delahaye, and R. Aalmoes, "The influence of traffic structure on airspace capacity," 2016.

[13] W. Schaberg, "A decentralized recovery method for air traffic conflicts," 2020.

[14] E. A. Irvine, B. J. Hoskins, K. P. Shine, R. W. Lunnon, and C. Froemming, "Characterizing north atlantic weather patterns for climate-optimal aircraft routing," *Meteorological Applications*, vol. 20, no. 1, pp. 80–93, 2013.

[15] B. Sridhar, N. Y. Chen, K. N. Hok, O. Rodionova, D. Delahaye, and F. Linke, "Strategic planning of efficient oceanic flights," 2015.

[16] O. Rodionova, M. Sbihi, D. Delahaye, and M. Mongeau, "North atlantic aircraft trajectory optimization," *IEEE Transactions on Intelligent Transportation Systems*, vol. 15, no. 5, pp. 2202–2212, 2014.

[17] O. Rodionova, D. Delahaye, B. Sridhar, and H. K. Ng, "Deconflicting wind-optimal aircraft trajectories in north atlantic oceanic airspace," 2016.

[18] L. Jacolin and R. Stengel, "Evaluation of a cooperative air traffic management model using principled negotiation between intelligent agents," in *Guidance, Navigation, and Control Conference and Exhibit*, p. 4103, 1998.

[19] M. Hagström and A. Lennartsson, "Aircraft navigation," *Encyclopedia of Aerospace Engineering*, 2010.

[20] S. Magill, "Effect of direct routing on air traffic control capacity," *2nd USA/Europe Air Traffic Management R&D Seminar*, 1998.

[21] O. Rodionova, M. Sbihi, D. Delahaye, and M. Mongeau, "Optimization of aicraft trajectories in north atlantic oceanic airspace," 2012.

[22] S. Gössling and A. Humpe, "The global scale, distribution and growth of aviation: Implications for climate change," *Global Environmental Change*, vol. 65, p. 102194, 2020.

[23] O. Rodionova, B. Sridhar, and H. K. Ng, "Conflict resolution for wind-optimal aircraft trajectories in north atlantic oceanic airspace with wind uncertainties," in *2016 IEEE/AIAA 35th Digital Avionics Systems Conference (DASC)*, pp. 1–10, IEEE, 2016.

[24] P. Koch, H. Wernli, and H. C. Davies, "An event-based jet-stream climatology and typology," *International Journal of Climatology: A Journal of the Royal Meteorological Society*, vol. 26, no. 3, pp. 283–301, 2006.

[25] H. David, *Conflict-free Direct Routing in European Airspace*. Eurocontrol, 91222 Bretigny-Sur-Orge Cedex, France, report no, 308 ed., 1997.

[26] M. S. Eby, "A self-organizational approach for resolving air traffic conflicts.," *The Lincoln Laboratory Journal*, 1994.

[27] M. R. Jardin, "Analytical relationships between conflict counts and air-traffic density," *Journal of guidance, control, and dynamics*, vol. 28, no. 6, pp. 1150–1156, 2005.

[28] K. Bilimoria, K. Sheth, H. Lee, and S. Grabbe, "Performance evaluation of airborne separation assurance in free flight," *AIAA Guidance, Navigation and Control Conference*, 2000.

[29] H. Q. Lee and K. D. Bilimoria, "Properties of air traffic conflicts for free and structured routing," in *AIAA Guidance, Navigation, and Control Conference and Exhibit*, p. 4051, 2001.

[30] C. A. Wells, P. D. Williams, N. K. Nichols, D. Kalise, and I. Poll, "Reducing transatlantic flight emissions by fuel-optimised routing," 2021.

[31] E. B. of ICAO, *On Board a Sustainable Future; 2016 Environmental Report*. ICAO, 999 University Street, Montréal, Quebec, Canada, 2016.

[32] A. Gardi, R. Sabatini, and S. Ramasamy, "Multi-objective optimisation of aircraft flight trajectories in the atm and avionics context," *Progress in Aerospace Sciences*, vol. 83, pp. 1 – 36, 2016.

[33] F. Imado, Y. Heike, and T. Kinoshita, "Research on a new aircraft point-mass model," *Journal of aircraft*, vol. 48, no. 4, pp. 1121–1130, 2011.

[34] D. G. Hull *et al.*, *Fundamentals of airplane flight mechanics*, vol. 19. Springer, 2007.

[35] H. K. Ng, B. Sridhar, and S. Grabbe, "A practical approach for optimizing aircraft trajectories in winds," in *2012 IEEE/AIAA 31st Digital Avionics Systems Conference (DASC)*, pp. 3D6–1, IEEE, 2012.

[36] J.-H. Kim, W. N. Chan, B. Sridhar, and R. D. Sharman, "Combined winds and turbulence prediction system for automated air-traffic management applications," *Journal of Applied Meteorology and Climatology*, vol. 54, no. 4, pp. 766–784, 2015.

[37] M. R. Jardin and A. E. Bryson Jr, "Neighboring optimal aircraft guidance in winds," *Journal of Guidance, Control, and Dynamics*, vol. 24, no. 4, pp. 710–715, 2001.

[38] J. Sorensen, "Concepts for generating optimum vertical flight profiles," 1979.

[39] S. Liden, "Optimum cruise profiles in the presence of winds," in *[1992] Proceedings IEEE/AIAA 11th Digital Avionics Systems Conference*, pp. 254–261, IEEE, 1992.

[40] F. Cheng and J. Gulding, "Computing wind-optimal routes for flight performance benchmarking," in *16th AIAA Aviation Technology, Integration, and Operations Conference*, p. 4361, 2016.

[41] K. Alton, *Dijkstra-Like Ordered Upwind Methods for Solving Static Hamilton-Jacobi Equations*. PhD thesis, University of British Columbia, 2010.

[42] E. Zermelo, "Über die navigation in der luft als problem der variationsrechnung," *Jahresbericht der deutschen Mathematiker–Vereinigung, Angelegenheiten*, vol. 39, pp. 44–48, 1930.

[43] H. K. Ng, B. Sridhar, S. Grabbe, and N. Chen, "Cross-polar aircraft trajectory optimization and the potential climate impact," in *2011 IEEE/AIAA 30th Digital Avionics Systems Conference*, pp. 3D4–1, IEEE, 2011.

[44] B. Girardet, L. Lapasset, D. Delahaye, C. Rabut, and Y. Brenier, "Generating optimal aircraft trajectories with respect to weather conditions," 2013.

[45] J. P. Snyder, "Map projections-a working manual," 1987.

[46] J. Hoekstra, R. Van Gent, and R. Ruigrok, "Conceptual design of free flight with airborne separation assurance," p. 4239, 1998.

[47] ICAO, *Procedures for Air Navigation Services Air Traffic Management*. International Civil Aviation Organisation, 999 University Street, Montréal, Quebec, Canada, 6 ed., 2016.

[48] P. Fiorini and Z. Shiller, "Motion planning in dynamic environments using velocity obstacles," *The International Journal of Robotics Research*, vol. 17, no. 7, pp. 760–772, 1998.

[49] S. Van Dam, M. Mulder, and R. Paassen, "The use of intent information in an airborne self-separation assistance display design," in *AIAA Guidance, Navigation, and Control Conference*, p. 5745, 2009.

[50] N. Durand and J.-B. Gotteland, "Genetic algorithms applied to air traffic management," in *Metaheuristics for hard optimization*, Springer, 2006.

[51] N. Durand, C. Allignol, and N. Barnier, "A ground holding model for aircraft deconfliction," in *29th Digital Avionics Systems Conference*, pp. 2–D, IEEE, 2010.

[52] N. Barnier and C. Allignol, "Trajectory deconfliction with constraint programming," *Knowledge Engineering Review*, vol. 27, no. 3, pp. pp–291, 2012.

[53] I. Dhief, N. H. Dougui, D. Delahaye, and N. Hamdi, "A new trans-atlantic route structure for strategic flight planning over the nat airspace," in *2017 IEEE Congress on Evolutionary Computation (CEC)*, pp. 1511–1518, IEEE, 2017.

[54] S. Chaimatanan, D. Delahaye, and M. Mongeau, "A hybrid metaheuristic optimization algorithm for strategic planning of 4d aircraft trajectories at the continental scale," *IEEE Computational Intelligence Magazine*, vol. 9, no. 4, pp. 46–61, 2014.

[55] J. Sun, J. M. Hoekstra, and J. Ellerbroek, "Openap: An open-source aircraft performance model for air transportation studies and simulations," *Aerospace*, vol. 7, no. 8, p. 104, 2020.

[56] E. E. Centre, *Base of Aircraft Data (BADA) Aircraft Performance Modelling Report*. Eurocontrol, Centre de Bois des Bordes, B.P. 15, F-91222 Bretigny-sur-Orge CEDEX France, 9 ed., 2009.

[57] J. Sun, J. Ellerbroek, and J. Hoekstra, "Flight extraction and phase identification for large automatic dependent surveillance–broadcast datasets," *Journal of Aerospace Information Systems*, vol. 14, no. 10, pp. 566–572, 2017.

[58] J. M. Hoekstra and J. Ellerbroek, "Bluesky atc simulator project: An open data and open source approach," in *Proceedings of the 7th International Conference on Research in Air Transportation*, vol. 131, p. 132, FAA/Eurocontrol USA/Europe, 2016.

[59] I. Metz, J. Hoekstra, J. Ellerbroek, and D. Kügler, "Aircraft performance for open air traffic simulations," in *AIAA Modeling and Simulation Technologies Conference*, p. 3522, 2016.

[60] T. E. Commission, *Laying Down Requirements for the Performance and Interoperability of Surveillance for the Single European Sky*. The European Commission, Brussels, 2011.

[61] FAA, *Automatic Dependent Surveillance—Broadcast (ADS–B) Out Performance Requirements To Support Air Traffic Control (ATC) Service; Final Rule*. Department of Transportation, 800 Independence Ave., S.W. Washington, DC 20591, 2010.